MINISTRY OF EDUCATION AND TRAINING MINISTRY OF SCIENCE AND TECHNOLOGY

VIETNAM ATOMIC ENERGY INSTITUTE

DAU DUC TU

STUDY ON SENSITIVITY AND UNCERTAINTY OF NUCLEAR DATA IN KINETIC PARAMETERS AND CRITICALITY ANALYSES FOR A CORE CONFIGURATION WITH 92 LOW ENRICHED FUEL BUNDLES OF THE DALAT NUCLEAR RESEARCH REACTOR

DISSERTATION FOR THE DEGREE OF DOCTOR OF PHILOSOPHY IN PHYSICS

HANOI - 2025

BỘ GIÁO DỤC VÀ ĐÀO TẠO BỘ KHOA HỌC VÀ CÔNG NGHỆ

VIỆN NĂNG LƯỢNG NGUYÊN TỬ VIỆT NAM

ĐẬU ĐỨC TỪ

NGHIÊN CỨU ĐỘ NHẠY VÀ ĐỘ BẤT ĐỊNH SỐ LIỆU HẠT NHÂN TRONG PHÂN TÍCH THÔNG SỐ ĐỘNG HỌC VÀ TỚI HẠN CHO VÙNG HOẠT 92 BÓ NHIÊN LIỆU ĐỘ GIÀU THẤP CỦA LÒ PHẢN ỨNG HẠT NHÂN ĐÀ LẠT

LUẬN ÁN TIẾN SĨ VẬT LÝ

Chuyên ngành: Vật lý Nguyên tử và Hạt nhân

Mã số: 9.44.01.06

Giáo viên hướng dẫn:

1. GS. TS. TRẦN HOÀI NAM

2. PGS. TS. NGUYỄN NHỊ ĐIỀN

Hà Nội - 2025

MINISTRY OF EDUCATION AND TRAINING MINISTRY OF SCIENCE AND TECHNOLOGY

VIETNAM ATOMIC ENERGY INSTITUTE

DAU DUC TU

STUDY ON SENSITIVITY AND UNCERTAINTY OF NUCLEAR DATA IN KINETIC PARAMETERS AND CRITICALITY ANALYSES FOR A CORE CONFIGURATION WITH 92 LOW ENRICHED FUEL BUNDLES OF THE DALAT NUCLEAR RESEARCH REACTOR

DISSERTATION FOR THE DEGREE OF DOCTOR OF PHILOSOPHY IN PHYSICS

Major: Nuclear and Atomic Physics

Code: 9.44.01.06

Supervisors:

1. **Prof. TRAN HOAI NAM**
2. **Assoc. Prof. NGUYEN NHI DIEN**

Hanoi - 2025

Declaration

I certify that this dissertation, entitled "Study on sensitivity and uncertainty of nuclear data in kinetic parameters and criticality analyses for a core configuration with 92 low enriched fuel bundles of the Dalat nuclear research reactor" is my original work, except where otherwise clearly indicated. I confirm that the dissertation submitted to the Nuclear Training Center, Vietnam Atomic Energy Institute, was primarily completed during my candidacy for a PhD degree under the supervision of Prof. Tran Hoai Nam and Assoc. Prof. Nguyen Nhi Dien.

DAU DUC TU

Acknowledgements

First of all, I would like to express my heartfelt gratitude to my supervisors, Prof. Tran Hoai Nam and Assoc. Prof. Nguyen Nhi Dien, for their invaluable support and encouragement throughout my research.

I would like to extend my sincere gratitude to Dalat Nuclear Research Institute and Nuclear Training Centre of Vietnam Atomic Energy Institute for permitting me to conduct this research.

I sincerely thank the leadership of the Reactor Center at Dalat Nuclear Research Institute, and all of my colleagues for their generous assistance during my research.

Finally, I want to express my gratitude to my family, who have consistently given me the confidence and motivation to complete my thesis.

Contents

List of symbols and abbreviations

AR	Automatic Regulating rod
ASA	Adjoint sensitivity analysis
BOC	Beginning of cycle
BROND	Russian Evaluated Nuclear Data Library
CENDL	Chinese Evaluated Nuclear Data Library
CIELO	Coordination International Evaluation Library Organization
CNDC	China Nuclear Data Center
CNDCN	Chinese Nuclear Data Cooperation Network
CRPs	Coordinated Research Projects
CSEWG	Cross Section Evaluation Working Group
DNRR	Dalat Nuclear Research Reactor
DPSA	Direct perturbation sensitivity analysis
ENDF	Evaluated Nuclear Data File
EOC	End of cycle
FBR	Fast Breeder Reactor
FSA	Forward sensitivity analysis
HEU	High Enriched Uranium
IAEA	International Atomic Energy Agency
INDEN	International Nuclear Data Evaluator Network
JEFF	Joint Evaluated Fission and Fusion File
JENDL	Japanese Evaluated Nuclear Data Library
JNDC	Japanese Nuclear Data Committee
LEU	Low Enriched Uranium
LWR	Light Water Reactor
NAA	Neutron Activation Analysis
NDS	Nuclear Data Section
NEA	Nuclear Energy Agency
NDM	Nuclear Data Measurement

NNDC	National Nuclear Data Center
NPS	Nuclear Physics Studies
NRDC	Nuclear Reaction Data Centres
NSDD	Nuclear Structure and Decay Data
OECD	Organization for Economic Cooperation and Development
PCM	Per Cent Mille (10^{-5})
PGNAA	Prompt Gamma Neutron Activation Analysis
PT	Perturbation Theory
R&T	Research and Training
RI	Radioisotope
SA	Sensitivity Analysis
ShR	Shim Rods
SR	Safety Rods
S/U	Sensitivity and Uncertainty
TENDL	TALYS based Evaluated Nuclear Data Library
TRIGA	Training, Research, Isotopes, General Atomics
UA	Uncertainty Analysis
WPEC	Working Party on International Nuclear Data Evaluation Cooperatio
Be $S(\alpha, \beta)$	Thermal scattering data for beryllium
C-nat $S(\alpha, \beta)$	Thermal scattering data for natural carbon
β_{eff}	Effective delayed neutron fraction
Λ	Neutron generation time
λ	Decay constant of delayed neutron precursors
l_p	Prompt neutron lifetime
Lwtr $S(\alpha, \beta)$	Thermal scattering data for hydrogen bound in light water
k_{eff}	Effective multiplication factor
ρ	Reactivity
ρ_{ex}	Excess reactivity

List of Tables

List of Figures

PREFACE

In the era of advanced scientific and technological development, computational modeling has become an indispensable tool in nuclear reactor physics and engineering. Modern reactor design, operation, and safety assessment rely extensively on high fidelity simulations capable of predicting the complex behavior of reactor cores under a wide range of conditions. Owing to the high cost, safety concerns, and operational limitations of full scale reactor experiments, computational reactor physics offers a practical and reliable means to explore core behavior, optimize configurations, evaluate safety margins, and support informed decision making. Among the various computational methods, Monte Carlo transport simulations have proven particularly powerful for their ability to model neutron behavior with high physical and geometric fidelity. Codes such as MCNP and SERPENT are widely used in both research and power reactor analyses, enabling the study of detailed particle interactions, transient phenomena, and safety related parameters under diverse operational scenarios.

At the foundation of every reactor physics simulation lies the nuclear data, a comprehensive set of evaluated quantities that describe the probabilities of neutron interactions with atomic nuclei. These evaluated quantities include fission, capture, elastic scattering, and inelastic scattering cross sections. Nuclear data are compiled into evaluated nuclear data libraries such as ENDF/B, JEFF, JENDL, and CENDL, which serve as essential input for all neutronic calculations. The accuracy and reliability of reactor simulations depend critically on the quality of these data. Differences in experimental measurements, evaluation methodologies, and theoretical models can lead to notable discrepancies between data libraries, directly affecting key reactor parameters such as the effective multiplication factor (k_{eff}). Although modern nuclear data libraries like ENDF/B-VIII.0, JEFF-3.3, JENDL-5, and CENDL-3.2 have significantly improved in coverage and accuracy by incorporating updated measurements, refined evaluation techniques, and covariance

information, residual uncertainties remain and must be rigorously quantified to ensure reliable reactor design and safety assessments.

Two categories of reactor physics parameters are particularly sensitive to the quality of nuclear data: criticality and kinetic parameters. The effective multiplication factor (k_{eff}) determines whether a reactor is subcritical, critical, or supercritical, thereby serving as a fundamental indicator of neutron economy and core stability. Accurate evaluation of k_{eff} is essential for fuel loading optimization, startup planning, and safety validation. Meanwhile, kinetic parameters such as the effective delayed neutron fraction (β_{eff}), neutron generation time (Λ), and prompt neutron lifetime (l_p) govern the reactor's time dependent response to reactivity changes. Although delayed neutrons constitute only a small fraction of all fission neutrons, they play a vital role in maintaining controllability and preventing prompt critical excursions. The β_{eff}, in particular, defines the margin between delayed and prompt critical states, while Λ and l_p influence transient power behavior and feedback responses. Even minor uncertainties in these parameters can significantly affect dynamic simulations, impacting predictions of power transients, reactivity insertion accidents, and scram effectiveness.

Given the interdependence between nuclear data and reactor performance, modern reactor analysis increasingly integrates sensitivity and uncertainty evaluation as essential components of the computational process. Sensitivity Analysis (SA) quantifies how perturbations in input parameters influence key reactor responses, providing insights into which isotopes and reaction channels most strongly affect outputs such as k_{eff}, β_{eff}. Uncertainty Analysis (UA), on the other hand, quantifies how uncertainties in the input data, represented by covariance matrices propagate through models to affect the variance of output quantities. Combined, SA and UA form a rigorous framework that enables the decomposition of total uncertainties, identification of dominant contributors, and prioritization of nuclear data improvements. The integration of these methodologies, supported by adjoint weighted perturbation theory and Monte Carlo simulation, enhances the interpretability and reliability of computational predictions in nuclear reactor

physics.

In summary, this dissertation analyzes the sensitivity and uncertainty of nuclear data for kinetic and criticality parameters in a core configuration comprising 92 low enriched fuel bundles from the Dalat nuclear research reactor. This research uses advanced Monte Carlo simulations along with comprehensive sensitivity and uncertainty analysis methods to clearly show how uncertainties in nuclear data affect reactor calculations. The results are expected to improve the reliability of reactor safety assessments, enhance the transparency of computation results, and support ongoing improvements in nuclear data evaluation. Through this systematic approach, the study aims to establish a solid methodological framework applicable not only to the DNRR but also to other reactors.

The following chapter presents a general overview of the theoretical background, the characteristics of the Dalat Nuclear Research Reactor, the computational tools and nuclear data libraries employed in this work.

Chapter 1 GENERAL OVERVIEW

1. Introduction

The rapid advancement of nuclear technology and its widespread application across nearly all aspects of human life have become increasingly evident. Among the most significant achievements of scientific research is the development of computer simulation, which has been extensively integrated into numerous scientific disciplines. Computer simulation has proven to be an invaluable tool, opening new areas of study and providing a qualitative impetus for the advancement of science and technology. Overall, the use of computer simulation has significantly improved the efficiency of scientific research by accelerating processes, reducing costs, and minimizing the time and resources required to achieve research objectives.

In the physical design of nuclear reactors, nuclear data libraries play a critical role in supporting calculations and simulations, necessitating rigorous analysis and evaluation of nuclear data uncertainties. Accurate and reliable nuclear data for the materials used in the reactor core are essential for designing and assessing new reactor concepts. This data includes neutron cross sections of various isotopes, which significantly influence the reactor's performance and safety. Consequently, evaluating the uncertainties associated with nuclear data is crucial for ensuring the safety, reliability, and effectiveness of reactor designs. Precise knowledge of cross section uncertainties can contribute to optimizing and enhancing the robustness of nuclear reactor physical designs.

For the safe operation of nuclear reactors, a comprehensive understanding of key reactor parameters, including physical parameters, the effective multiplication factor, and kinetic parameters, is essential. This understanding allows for accurate predictions of reactor behavior under various operational conditions, thereby supporting the effective implementation of safety measures and emergency responses. In particular, evaluating kinetic parameters, such as neutron generation time, prompt neutron lifetime, and delayed neutron fractions, under different conditions provides valuable insights into reactor dynamics during both normal and transient states. This

knowledge enhances safety standards and the development of robust emergency response strategies, ultimately helping to prevent accidents and ensure the safe operation of nuclear reactors.

In nuclear reactor simulations, computational models and methods play a critical role. A variety of computer codes have been developed to perform reactor calculations and simulations using different techniques, such as deterministic transport methods and the Monte Carlo method. Monte Carlo-based transport codes, including MCNP [1], MVP [2], SERPENT [3], among others, are widely employed for the simulation and analysis of nuclear reactors. These codes enable researchers and engineers to model diverse scenarios and assess potential risks under various operational conditions. By utilizing these advanced computational tools, it is possible to develop detailed models for reactor design, maintenance planning, and emergency preparedness. However, the accuracy of such simulations strongly depends on the assumptions, input parameters, and nuclear data provided by the user. Inaccurate inputs or unrealistic assumptions may lead to results that do not accurately represent the behavior of actual nuclear reactors.

To address the limitations associated with the data, models, and methods employed in reactor analyses, it is essential to enhance the realism of predictions through comprehensive uncertainty quantification. This approach enables a detailed assessment and definition of safety margins, forming the basis of methodologies commonly referred to as best estimate plus uncertainty. Figure 1.1 illustrates the concept of safety margins, along with two methodologies regarded as realistic or best estimate approaches for conducting safety analyses.

In analyzing a nuclear reactor, the accuracy of the kinetic and criticality parameters depends heavily on the quality of the nuclear data and modeling assumptions. Uncertainties from both physical and numerical sources inherently impact every calculation in reactor physics. These include limitations in evaluated nuclear data files, approximations in neutron transport or diffusion theory, discretization of the geometry and energy domains, boundary conditions, and user defined input parameters. Therefore, understanding

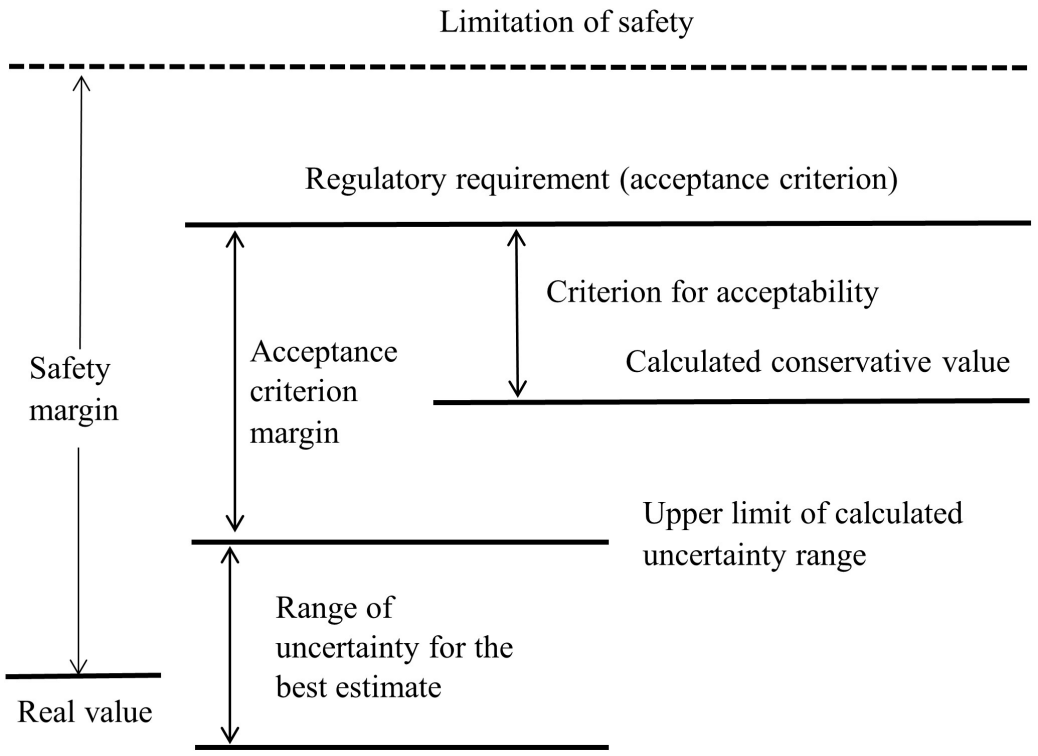

Figure 1.1: The concept of safety margins as defined by the IAEA [4].

and quantifying these uncertainties is essential to ensure the reliability of the calculated effective multiplication factor and kinetic parameters. Uncertainty analysis aims to quantify the total variability in the calculated parameters that results from the combined effects of uncertainties in nuclear data and modeling inputs. In contrast, sensitivity analysis identifies the degree to which each specific input, such as the cross sections, fission yields, or delayed neutron data for main isotopes affects reactor responses. The sensitivity analysis enhances this process by identifying the importance of individual isotopes and reactions in contributing to the overall uncertainty. These results offer valuable guidance for improving the evaluated nuclear data and refining the reactor core model. It not only measures the confidence level of the simulation results but also aids future improvements in nuclear data, model validation, and safety margin assessment for reactors. In this research, the stochastic Monte Carlo approach provides a robust means of propagating nuclear data uncertainties by sampling input parameters using random methods, followed by statistical evaluation of the output quantities. The resulting ensemble of simulations enables the estimation of statistical descriptors, such

as the mean, variance, and confidence intervals, for the kinetic and criticality parameters.

Extensive research has focused on determining kinetic parameters and the effective multiplication factor for various reactor types using Monte Carlo simulations [5–10]. Notable S/U studies have been carried out for several research reactors, including the TRIGA Mark II and the RSG-GAS multipurpose reactor, employing codes such as SUSD3D and MCNP. [11–19]. The DNRR has utilized various deterministic and Monte Carlo computational tools for core physics evaluations, including neutronics analysis, burnup calculations, safety assessments, and in-core fuel management. Early studies utilized the WIMSD/CITATION code system to evaluate burnup distributions of the HEU-fueled core and to benchmark the calculated results against experimental measurements [20]. In addition, this code system was used to generate data for the HEU-based DNRR configuration, which later served as the foundation for the development of advanced ICFM methodologies, such as genetic algorithms, differential evolution, and their improved variants [21]. Further neutronic analyses of the HEU core were conducted using the MCNP5 and SRAC codes. The calculated effective multiplication factors closely matched between the two codes, with differences of less than 55 pcm, while deviations from experimental measurements were approximately 119 pcm. Regarding power distribution, the relative deviations in the core's central region were under 4%, whereas about 7% deviations were observed in the outer core region [22]. A detailed criticality analysis of 49 startup configurations was performed using the SRAC and MCNP5 codes with various nuclear data libraries, including ENDF/B and JENDL. The differences in calculated criticality values ranged from 770 pcm, depending on the library used (ENDF/B-VII.0, JENDL-3.3, and JENDL-4.0). For the operational setup with 88 fuel bundles, the gap between calculated and measured k_{exteff} values remained within 330 pcm [23]. The coupled PARCS/Serpent model demonstrated potential applicability for both steady state and transient reactor analyses [24].

For these reasons, uncertainty analysis is a critical component of simulation modeling, particularly when employing nuclear data and kinetic parameters that play a key role in reactor transient analysis and control. In this study, the thesis presents Sensitivity and Uncertainty (S/U) analyses of nuclear data related to the criticality and kinetic parameters of the Dalat Nuclear Research Reactor (DNRR). The analyses are performed using the MCNP6 code [1] in combination with the latest nuclear data libraries, including ENDF/B-VIII.0 [25], JEFF-3.3 [26], JENDL-5.0 [27], and CENDL-3.2 [28].

2. The role of nuclear data libraries

Nuclear data provide the empirical foundation for research in a wide range of scientific fields, including nuclear energy, safety, security, and safeguards, as well as numerous other applications. These data also support the development of technologies that impact various aspects of daily life. For example, nuclear data are essential in the discovery of Nobel Prize winning particles, such as the Higgs boson, as they determine how particles interact with detectors. Nuclear data encompass a broad spectrum of structural and reaction quantities, including scattering and reaction cross sections (typically as functions of energy and angle), nuclear masses, level properties, decay modes and parameters, neutron and photon spectra from reactions, and many other related quantities. Such data are crucial for characterizing each nuclear isotope and facilitating reactions involving neutrons, protons, deuterons, alpha particles, and photons. In cases where experimental data are unavailable, model predictions are employed to generate the necessary database [29].

Due to the complexity of nuclear data evaluation and the diverse expertise required for this work, as well as the critical role of nuclear data in both fundamental and applied research, numerous organizations have been established to coordinate activities, enhance communication, and promote collaboration among evaluators. The development of nuclear data libraries involves six interconnected stages: measurement, compilation, evaluation, processing, validation, and application. These stages collectively support a wide range of scientific fields and end user applications. Various groups

contribute to the generation and evaluation of nuclear data, particularly for nuclear reactions. These include the International Nuclear Data Evaluator Network (INDEN) [30], the International Network of Nuclear Reaction Data Centres (NRDC) [31], and the U.S. National Nuclear Data Center (NNDC) [32], all operating under the auspices of the Nuclear Data Service (NDS) of the International Atomic Energy Agency (IAEA) [33]. Additional key contributors include the Cross Section Evaluation Working Group (CSEWG) [34], in collaboration with U.S. and Canadian national laboratories, as well as the Nuclear Energy Agency (NEA) of the Organization for Economic Cooperation and Development (OECD), through its Working Party on International Nuclear Data Evaluation Cooperation (WPEC) [35], and the Japanese Nuclear Data Committee (JNDC) [36].

These organizations have worked to address differences among nuclear reaction data libraries developed in various countries, including the Evaluated Nuclear Data File (ENDF) in the United States [25], the Joint Evaluated Fission and Fusion File (JEFF) in Europe [37], the TALYS based Evaluated Nuclear Data Library (TENDL) [38], the Japanese Evaluated Nuclear Data Library (JENDL) [36], the Russian Evaluated Nuclear Data Library (BROND) [39], and the Chinese Evaluated Nuclear Data Library (CENDL) [28]. In addition, the WPEC subgroups [35] and the IAEA Nuclear Data Section's Coordinated Research Projects (CRPs) [40] have contributed to the improvement of data evaluation methodologies, data formats, and both general purpose and application specific evaluated data sets. In the field of nuclear structure, evaluation efforts are coordinated by the U.S. Nuclear Data Program [41], managed by the U.S. National Nuclear Data Center (NNDC), the IAEA Nuclear Data Section (NDS) [33], and the Nuclear Structure and Decay Data (NSDD) Network [42]. Collaboration among these organizations fosters improved consistency and accuracy in global nuclear data evaluations and standards.

Nuclear data have a significant impact on the physical design, efficiency, and operation of advanced reactors, as well as on applications related to security. The development of advanced reactors and small reactors, many

of which employ fuels, coolants, and moderators different from those used in existing reactor technologies, has created a growing need for improved nuclear data, including new differential and integral measurements and evaluations. Security related applications are even more diverse, involving a wide array of detectors, systems, and interaction scenarios. Notably, there is substantial overlap in the nuclear data requirements for reactor technologies and security applications, particularly in the context of small reactors [29].

Nuclear data serve as the cornerstone for the development and application of nuclear science and technology. Accordingly, comprehensive examination and evaluation of nuclear data are essential to establish a cohesive and reliable body of information. Nuclear data are applied across a wide range of fields within nuclear science and technology, spanning both energy related and non energy related domains. In the energy sector, nuclear data support the design of fission reactors, management of nuclear fuel cycles, assurance of nuclear safety, reactor monitoring, radiation shielding and dose assessment, nuclear waste disposal, transmutation of radioactive materials, development of accelerator driven systems, fusion device design, and plasma processing technologies. Beyond the energy sector, nuclear data play a vital role in areas such as radiation therapy for cancer treatment, production of radioisotopes for medical and industrial applications, radiation protection and worker safety, nuclear safeguards, nuclear waste treatment and recycling, environmental monitoring and remediation, materials research, process control, mineral and oil exploration, and fundamental research in nuclear astrophysics and education. The collection, evaluation, and dissemination of nuclear data represent a complex and challenging endeavor that depends on the contributions of experts from both fundamental and applied sciences worldwide.

3. Reactor core analysis and uncertainty sources

Reactor core analysis involves the simulation and evaluation of the physical and neutronic behavior of a nuclear reactor core under both normal and transient conditions. This process is fundamental to core design, fuel management, and safety assessment. However, the accuracy of such analyses is inherently influenced by multiple sources of uncertainty. A primary

source is nuclear data, particularly neutron cross sections, which directly affect neutron transport and reaction rate calculations. Inaccuracies or limitations in these data can lead to errors in predicting key parameters such as power distribution, reactivity, and fuel burnup. Additional uncertainties arise from reactor operating conditions, including temperature, coolant flow rate, and power level, all of which are subject to measurement errors and operational variability. Manufacturing tolerances further contribute by introducing deviations in fuel enrichment, fuel density, and geometric dimensions from their nominal specifications, thereby altering the core's physical configuration. During reactor operation, changes in fuel composition due to burnup introduce further uncertainties in isotopic inventories and their associated reactivity effects. Moreover, computational models and numerical methods used for core simulations introduce algorithmic approximations and discretization errors, often referred to as computational bias. To ensure the reliability of reactor core predictions, comprehensive uncertainty analysis is essential. Such analysis involves quantifying individual sources of uncertainty, understanding their interactions, and evaluating their impact on key safety and performance metrics. This is critical for regulatory compliance, risk informed decision making, and upholding high standards of nuclear safety.

In general, the primary sources of input variability that contribute to uncertainty in reactor analysis include nuclear data, reactor operating conditions, manufacturing tolerances, fuel burnup, induced technological changes, and computational biases. To accurately assess their impact, it is essential to conduct a comprehensive analysis of all sources of uncertainty. Such an analysis must cover the entire process and rely on rigorous methodologies, beginning with the nuclear cross section data and extending through the calculation tools and procedures, review processes, and the qualification of the nuclear analysts involved [43].

Nuclear data represent the primary source of uncertainty in this context and are classified as aleatory uncertainties. Such uncertainties directly

influence the solutions of neutron transport or diffusion equations by affecting quantities such as microscopic cross sections, energy and angular distributions, the average number of neutrons per fission, neutron spectra, and decay constants. Nuclear data libraries compile information generated through the six interconnected steps described in Section 2., with each step contributing to the overall uncertainty in the nuclear data.

The second category of uncertainties arises from reactor operating conditions, including the temperature and density of the moderator, fuel temperature, boron concentration, and irradiation history. These factors influence neutron behavior within the reactor core, thereby contributing to variations in calculated reactor parameters. It is essential to carefully quantify and account for uncertainties in operating conditions to ensure the accuracy and reliability of reactor calculations and analyses [43].

The third category of uncertainties comprises technological uncertainties, which are also classified as aleatory uncertainties. These arise from manufacturing standards and process deviations, affecting components of the nuclear reactor such as geometrical dimensions and configurations, as well as characteristics of nuclear fuel, including enrichment, density, and other material properties [43].

The fourth category of uncertainties is associated with burnup and is arguably the most challenging to quantify. Burnup influences nearly all other sources of uncertainty by altering material compositions over time, thereby modifying the nuclear data uncertainty component. As fuel assemblies undergo burnup, the mechanical and structural properties of the fuel rod, fuel meat, gap, and cladding evolve due to various phenomena, including densification, swelling, fission gas release, cladding creep down, creep out, oxidation, hydrogen uptake, among others. These changes also affect thermal behavior, leading to variations in fuel and moderator temperatures. In addition, burnup can cause fuel relocation and structural deformation, further contributing to technological uncertainties [43].

Finally, computational models and numerical methods, including the underlying equations, approximations, and algorithms represent a source of fundamental uncertainty, as they can introduce inaccuracies or biases into reactor analysis. These uncertainties, often referred to as computational biases, may arise from model simplifications or numerical discretization. In some cases, they can be quantified by comparison with more accurate reference models, such as continuous energy Monte Carlo simulations rather than multigroup deterministic solvers, or transport solvers instead of diffusion solvers. This category of uncertainty also includes user effects, which reflect variations in results due to the level of proficiency and experience in applying specific computational codes.

4. Uncertainty and sensitivity analysis

Uncertainty and sensitivity analyses are essential tools for the evaluation of complex engineering systems, particularly in the modeling and simulation of nuclear reactors. Uncertainty analysis focuses on identifying and quantifying potential errors or variations in input parameters, such as nuclear data, geometric dimensions, material properties, and operating conditions and assessing how these uncertainties propagate through computational models to affect output results. In contrast, sensitivity analysis examines how variations in individual input parameters influence specific output quantities, thereby identifying the inputs that most significantly impact key results, including reaction rates, power distributions, neutron fluxes, and temperature fields. While uncertainty analysis quantifies the range or spread of output values due to input variability, sensitivity analysis highlights the most influential parameters. These analyses serve complementary purposes: together, they enhance model reliability, guide data collection efforts by indicating where greater accuracy is required, and support safety assessments by identifying critical parameters that must be tightly controlled. In nuclear engineering, where decisions must be supported by a high degree of confidence, the combined application of uncertainty and sensitivity analyses is vital for model validation and for ensuring that reactor performance predictions are both accurate and robust.

In the context of nuclear data, uncertainty analysis assesses how input data uncertainties propagate and affect output results, while sensitivity analysis identifies the isotopes, reaction cross sections, and energy ranges that have the most significant impact on specific output quantities. To evaluate and analyze uncertainties in input data and their influence on reactor physics parameters, two primary tasks are required: Sensitivity Analysis (SA) and Uncertainty Analysis (UA).

The SA is the first critical task that must be addressed. The SA determines the impact of perturbations in input parameters on the responses of interest. This step is essential, as many subsequent analyses either depend on its results or can be significantly simplified based on its findings. Specifically, the SA provides the foundation for the UA, the identification of key nuclear data, and the reduction of input parameter space. Global sensitivity evaluation examines the effects of varying an input parameter in the presence of variations in other input parameters, typically employing sampling methodologies to explore the full range of input values and their interactions. In contrast, local sensitivity analysis focuses on the effect of perturbing a single input parameter while keeping all others fixed. This local analysis often relies on linear perturbation theory and is commonly implemented using adjoint-based computations. The sensitivity evaluation activities conducted in this thesis for reactor core simulations are detailed in Chapter 2.

In general, the sensitivity coefficient (S) can be defined as the ratio of the fractional change in a response (Ψ) to the corresponding fractional change in an input parameter (α), as expressed by the following relation [43–45]:

$$S_{\Psi,\alpha} = \frac{\partial\Psi/\Psi}{\partial\alpha/\alpha}. \tag{1.1}$$

Several studies on the application of Sensitivity Analysis (SA) can be found in the literature, including [14, 16, 23, 46–53].

The second major task is the UA, which involves the propagation of input parameter uncertainties to the responses of interest. Comprehensive details regarding the full core calculations performed in this study, based on

reactor core simulations, are provided in Chapter 2, with a brief introduction to this topic presented below. The UA approaches are generally classified into two categories: deterministic based methods and sampling based methods. The former relies on Perturbation Theory (PT), while the latter employs random sampling techniques. Perturbation theory provides the theoretical foundation for deterministic based methods and has been successfully implemented in various computational codes [54, 55]. To quantify the uncertainty (U) in the responses due to input parameter variations, the sandwich rule is applied. This rule combines the sensitivity matrix $[S]$, representing the response sensitivities to input parameters, with the covariance matrix $[C]$ of the input parameters, as follows [45]:

$$U^2 = [S]^{\mathrm{T}} \cdot [C] \cdot [S]. \tag{1.2}$$

One limitation of approaches based on the PT is that they rely on first order approximations. As a result, these methods may produce inaccurate uncertainty estimates when applied to non linear systems or systems subject to large perturbations. In contrast, sampling based techniques for uncertainty quantification involve random sampling of input parameters from their joint probability distributions, with each random sample used in a separate simulation to compute the integral observable of interest. The uncertainty associated with the integral observable is then derived from the statistical analysis of the Monte Carlo simulation results. Transport based codes are particularly well suited for sensitivity and uncertainty analyses in full core calculations, especially those that do not depend on multigroup cross section data. Several computational codes, such as SCALE (TSUNAMI-3D), MCNP, and SERPENT, are widely used for S/U analyses owing to their capability to process continuous energy nuclear data libraries. In these methods, sensitivities are computed and subsequently combined with covariance matrices to estimate uncertainties. Numerous studies have applied both deterministic and sampling based uncertainty propagation approaches [46, 56–59].

5. Brief overview of the Dalat nuclear research reactor

The General Atomic Company developed the well known nuclear reactor design called TRIGA (Training, Research, Isotopes, General Atomics). It

has been built in 66 reactors across 24 countries around the world. Of these, five TRIGA reactors have operated in Southeast Asia as follows: Thailand has the TRIGA Mark III reactor, which was built in Bangkok in 1962. In addition, there are four TRIGA Mark II reactors in Indonesia (Bandung, 1965; Yogyakarta, 1979), Malaysia (Kuala Lumpur, 1982), and Vietnam (Dalat, 1960) [60].

The Dalat Nuclear Research Reactor (DNRR), the TRIGA Mark II reactor, was constructed in the early 1960s and operated at a power of 250 kW from 1963 to 1968. It remained inactive from 1968 until March 1975, and by the end of that month, all TRIGA fuels were unloaded and returned to the United States. Reconstruction and upgrading to 500 kW for the DNRR began in 1982, achieving first criticality on November 1, 1983. In February 1984, the nominal power of 500 kW was reached, with the initial working core loaded with 88 VVR-M2 fuel assemblies, including 36% High Enriched Uranium (HEU). In September 2007, the DNRR started to install the first six Low Enriched Uranium (LEU) fuel bundles, which have an enrichment level of 19.75%. By 2009, the DNRR completed the construction of a core mixture of HEU and LEU, consisting of 92 fuel bundles made of HEU and 12 LEU. In December 2011, the DNRR successfully converted the reactor core to use LEU fuel, which included 92 LEU and 12 beryllium rods surrounding a neutron trap at the center of the reactor core. Table 1.1 illustrates the primary parameters of the DNRR [22–24, 61–65].

When the DNRR was upgraded to 500 kW, most of the core structures from the original TRIGA reactor were retained. These components include aluminum tanks, graphite reflectors, thermal columns, horizontal beam tubes, concrete shielding, and other associated structures. The aluminum tank is cylindrical in design, with a height of 6.26 meters and a diameter of 1.98 meters. To enhance cooling efficiency through natural convection, an inner cylindrical extraction well is located within the graphite reflector and positioned directly above the reactor core. A vertical sectional view of the reactor is presented in Figure 1.2 [61, 62, 64].

Table 1.1: Design specifications of the DNRR with LEU fuel.

Parameter	**Value**
Reactor	
Reactor type	Pool type
Fuel type	Russian VVR-M2
Cooling system	Natural convection
Moderator and coolant	Water
Reflector	Graphite, beryllium, and water
Nominal power (kW)	500
Core	
Number of fuel bundles	92
Regulating rod (stainless steel)	1
Shim rod (B_4C)	4
Safety rod (B_4C)	2
Beryllium rod	12
Irradiation channel	4
Fuel	
U-235 enrichment (wt%)	19.75
Number of fuel elements	3
Outermost element (hexagonal)	1
Inner elements (circular)	2
Fuel element thickness (mm)	2.5
Fuel meat thickness (mm)	0.94
Cladding thickness (mm)	0.78
Cladding material	Al
Fuel meat material	UO_2-Al
Coolant channel width (mm)	2.5–3.0
Total length of a fuel bundle (mm)	865
Active fuel length (mm)	600

The reactor core is cylindrical in shape, with a height of 60 cm and a diameter of 44.2 cm. Cooling is achieved through natural convection. The core consists of 92 WWR-M2 type LEU fuel bundles, 12 beryllium rods, a neutron trap located at the center of the core, three irradiation positions within the core, and seven control rods. The control rods include one Automatic Regulating rod (AR), four Shim Rods (ShR), and two Safety Rods (SR). The AR rod is made of stainless steel, whereas the ShR and SR rods are composed of boron carbide (B_4C) [61, 62, 64]. A cross sectional view of the reactor pool tank is shown in Figure 1.3.

The reactor core includes a neutron trap, one wet irradiation channel (1-4), and two dry irradiation channels (7-1 and 13-2). Most radioisotopes are produced in the neutron trap, which provides the highest thermal neutron

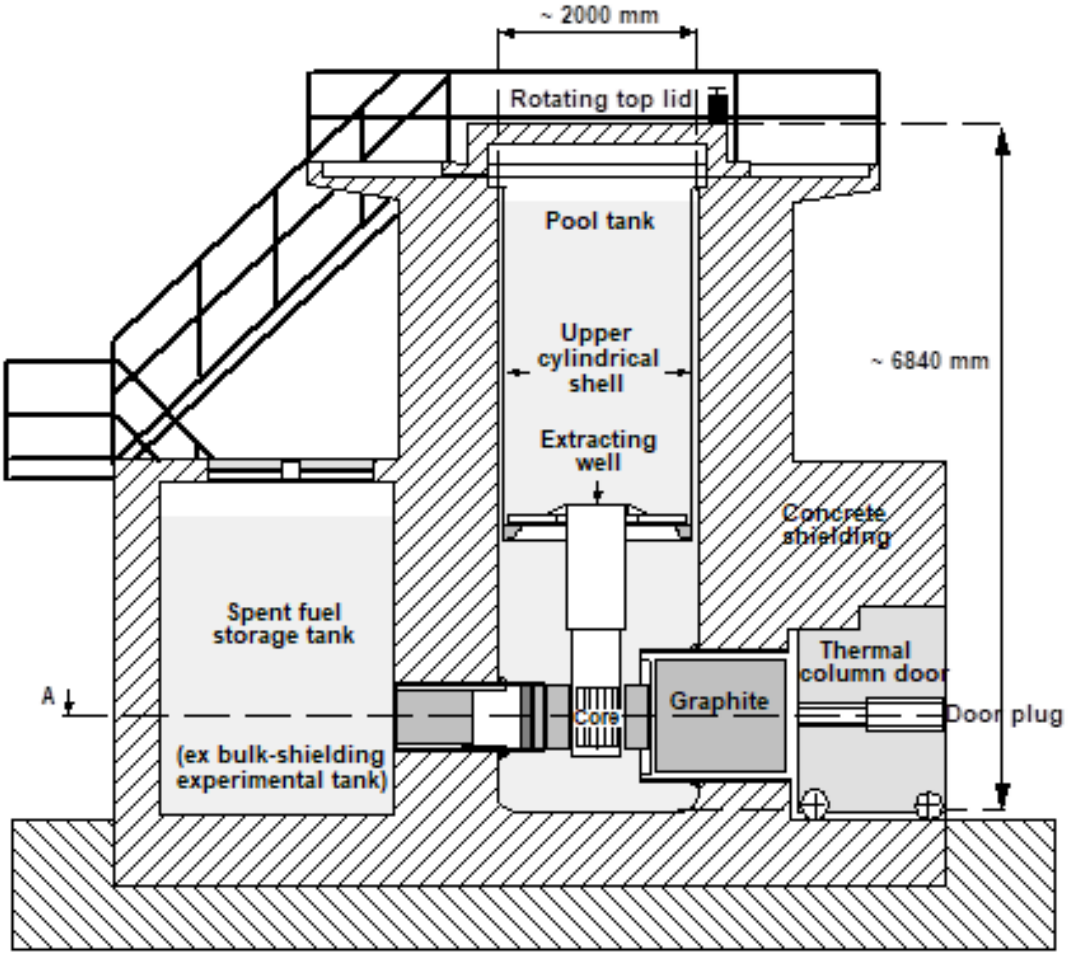

Figure 1.2: Vertical section view of the DNRR.

flux, approximately 2.12×10^{13}(n.cm^{-2}.s^{-1}), and in the wet irradiation channel 1-4, with a thermal neutron flux of approximately 1.07×10^{13}(n.cm^{-2}.s^{-1}). The two pneumatic transfer channels, 7-1 and 13-2, have thermal neutron fluxes of about 4.23×10^{12}(n.cm^{-2}.s^{-1}), and are primarily used for Neutron Activation Analysis (NAA) applications [62–65].

Outside the reactor core, there are a rotary specimen rack, a thermal column, and four beam ports. The rotary specimen rack, used for both Neutron Activation Analysis (NAA) and Radioisotope (RI) production, contains 40 wet irradiation positions with a thermal neutron flux of approximately 4.23×10^{12} (n.cm^{-2}.s^{-1}). The thermal column, with a thermal neutron flux of about 1.25×10^{11} (n.cm^{-2}.s^{-1}), is also employed in NAA applications. The four beam ports, including beam tubes No.1, 2, 3, and 4, serve various purposes such as Nuclear Data Measurement (NDM), Prompt Gamma

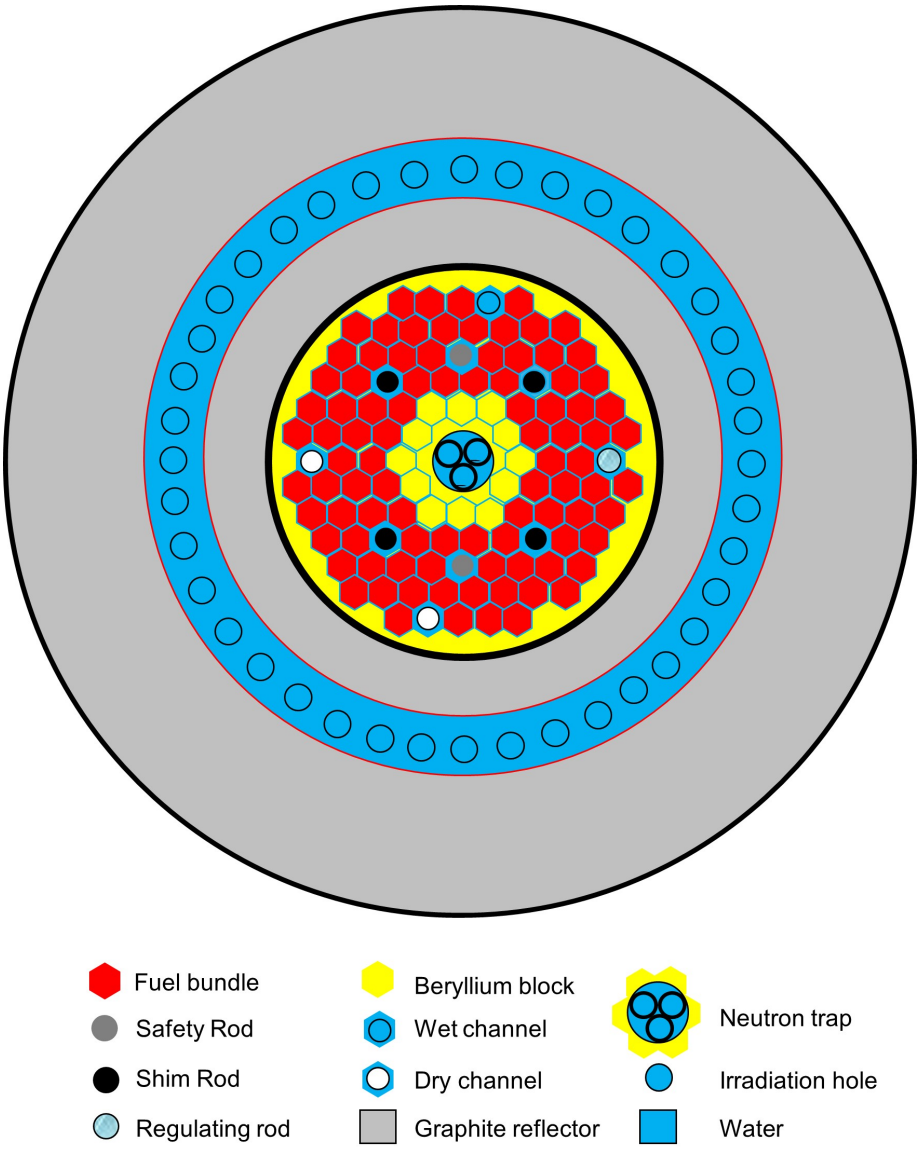

Figure 1.3: Horizontal cross section view of the DNRR pool tank.

Neutron Activation Analysis (PGNAA), Nuclear Physics Studies (NPS), and Research and Training (R&T). The applications of these irradiation facilities are summarized in Table 1.2 [62–64].

Although the DNRR operates at relatively low power and neutron flux, it has made significant contributions to Vietnam's social economic development. The reactor supports a wide range of applications in nuclear engineering and the use of radioactive isotopes across medical, agricultural, industrial, geological, hydrological, and environmental fields. Furthermore,

Table 1.2: Physical characteristics of irradiation facilities in the DNRR.

Irradiation facility –	**Thermal neutron flux** ($n.cm^{-2}.s^{-1}$)	**Applications** –
Inside the reactor core		
Neutron trap	2.12×10^{13}	RI, NAA, R&T
Channel 1-4	1.07×10^{13}	RI, NAA, R&T
Channel 7-1	4.20×10^{12}	NAA, R&T
Channel 13-2	4.40×10^{12}	NAA, R&T
Outside the reactor core		
Rotary specimen	4.23×10^{12}	NAA, RI, R&T
Thermal column	1.25×10^{11}	NAA, R&T
Beam port 1	1.61×10^{6}	R&T, NDM, NAA, PGNAA, NPS, ...
Beam port 2	1.02×10^{6}	R&T, NDM, NAA, PGNAA, NPS, ...
Beam port 3	3.01×10^{5}	R&T, NDM, NAA, NPS, ...
Beam port 4	4.50×10^{5}	R&T, NDM, NAA, NPS, ...

the DNRR's focus on reactor engineering, nuclear physics, and applied research has helped to develop a competent and skilled workforce, while fostering national expertise in these areas [63].

6. Objectives of this Dissertation

The principal objective of this dissertation is to perform comprehensive evaluations of the sensitivity and uncertainty associated with nuclear data used in the analysis of the criticality and kinetic parameters of the Dalat Nuclear Research Reactor (DNRR), which operates with 92 low enriched uranium (LEU) fuel bundles. The study aims to assess how the most recent evaluated nuclear data libraries influence main reactor physics parameters and to quantify their corresponding uncertainties. This work contributes to improving the accuracy and reliability of reactor physics calculations and provides essential feedback for the continuous refinement of evaluated nuclear data.

To achieve these goals, a 3D computational model of the DNRR core was developed using MCNP6. The analyses used four evaluated nuclear data libraries, which are ENDF/B-VIII.0, JEFF-3.3, JENDL-5, and CENDL-3.2, to perform a systematic investigation of their effects on both reactor criticality and kinetic behavior. The study focuses on the major neutronic parameters, including the effective multiplication factor (k_{eff}), effective delayed neutron fraction (β_{eff}), neutron generation time (Λ), and prompt neutron

lifetime (l_p). Through sensitivity and uncertainty (S/U) analysis, the research identifies the dominant isotopes and reaction channels contributing to the overall uncertainty of these parameters, thereby providing a quantitative basis for prioritizing nuclear data improvements.

In addition to the nuclear data evaluation, this work also investigates the influence of operational factors, such as fuel burnup, control rod position, and temperature of fuels on the kinetic parameters of the reactor. By examining the behavior of β_{eff}, Λ, and l_p under different core conditions, the dissertation provides insights into the reactor's dynamic response and contributes to enhancing the safety and efficiency of its operation.

The original contributions of this dissertation, supported by the author's published research, can be summarized as follows:

1. Development of a detailed three dimensional computational model of the DNRR using the MCNP6 code, validated against experimental measurements and benchmarked using the Serpent 2 code.

2. Execution of comprehensive sensitivity and uncertainty analyses for the effective multiplication factor (k_{eff}) and the effective delayed neutron fraction (β_{eff}), focusing on the key isotopes in the fuel, moderator, reflector, and structural materials. These analyses quantify how uncertainties in evaluated nuclear data propagate to reactor responses.

3. Estimation of the kinetic parameters (β_{eff}, Λ, and l_p) using both the adjoint weighted and prompt methods, with additional verification via the $1/v$ absorber insertion approach. Comparisons across nuclear data libraries were performed to evaluate consistency and reliability.

4. Assessment of the sensitivity of kinetic parameters to operating conditions such as fuel burnup, control rod movement, and temperature of fuels variations, providing essential input for the prediction of reactivity feedback and transient behavior.

5. Identification of the major contributors to the uncertainty of both criticality and kinetic parameters, with emphasis on the dominant roles of

the elastic and capture reactions of H-1, U-235, Al-27, Be-9, and B-10. The results offer practical guidance for nuclear data evaluators to refine cross section and covariance datasets in future releases.

The results of this research are expected to enhance the predictive capability of Monte Carlo based reactor simulations, improve the reliability of uncertainty quantification methods, and strengthen the scientific foundation for reactor safety assessments. Furthermore, the findings serve as valuable technical input for the ongoing development of evaluated nuclear data libraries and for the safe and efficient operation of the DNRR and similar research reactors worldwide.

7. Dissertation outline

This thesis is organized into five main sections, along with additional sections that include relevant publications, an appendix, and the reference list.

- **Introduction** establishes the scientific motivation and objectives of the dissertation, emphasizing its contribution to improving the reliability and accuracy of reactor safety and performance assessments.
- **Chapter 1** presents a comprehensive overview of the theoretical and methodological framework underpinning this study. It describes the configuration of the Dalat Nuclear Research Reactor (DNRR), the computational codes and modeling techniques employed, and the evaluated nuclear data libraries utilized in the simulations. Furthermore, it outlines the methodologies used to determine kinetic parameters and the procedures adopted for conducting sensitivity and uncertainty analyses. Particular emphasis is placed on the significance of nuclear data, uncertainty quantification, and sensitivity evaluation in reactor physics, highlighting how variations in nuclear data, operational conditions, manufacturing tolerances, and computational models influence the accuracy and reliability of reactor core simulations. Finally, this chapter establishes the context for subsequent research by defining the dissertation's main objectives.

- **Chapter 2** describes in detail the methods, models, and data used in the study. It begins by explaining the theoretical background of reactor simulations, introducing both deterministic and Monte Carlo methods, and emphasizing the advantages of MCNP6 for detailed three dimensional transport analysis. The configuration and characteristics of the Dalat Nuclear Research Reactor (DNRR) with LEU fuel are then described, including its geometry, control rods, and fuel design. Next, the chapter reviews major evaluated nuclear data libraries (ENDF/B-VIII.0, JEFF-3.3, JENDL-5, and CENDL-3.2) and summarizes the sensitivity and uncertainty (S/U) analysis approach based on perturbation theory and the sandwich rule. Finally, it explains the procedures for calculating kinetic parameters, such as the effective delayed neutron fraction (β_{eff}), neutron generation time (Λ), and prompt neutron lifetime (l_p), using the adjoint weighted and prompt methods, as well as the *1/v* absorber insertion method.

- **Chapter 3** performs comprehensive sensitivity and uncertainty (S/U) analyses of the most recent evaluated nuclear data libraries for the operational core of the DNRR employing LEU fuel. The study systematically investigates the influence of the ENDF/B-VIII.0, JEFF-3.3, JENDL-5, and CENDL-3.2 libraries on reactor criticality and the corresponding S/U characteristics. The results of criticality calculations are presented and validated against experimental measurements to ensure the accuracy and reliability of the computational models. Furthermore, the chapter provides an evaluation of the DNRR kinetic parameters and their associated uncertainties arising from nuclear data. The adjoint weighted and prompt methods were employed to determine the effective delayed neutron fraction (β_{eff}), whereas the prompt neutron lifetime (l_p) was obtained using both the adjoint weighted technique and the *1/v* absorber insertion method. Sensitivity coefficients were derived from first order perturbation theory, and the propagation of nuclear data uncertainties was performed using the linear Sandwich Rule formalism. The analysis also accounts for variations in reactor operating conditions, including

fuel burnup, fuel temperature, and control rod positioning, with evaluations carried out at both the beginning and end of the reactor cycle to compare methodologies and the effects of different nuclear data libraries.

- **Conclusions and future work** summarizes the main findings and conclusions of the study, emphasizes the scientific contributions of the dissertation, and suggests potential directions for future research.

Chapter 2 METHODS AND MODELLING

2.1 Introduction

Simulation calculation is an essential tool in nuclear physics research, particularly in situations where experimental studies are difficult, prohibitively expensive, hazardous, or impractical. Its main applications include nuclear reactor design, nuclear safety analysis, optimization of reactor physical and technical parameters, support for experimental investigations, and the development of new equipment and technologies. Although simulation calculations provide significant advantages, they cannot fully replace experimental research due to inherent uncertainties in the models and nuclear data employed. Therefore, it is crucial to rigorously evaluate these uncertainties to ensure reliable and accurate results. In this context, neutron physics, thermal hydraulic simulation models, and high quality nuclear data are fundamental to comprehensive and credible studies [66].

Computer models in nuclear physics are employed to simulate the three dimensional core structure of nuclear reactors and to solve neutron transport or diffusion equations for the purpose of investigating the physical characteristics of the reactor. Two principal approaches are used in these simulations: deterministic methods and Monte Carlo methods. Each approach offers distinct advantages and limitations, and the choice between them depends on the specific objectives of the study and the computational resources or time available [67].

The Monte Carlo technique is a stochastic statistical method that derives solutions by simulating individual particle histories and recording specific characteristics (tallies) of their average behavior. The results represent solutions to the neutron transport equations. This method offers several advantages, including ease of implementation, accurate representation of complex geometries, direct use of nuclear data libraries with continuous neutron energy spectra, and the capability to perform high precision reactor calculations, typically achieving uncertainties of approximately 300 pcm in $\Delta k/k$ for criticality evaluations [68]. However, the Monte Carlo method also presents certain limitations, notably the substantial computational resources required

and the long calculation times needed to reduce statistical uncertainties to acceptable levels. Prominent Monte Carlo based codes for nuclear reactor physics calculations include MCNP (USA), SERPENT (Finland), MVP/G-MVP (Japan), SCALE (USA), among others [1–3, 67, 69]. This approach is particularly well suited for static problems or scenarios involving slowly varying conditions, and it is commonly employed as a benchmark for validating deterministic models.

The deterministic method solves the neutron diffusion equation using space time discretization and a non continuous neutron energy spectrum, in which neutron energies are divided into multiple groups. By simplifying the geometry typically representing it as lattice cells dividing it into small regions, and applying a mesh to solve the corresponding differential equations, the spatial variables are discretized [2]. The neutron energy spectrum is segmented into discrete groups, each covering a defined energy range with constant properties. Widely used deterministic codes include SRAC (Japan), DRAGON and APOLLO (France), WIMSD (UK), CITATION, OpenMOC (USA), and CASMO (Sweden) [70–73]. This method offers significant advantages in terms of computational efficiency, making it well suited for rapid analyses and fundamental evaluations. Moreover, deterministic approaches can be coupled with thermal hydraulic calculation tools to facilitate the analysis of transient conditions in nuclear facilities [74]. However, a key limitation is that the geometry is idealized (e.g., as lattice cells) rather than modeled in full detail, which may lead to uncertainties associated with material homogenization and an inability to accurately represent complex structural features.

As previously discussed, the nuclear data libraries used in computer codes are fundamental to reactor physics calculations and have a direct impact on the computational results. Nuclear data encompass a wide range of properties, including fission yields, gamma decay energies, decay chains, isotope lifetimes, and cross sections for various interactions with different particles. For example, the ENDF/B-VIII.0 nuclear data library incorporates updated nuclear data standards and offers improved thermal neutron scattering data. In addition, it includes the latest evaluations from the Coordination

International Evaluation Library Organization (CIELO) pilot projects for key neutron reactions involving H-1, O-16, Fe-56, U-235, U-238, and Pu-239 [75]. The construction of these libraries was carried out using the NJOY code, and the S(α, β) thermal scattering data for materials such as beryllium, graphite, and hydrogen in light water were also generated as part of this process [76].

With the continuous efforts of international nuclear data centers, several evaluated nuclear data libraries have been developed to support nuclear reactor analysis, including ENDF/B, JENDL, JEFF, CENDL, BROND, and TENDL. ENDF/B-VIII.0, released in 2018, is the latest version of the ENDF/B library and contains cross section data for 557 nuclides. This version incorporates significant updates for light nuclei, structural materials, actinides, fission energy release, prompt fission neutron spectra, and thermal neutron scattering data [25]. The Japan Atomic Energy Agency (JAEA) released JENDL-5 in 2021, which provides comprehensive evaluated data for 795 nuclides (ranging from Z = 1 to Z = 100) and a thermal scattering sub library for 37 materials, covering nuclear reactions, decays, thermal scatterings, and fission product yields [27]. This represents a substantial enhancement over JENDL-4.0, which included data for 406 nuclides and 15 materials. Similarly, JEFF-3.3, released by the OECD/NEA in 2017, provides evaluated data for 562 nuclides [26]. The latest version of the Chinese Evaluated Nuclear Data Library (CENDL-3.2), issued in 2020, contains cross section data for 240 isotopes [28]. In addition, BROND-3.1, released by Russia in 2016, includes data for 372 nuclides, while the TENDL-2015 library, developed by NRG and CEA and released in 2016, covers data for approximately 2800 isotopes [77]. Ongoing efforts continue to enhance the accuracy and reliability of these nuclear data libraries. To support these developments, sensitivity and uncertainty (S/U) analysis plays a critical role in quantifying the sensitivity profiles of isotopes, reaction cross sections, and energy groups, as well as evaluating the uncertainties in computational results [14]. The present study aims to assess the impact of the latest nuclear data libraries, namely ENDF/B-VIII.0, JEFF-3.3, JENDL-5, and CENDL-3.2, on the criticality

and S/U analysis of the Dalat Nuclear Research Reactor (DNRR) with low enriched uranium (LEU) fuel.

The kinetic parameters of a research reactor, such as the β_{eff}, Λ, and l_p, are critical characteristics associated with reactor safety, kinetics, and transient analysis [10, 78–84]. Delayed neutrons are produced in the reactor core through the decay of radionuclides formed as fission products. For example, neutrons are emitted during the beta decay of isotopes such as iodine and bromine. The temporal delay of these neutrons depends on the lifetimes of the corresponding fission products. Although delayed neutrons constitute less than 1% of the total neutron population, they play a vital role in defining the safety related characteristics of the reactor core [10, 16, 84, 85]. Kinetic parameters are influenced by factors such as fuel burnup, fuel type, core configuration, and operational conditions [10, 80, 85]. Therefore, the precise evaluation of these parameters is essential for enhancing reactor safety and ensuring effective operation.

In this study, the β_{eff} was evaluated using two approaches: the adjoint weighted method and the prompt method. The l_p was calculated using the adjoint weighted method and the $1/v$ absorber insertion method. The Λ was determined using the adjoint weighted method. The adjoint weighted method, based on perturbation theory and adjoint flux, offers high fidelity evaluations. In contrast, the prompt method relies on the ratio of prompt to total fission neutrons, and the $1/v$ absorber insertion method assumes a linear relationship between reactivity and a small, uniformly inserted B 10 content. While the adjoint weighted method provides a rigorous assessment, the prompt method and the $1/v$ absorber insertion method serve as comparative baselines.

2.2 The Dalat nuclear research reactor with low enriched uranium fuel

2.2.1 *The reactor core*

The reactor core of the Dalat Nuclear Research Reactor (DNRR) is housed within an aluminum cylindrical tank with a height of 60 cm and a

diameter of 44.2 cm. The reactor core comprises vertically arranged fuel assemblies, beryllium blocks, control rod guide tubes, irradiation channels, and other structural components. These elements are secured by two perforated plates, known as grid plates, located at the bottom of the core. The grid plates contain 121 holes arranged in a hexagonal lattice pattern, where each cell has a hexagonal cross section with a width of 35 mm across its parallel sides. Among these, 114 hexagonal cells are available for positioning fuel assemblies, beryllium blocks, or irradiation channels. The remaining seven cells are specifically designated for control rod guide tubes, which have an inner diameter of 33 mm. All control rod guide tubes are wet type designs, featuring perforations at their lower sections to enhance coolant circulation and facilitate water expulsion during rapid rod insertion. The reactor core is supported by a structural frame and is positioned approximately 60 cm above the bottom of the aluminum tank. The configuration of the DNRR core with 92 low enriched uranium (LEU) fuel assemblies is illustrated in Figure 2.1 [20, 21, 61, 62, 64, 86].

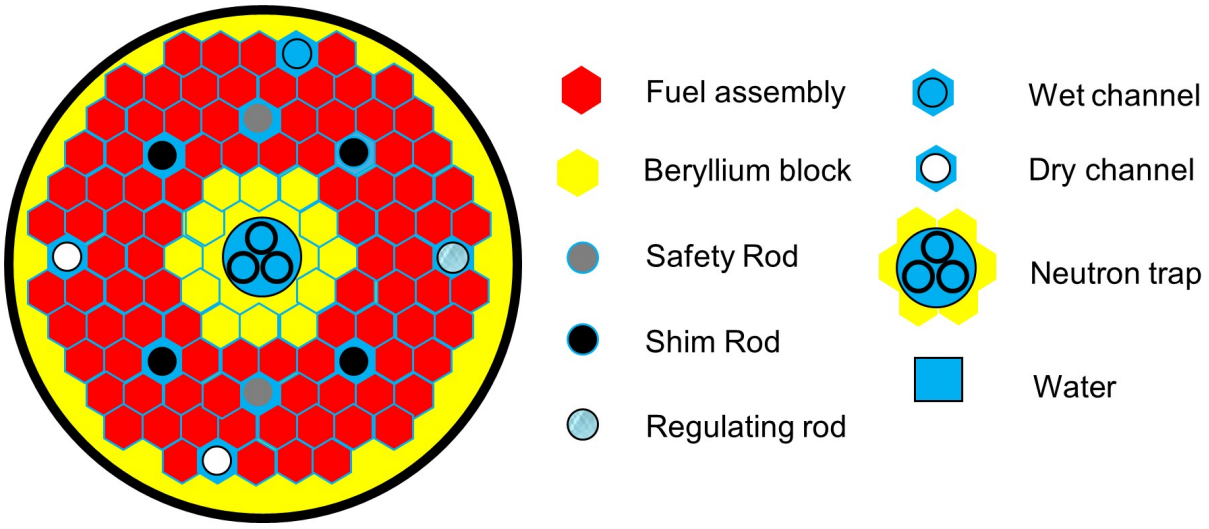

Figure 2.1: Configuration of the reactor core with 92 LEU fuel bundles.

The reactor core is configured with 92 LEU fuel assemblies containing 19.75% enriched uranium, three irradiation channels (including two dry channels and one wet channel), 12 beryllium rods that function as surrounding

neutron traps, and an additional neutron trap incorporating three wet channels. The fuel assemblies are VVR-M2 tubular fuel elements manufactured in Russia. Each assembly consists of three coaxial annular fuel tubes, along with a header and a tail section. The outermost fuel tube has a hexagonal cross section with a width of 32 mm across its parallel sides, while the two inner tubes are circular with outer diameters of 22 mm and 11 mm, respectively. The beryllium rods also feature a hexagonal cross-section, measuring 32 mm across the parallel sides [62].

Several vertical irradiation facilities are incorporated within the reactor core. The central region of the core comprises 12 cells designed to accommodate 12 beryllium blocks arranged around a hollow space filled with water, forming the central neutron trap. Additionally, multiple cells located at the periphery of the core are designated for both wet and dry irradiation channels. Currently, cell 1-4 functions as a wet irradiation channel, while cells 7-1 and 13-2 are utilized as pneumatic (dry) irradiation channels [62, 63, 65].

2.2.2 *The fuel bundles*

The LEU fuel bundles employed in the reactor core are of the VVR-M2 type, manufactured in Russia. The VVR-M2 design consists of several coaxial fuel rods (fuel elements). The outermost fuel element has a hexagonal cross section, measuring 32 mm across its parallel sides, while the two inner fuel elements are circular with outer diameters of 22 mm and 11 mm, respectively. Each fuel element comprises three layers: the fuel meat, made of a UO_2-Al dispersion containing 49.7 g of uranium enriched to 19.75%, has a thickness of 0.94 mm; this is surrounded by two layers of aluminum alloy cladding with a total thickness of 0.78 mm. The fuel rod design includes two cooling channels utilizing light water for neutron moderation and heat removal, as well as two cladding layers enclosing the central fuel meat. Water flows through a gap of 2.5–3 mm between the fuel elements to enhance cooling efficiency. The total length of the fuel assembly is 865 mm, with an active fuel length of 600 mm, while the remaining non fuel structural components are made of aluminum alloy. The design specifications of the VVR-M2 LEU fuel bundle are illustrated in Figure 2.2 [62].

Table 2.1: Design parameters of the VVR-M2 LEU fuel bundle.

Parameter	**Value**
Number of fuel tubes	3
Hexagonal tube	1
Cylindrical tube	2
Length of fuel bundle (mm)	
Total length	865
Fuel length (active height)	600
Fuel and cladding	
Cladding material	Al
Fuel meat thickness (mm)	0.94
Cladding thickness (mm)	0.78
Fuel material	UO_2-Al
Total U-235 mass (g)	49.7
U-235 enrichment (wt%)	19.75
Fuel composition (wt%)	
U-234	0.14
U-235	12.60
U-238	22.26
Al-27	65.00

The head of the fuel bundle, which is slightly wider than the outermost fuel element at 35 mm across its parallel sides but retains a hexagonal shape, connects the outermost fuel element to the fuel assembly structure. This design allows adjacent fuel assemblies to provide mutual support at the top of the core through the contact of their header edges. The fuel head is equipped with six holes to facilitate water flow between the fuel tubes and to allow the release of water from the assembly. Additionally, the upper part of the header is designed to accommodate a specialized handling tool for fuel assembly manipulation. At the bottom of the core, the fuel assemblies are secured by inserting their tail sections into openings on two grid plates. The Russian VVR-M2 type LEU fuel bundle, including its cross sectional views and dimensional specifications, is illustrated in Figure 2.2 [62].

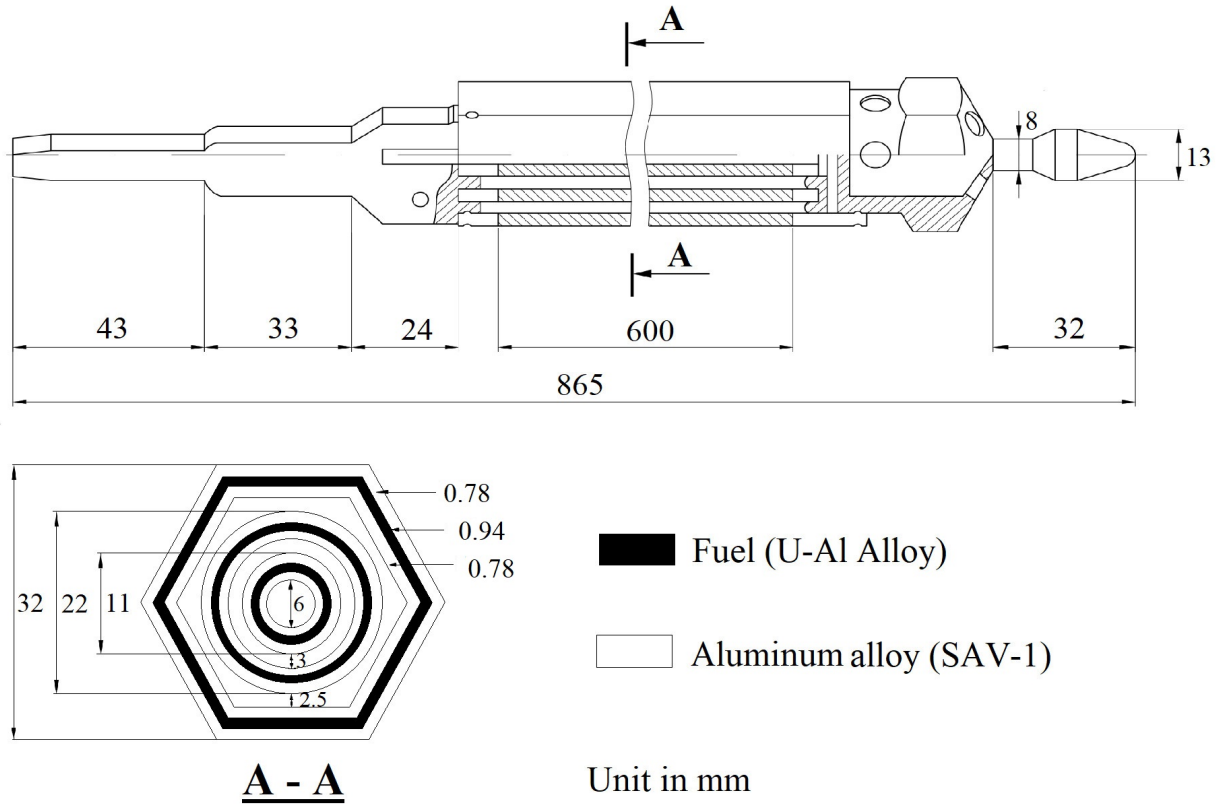

Figure 2.2: Cross sectional views and dimensional parameters of the Russian VVR-M2 type LEU fuel bundle.

2.2.3 *Control rods*

The reactor control and protection system comprises seven control rods symmetrically positioned within the reactor core. These include two safety rods (SR), four shim rods (ShR), and one automated regulator rod (AR). The AR rod is fabricated from stainless steel, whereas the ShR and SR rods are constructed from boron carbide (B_4C) with a density of 1.7 g/cm^3. Each rod has an absorption length of 650 mm, sufficient to cover the entire active core height. The control rods have an outer diameter of 27 mm, which includes both the absorbent material and the stainless steel cladding. All control rods operate within wet channels, and their guide tubes are made of aluminum. The configuration and design of the DNRR control rods are depicted in Figure 2.3 [23, 62].

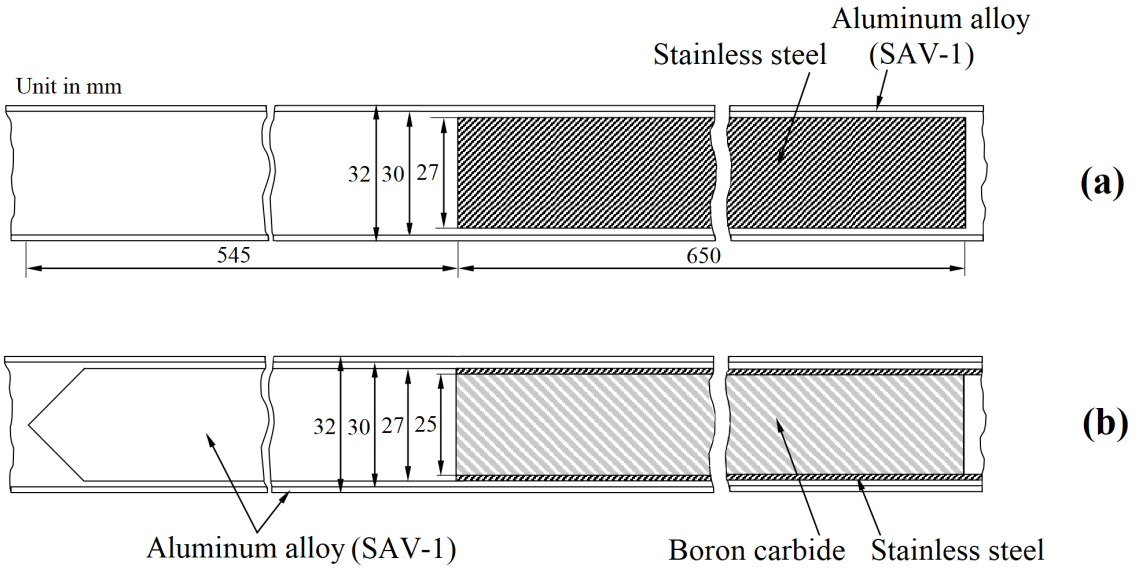

Figure 2.3: The control rods of the DNRR.

Both SR can be rapidly inserted into the reactor core, with each rod independently capable of terminating the fission chain reaction and shutting down the reactor. The four ShR are designed to compensate for the reactor's excess reactivity and also contribute to reactor shutdown. When partially withdrawn, the ShR can be freely dropped into the core, providing greater negative reactivity than the SR and ensuring that the reactor reaches a deeply subcritical state upon shutdown. The maximum withdrawal speed of either a SR or ShR is 3.4 mm/s. The AR is responsible for controlling the reactor power during automatic operation, with a maximum withdrawal speed of 20 mm/s. In emergency conditions, all SR and ShR are designed to be fully inserted into the reactor core within one second [62].

2.3 Code and reactor model

2.3.1 *MCNP6 code*

The MCNP6 code (Monte Carlo N-Particle) is a general purpose, continuous energy, generalized geometry, and time dependent Monte Carlo code capable of simulating the transport of 37 different particle types across a wide range of energies. Its applications include criticality analysis, shielding design, dosimetry, detector response modeling, and other areas of reactor

and radiation physics. The origin of MCNP dates back to 1977, when various Monte Carlo codes developed for specific applications were integrated to form the first generic Monte Carlo particle transport code. Since then, MCNP has evolved into a comprehensive and versatile tool, serving as a significant repository of physics knowledge and computational expertise. To perform a simulation, the user prepares an input file specifying the problem definition, including geometry, material compositions, selected cross section data, source characteristics, desired tallies or outputs, and any variance reduction techniques employed to enhance computational efficiency [67].

The Monte Carlo method and the deterministic transport method represent fundamentally different approaches to solving neutron transport problems. The discrete ordinates method, as a deterministic technique, solves the transport equations to determine the average behavior of particles within the system. In contrast, the Monte Carlo method derives solutions by simulating individual particle histories and recording specific characteristics of their collective behavior. Beyond these differing methodologies, the two approaches also differ conceptually in defining what constitutes a solution. It is often stated that the Monte Carlo method solves the integral form of the transport equation, whereas the discrete ordinates method addresses the integral differential form. However, this distinction is somewhat misleading for two reasons. First, the integral and integral differential transport equations are mathematically equivalent, and solving one inherently satisfies the other. Second, the Monte Carlo method does not require explicit formulation of the transport equation to solve a given problem; instead, it effectively addresses transport phenomena by tracking particle histories through stochastic simulation. Nevertheless, it is possible to construct a probability equation that describes particle scattering in phase space, which corresponds precisely to the integral form of the transport equation [67].

The Monte Carlo method is particularly well suited for addressing complex, three dimensional, and time dependent problems in neutron and particle transport. Unlike deterministic approaches, it does not require the introduction of phase space regions or the use of average approximations in

space, energy, or time. Instead, the method relies on an accurate and detailed representation of the physical data for each element of the problem. Monte Carlo simulations model stochastic transport processes, including the interactions between nuclear particles and materials, making the method especially valuable for analyzing complex scenarios that deterministic algorithms may be unable to characterize effectively. The method simulates the sequence of individual probabilistic events that define a particle's history from birth to termination, and these histories can also be generated in parallel to improve computational efficiency. The probability distributions governing these events are sampled statistically, thereby providing a comprehensive representation of the underlying physical phenomena [67].

Monte Carlo simulations are typically performed on computers due to the large number of iterations required to accurately represent stochastic events. The statistical sampling technique employed by the method is based on the random selection of numbers, analogous to games of chance in a casino, which is the origin of the term "Monte Carlo." The Monte Carlo method is recognized for its high accuracy and is widely used in particle transport simulations for conducting numerical experiments. The approach involves carefully tracking the trajectories of numerous particles from their points of origin until their final outcomes, such as absorption or escape from the system. Throughout this process, probability distributions are sampled stochastically, using nuclear data to determine the outcomes at each stage of a particle's lifetime [67].

The MCNP code models neutrons and photons as particles that travel in straight line paths between successive collisions. Figure 2.4 illustrates the random trajectory of a neutron interacting with a solid material capable of undergoing nuclear fission. Random numbers uniformly distributed between 0 and 1 are sampled to determine the occurrence, location, and timing of interactions, governed by the underlying physics principles and probabilities derived from nuclear data. In the example depicted, the first event involves a neutron collision with the solid material. In the second event, nuclear fission takes place, resulting in the termination of the incident neutron and

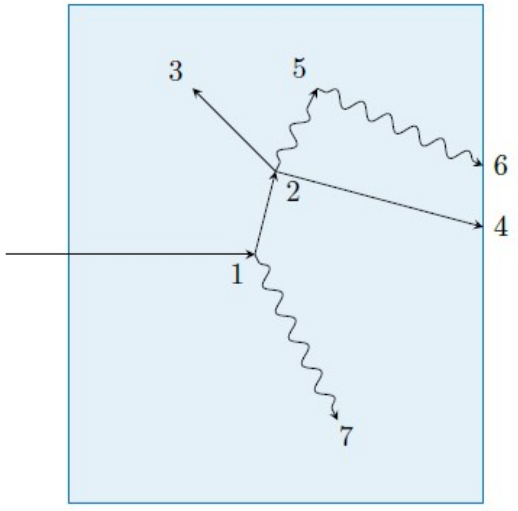

Event Record:
1: Scattering of neutrons and production of photons.
2: Fission and production of photons.
3: Capture of neutrons.
4: Leakage of neutrons.
5: Scattering of photons.
6: Leakage of photons.
7: Capture of photons.
The zigzag lines are used to show the trajectory of photons or neutrons. However, the MCNP code simplifies photon and neutron travel as a straight line between collision events.

Figure 2.4: The random walks of the different particles [67].

the production of two neutrons and a photon. One of these neutrons and the photon are retained for subsequent tracking. During the third event, the primary fission neutron is captured and terminated. The previously stored neutron is then released and, in the fourth event, exits the material through a randomly determined path. The photon generated from fission undergoes a collision at the fifth event but escapes the material during the sixth event. Finally, in the seventh event, photons remaining from the initial interaction are captured. It is noteworthy that MCNP manages the particle bank using a last in, first out (LIFO) protocol, where the most recently stored particle is the first to be processed. Upon completion of a particle history, further event simulations progressively refine the understanding of neutron and photon distributions, enabling the calculation of desired quantities along with their associated statistical uncertainties [67].

The processed data from nuclear data evaluations are formatted for use in the MCNP code through tools such as NJOY, which generate ACE formatted nuclear data libraries [76]. Various nuclear data tables are available to describe different types of interactions involving neutrons, including neutron induced photon production, photon interactions, neutron dosimetry or activation, and thermal particle scattering represented by $S(\alpha, \beta)$ data. For example, the thermal scattering library based on ENDF/B-VIII.0 includes data for 34 materials and encompasses 253 evaluations [87]. Photon

interaction tables are available for all elements with atomic numbers from 1 to 100. The MCNP code is capable of modeling processes such as elastic and inelastic scattering, photoelectric absorption, pair production, and fluorescence emission. Scattering angular distributions are refined using atomic form factors and incoherent scattering functions. Additionally, the MCNP database contains cross section data for approximately 2000 dosimetry and activation reactions, covering more than 400 target nuclei in both ground and excited states. These cross sections can be employed as energy dependent response functions for calculating reaction rates but are not suitable for use as transport cross sections in neutron transport simulations [67].

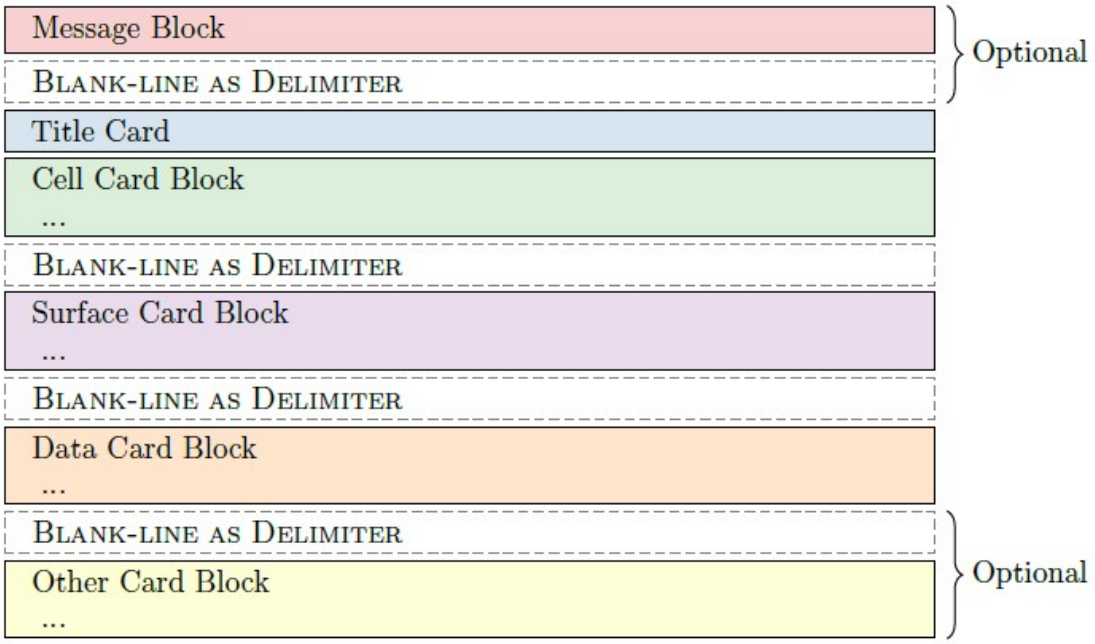

Figure 2.5: The format of the MCNP6 input file [67].

The MCNP6 represents not only a simple and precise integration of the functionalities of MCNP5 and MCNPX, but also a significant advancement beyond the combined capabilities of these two codes. It is the first version to implement adjoint weighted tallies for perturbation theory in continuous energy Monte Carlo simulations. The use of adjoint weighted tallies in MCNP6 requires the application of integrated fission probabilities, a technique previously employed in MCNP5 for the calculation of adjoint weighted reactor kinetics parameters. MCNP6 also enables the computation of sensitivity coefficients for the multiplication factor (k) with respect to specific

cross sections. The input structure of MCNP6 consists of three required blocks and an optional block, as illustrated in Figure 2.5. Each block is separated by a single empty line, which may also serve as an optional end of input indicator. It is essential to avoid including additional empty lines between blocks, as this may cause the input to be ignored and lead to confusing or fatal errors during execution [67].

2.3.2 *The reactor model*

MCNP6 employs an accurate geometric modeling framework capable of representing arbitrary three dimensional configurations of user defined materials within geometric cells. These cells are defined by the intersection, combination, or exclusion of regions bounded by surfaces, with Boolean operators used to combine fundamental geometric shapes such as spheres, boxes, and cylinders. This capability enables detailed and precise modeling of complex systems, including nuclear reactors such as the DNRR. By specifying geometric cells with high accuracy, users can achieve precise neutron transport simulations. Furthermore, MCNP6 incorporates advanced features, including variance reduction techniques and parallel processing, which enhance computational efficiency. These capabilities make MCNP6 a powerful and versatile tool for investigating neutron behavior across a wide range of applications in nuclear science and engineering [67].

The DNRR comprises numerous complex components that can be simulated with high accuracy using MCNP6. A critical aspect in modeling the DNRR with MCNP6 is the precise representation of both material compositions and geometric configurations. The DNRR model includes a water tank, 92 fuel assemblies, four control rods, two safety rods, one regulating rod, two irradiation channels (one wet and one dry), 12 beryllium rods surrounding the neutron trap, a rotary specimen rack containing 40 wet irradiation channels, a graphite reflector, four horizontal neutron beam ports, a thermal column, and other structural features. Detailed descriptions of the DNRR structures are provided in Section 2.2.1. Figures 2.6 and 2.7 illustrate the vertical and horizontal cross sectional views of the DNRR model generated using MCNP6.

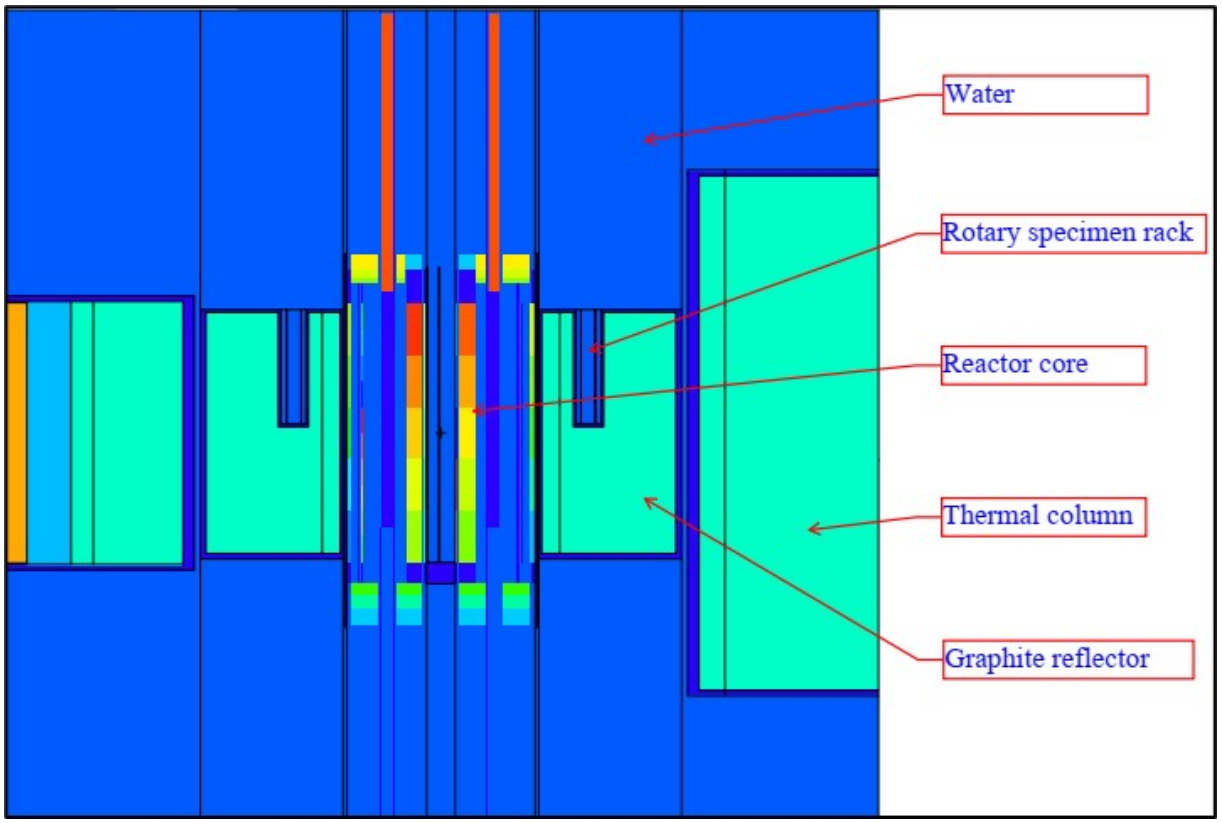

Figure 2.6: The vertical views of the DNRR model using the MCNP6.

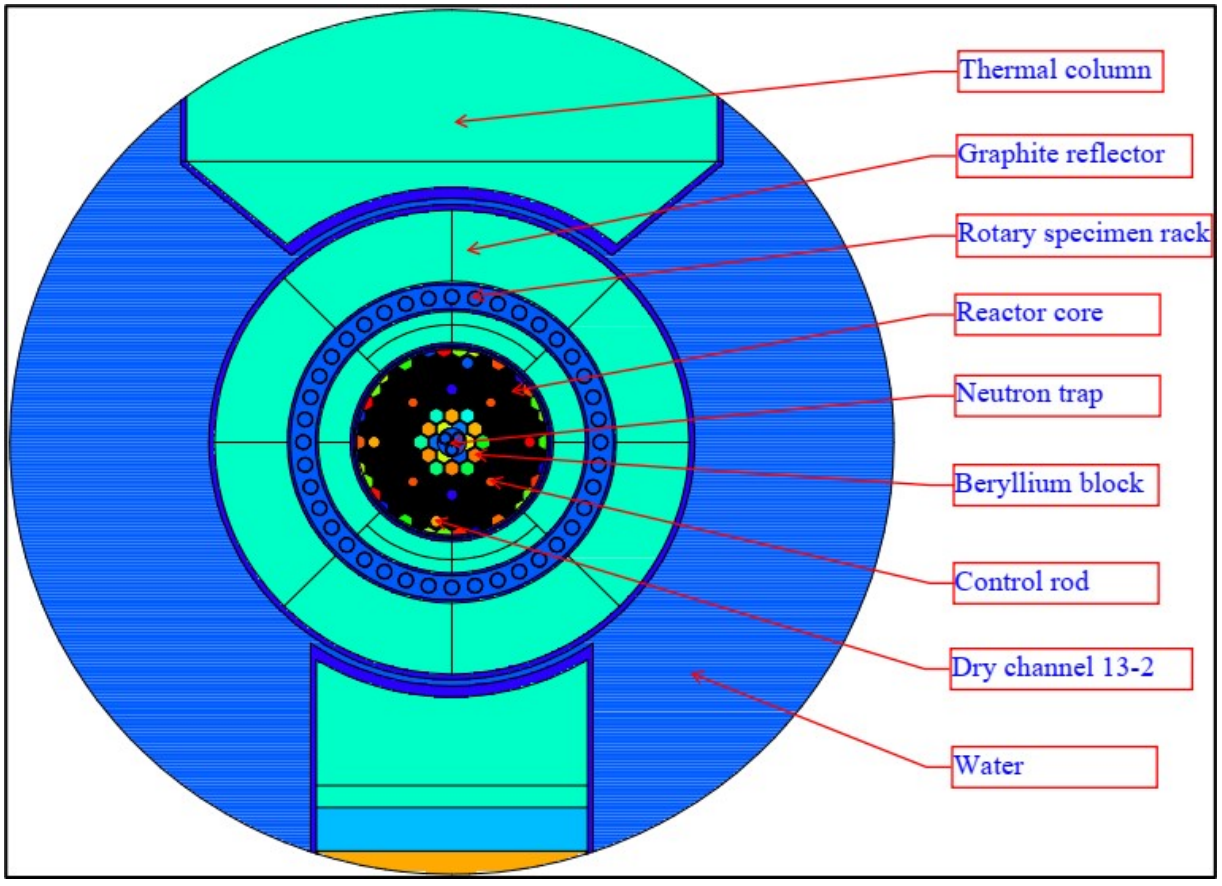

Figure 2.7: The horizontal views of the DNRR model using the MCNP6.

The DNRR model, comprising both the water tank and reactor core, has an approximate diameter of 200 cm and a height of 185 cm.

Accurate definition of all core components in the MCNP6 model is essential for reliable simulation of the DNRR behavior. To simplify calculations and enhance model quality while preserving the core's neutronic characteristics, homogenization was applied at the top and bottom regions of certain components, including the fuel assemblies, beryllium rods, and both dry and wet irradiation channels [22–24]. This homogenization process reduces geometric complexity without compromising the accuracy of material properties. According to Chu et al. (2024) [23], the difference in the calculated effective multiplication factor (k_{eff}) between the homogenized and non homogenized models was less than 20 pcm, indicating negligible impact on criticality results. The effect of beryllium poisoning in the reactor core was included in the reactor model. The MCNP6 simulations were performed using 500 active cycles following 50 inactive cycles, with each cycle tracking 10^6 neutron histories, to ensure that the statistical uncertainty of k_{eff} remained below six pcm [67].

2.4 Nuclear data libraries

2.4.1 *Evaluated Nuclear Data File (ENDF)*

The Evaluated Nuclear Data File (ENDF) format for nuclear data libraries was introduced at the CSEWG meeting in 1966 to provide a standardized database intended for reactor physics calculations [88]. A nuclear data library is a compilation of evaluated data prepared by accredited organizations and structured to support various applications, including reactor design and analysis. The ENDF format libraries consist of collections of nuclear data evaluations organized in a standardized format to facilitate consistent use in nuclear data processing codes. In addition to establishing a common basis for all nuclear data evaluations, the development of an evaluated nuclear data file was essential for performing accurate reactor design calculations. This system, referred to as ENDF/B (with "B" designating the version series), has undergone multiple revisions. Table 2.2 provides a concise summary of the major ENDF versions released to date, along with

information on their formats, evaluation methodologies, and associated documentation [88, 89].

The ENDF/B library provides comprehensive nuclear data essential for a wide range of applications in reactor physics and nuclear engineering. It includes neutron cross sections and distributions, photon production from neutron interactions, limited data on charged particle production from neutron reactions, photo atomic interaction data, thermal neutron scattering information, and radionuclide production and decay data. The library offers complete evaluations for numerous materials, ensuring the accuracy and reliability of nuclear data used in criticality safety assessments and neutron transport simulations. This detailed dataset enables precise modeling and prediction of nuclear reactions, thereby supporting the design and analysis of nuclear systems. As a result, the ENDF/B library serves as an invaluable resource for researchers and engineers involved in nuclear projects requiring dependable data for criticality safety evaluations.

Table 2.2: Overview of ENDF versions and formats.

Library version	**Release year**	**Format**
ENDF/B-I	July 1968	ENDF-1 format [90]
ENDF/B-II	Aug. 1970	ENDF-2 format [91, 92]
ENDF/B-III	late 1972	ENDF-3 format [91, 92]
ENDF/B-IV	Feb. 1975	ENDF-4 format [93]
ENDF/B-V.0	July 1979	ENDF-5 format [94]
ENDF/B-V.1	1983	ENDF-5 format [94]
ENDF/B-V.2	Jan. 1985	ENDF-5 format [94]
ENDF/B-VI.0	July 1990	ENDF-6 format, 1990 revision [95]
ENDF/B-VI.1	Sep. 1991	ENDF-6 format, 1991 revision [95]
ENDF/B-VI.2	June 1993	ENDF-6 format, 1991 revision [95]
ENDF/B-VI.3	May 1995	ENDF-6 format, 1993 revision [95]
ENDF/B-VI.4	Dec. 1996	ENDF-6 format, 1993 revision [95]
ENDF/B-VI.5	1997–1998	ENDF-6 format, 1997 revision [95]
ENDF/B-VI.6	1998–1999	ENDF-6 format, 1997 revision [95]
ENDF/B-VI.7	1999–2000	ENDF-6 format, 1997 revision [95]
ENDF/B-VI.8	2001	ENDF-6 format, 2001 revision [95]
ENDF/B-VII.0	Dec. 2006	ENDF-6 format, 2009 revision [96]
ENDF/B-VII.1	Dec. 2011	ENDF-6 format, 2011 revision [96]
ENDF/B-VIII.0	Dec. 2017	ENDF-6 format, 2017 revision [25]

In addition to core neutron data, the library contains decay data, fission product yields, and thermal scattering law information, making it a

versatile tool for diverse applications in nuclear engineering. Access to the ENDF/B library is provided through various software packages and data processing tools, facilitating detailed simulations and analyses. The data within the library undergo rigorous evaluation and validation and are only modified or replaced when necessary to reflect improvements in nuclear data standards or evaluations [88, 89].

With support from the United States and the global nuclear research community, the Cross Section Evaluation Working Group (CSEWG), which oversees the ENDF library project, has released the updated ENDF/B-VIII.0 library. The library is available in both the traditional ENDF-6 format and the more recent Generalized Nuclear Database Structure (GNDS) format, providing flexible access to its extensive collection of evaluated data. Enhancements in ENDF/B-VIII.0 include updated data for neutron reactions involving metals, actinides, structural materials, light nuclei, and dosimetry cross sections, as well as improvements in fission energy release data, decay data, charged particle interactions, and thermal neutron scattering information. These advancements are designed to improve the modeling of neutron interactions with materials, particularly for low energy neutron reactions in molecular systems [25].

2.4.2 *Joint Evaluated Fission and Fusion Nuclear Data Library (JEFF)*

The OECD Nuclear Energy Agency (NEA) was established on February 1, 1958, originally under the name European Nuclear Energy Agency within the framework of the Organisation for European Economic Cooperation (OEEC). Today, the NEA operates as part of the OECD and comprises 34 member countries. These include Australia, Austria, Belgium, Bulgaria, Canada, the Czech Republic, Denmark, Estonia, Finland, France, Germany, Greece, Hungary, Iceland, Ireland, Italy, Lithuania, Luxembourg, Mexico, the Netherlands, Norway, Poland, Portugal, Romania, the Slovak Republic, Slovenia, Spain, Sweden, Switzerland, Turkey, the United Kingdom, and two

non-European OECD members: the United States and Japan. The development of the JEFF project under the auspices of the NEA is illustrated in Figure 2.8 [37].

The primary objective of the Joint Evaluated Fission and Fusion (JEFF) Project is to develop a comprehensive reference nuclear data library through collaborative efforts among the member countries of the OECD Nuclear Energy Agency (NEA) Data Bank. The JEFF Nuclear Data Library represents the outcome of contributions from the 34 OECD member countries participating in the NEA Data Bank. The project integrates the work of multiple specialized working groups across various scientific disciplines to produce thoroughly reviewed nuclear data sets applicable to both fission (JEF and JEFF libraries) and fusion (EFF libraries) applications. For fission related applications, the JEFF library provides a wide range of data types, including neutron and proton interaction cross sections, radioactive decay data, fission yield data, thermal scattering law data, and photo atomic interaction data.

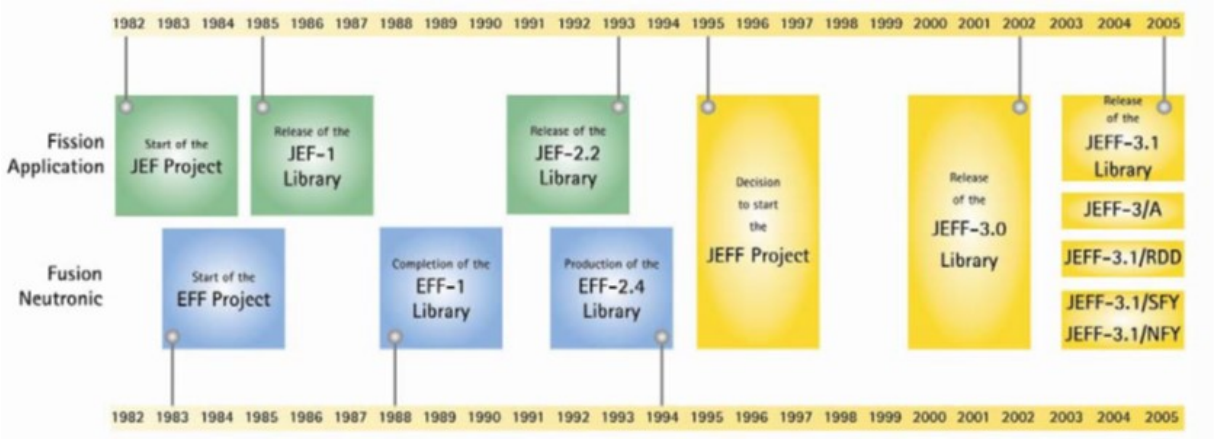

Figure 2.8: The progression of the JEFF project [37]

The release of the JEFF-3.3 library in 2017 represented a significant update and expansion of previous versions. This library includes evaluated data for neutrons, protons, deuterons, tritons, helions, alpha particles, radioactive decay, fission yields, neutron activation, and thermal neutron scattering for 20 different compounds. Additionally, it includes specialized sublibraries for incident alpha particles, deuterons, gamma rays, helium-3,

protons, and tritons, all formatted in the ENDF structure, similar to the ENDF/B-VIII.0 library. JEFF-3.3 serves as a versatile resource applicable to a wide range of nuclear technology fields, encompassing both energy and nonenergy sectors. The primary objective of this library is to enhance the accuracy of nuclear data for neutron transport calculations. These calculations are essential for the design, performance evaluation, and safety analysis of power and research reactors, as well as for criticality safety assessments of spent nuclear fuel, nuclear safeguards, nuclear security, and fundamental scientific research [26].

2.4.3 *Japanese Evaluated Nuclear Data Library (JENDL)*

The first version of the Japanese Evaluated Nuclear Data Library (JENDL), JENDL-1, was released to the public in 1977. This initial version contained neutron induced reaction cross sections for 72 nuclides, primarily intended for applications in Fast Breeder Reactor (FBR) systems [97]. Since its introduction, the JENDL library has undergone numerous revisions to meet the evolving requirements of fast reactors, thermal reactors, Light Water Reactor (LWR), fusion reactors, and neutron shielding applications [98]. The latest edition, JENDL-5, released in 2021, features substantial updates to the data for minor actinides and fission products. Furthermore, this version includes significantly expanded covariance data for actinides, enhancing its suitability for neutronic calculations in fission reactor analyses compared to earlier versions [27]. The characteristics of the JENDL nuclear data library are summarized in Table 2.3 [27, 36, 97–100].

JENDL-5 incorporates several special purpose data files to enhance its applicability in diverse nuclear analyses. These include activation cross sections, high energy dosimetry data, fission product yields, and photonuclear reaction data. Significant improvements have also been made in the thermal scattering law data, alongside extensions in the upper energy limits, the range of reaction types, target nuclides, and covariance information. The structure of JENDL-5 comprises 11 sublibraries, which collectively provide comprehensive nuclear data. These sublibraries cover neutrons, thermal scattering laws, fission product yields, decay data, protons, deuterons, alpha

Table 2.3: Characteristics of the JENDL nuclear data library.

Library version	**Release year**	**Application**	**Nuclide**[a]	γ **-production**[b]	**Covariance**[c]	**DDX**[d]
JENDL-1	1977	FBR	72	0	0	0
JENDL-2	1982	FBR, LWR	181	0	0	0
JENDL-3.0	1989	General	171	59	1	0
JENDL-3.1	1990	General	324	59	1	0
JENDL-3.2	1994	General	332	66	1	0
JENDL-3.3	2002	General	337	114	20	60
JENDL-4.0	2010	General	406	354	95	318
JENDL-5	2021	General	795	794	105	337

[a] Number of isotopes and natural elements.
[b] Number of nuclides containing secondary γ-ray production data.
[c] Number of nuclides containing covariances.
[d] Number of nuclides containing double-differential cross sections $d^2\sigma/dE/d\omega$.

particles, photonuclear data, photon atomic data, electron atomic data, and atomic relaxation data [27].

2.4.4 *Chinese Evaluated Nuclear Data Library (CENDL)*

Since the 1970s, the development of the Chinese Evaluated Nuclear Data Library (CENDL) has been a collaborative effort between the China Nuclear Data Center (CNDC) and the Chinese Nuclear Data Cooperation Network (CNDCN). This initiative, referred to as the CENDL project, has progressed through the active engagement of the CENDL working group, combining resources and expertise in both experimental measurements and nuclear data evaluations. As a result of these sustained efforts, several major versions of the CENDL library have been released: CENDL-1.0 in 1985 [101, 102], CENDL-2.0 in 1993 [101, 102], CENDL-3.0 in 2000 [103], CENDL-3.1 in 2009 [104], and the most recent CENDL-3.2 in 2020 [28]. These versions were primarily developed to provide evaluated neutron reaction data covering a broad range of nuclides, from light elements to heavy nuclei. The overall structure and content of the CENDL nuclear data library are summarized in Table 2.4 [28].

In the most recent phase of the CENDL project, significant advancements have been made in nuclear reaction modeling, experimental measurement techniques, data evaluation methodologies, visualization systems for data assessment, and benchmark testing tools. These developments have

contributed to enhancing the quality and reliability of the newly evaluated nuclear data. As a result of these efforts, a new neutron data library, CENDL-3.2, has been produced. This latest version encompasses evaluated data for 272 nuclides, representing a substantial expansion compared to the 37 nuclides included in the initial CENDL-1.0 release. The construction of CENDL-3.2 was aimed at providing high precision and comprehensive nuclear data to support modern applications in nuclear science, engineering, technology, and other related fields [28].

Table 2.4: Summary of the CENDL nuclear data library versions.

Library version	**Release year**	**Application**	**Nuclide**	**Format**
CENDL-1.0	1985	General	36	ENDF-5
CENDL-2.0	1993	General	54	ENDF-6
CENDL-3.0	2000	General	200	ENDF-6
CENDL-3.1	2009	General	200	ENDF-6
CENDL-3.2	2020	General	272	ENDF-6

2.5 Methods for sensitivity/uncertainty analysis

2.5.1 *Sensitivity/uncertainty theory*

A first order perturbation theory based method can propagate uncertainty in the reaction cross sections to the full core calculation by simulating the core of a reactor. Uncertainties are transmitted from the input parameter covariance data to the responses of interest via the sandwich rule, which necessitates calculating sensitivity coefficients. This process is divided into two parts: sensitivity analysis and uncertainty analysis. Consider the linear system shown below [45, 52, 53, 105, 106].

$$\Psi(\alpha).\varphi = \theta(\alpha). \tag{2.1}$$

In which: Ψ is a vector of operators that works linearly on the state vector φ, however, there is the possibility that they have a nonlinear reliance on the parameter of the system. These operators may be differential, integral, ...
φ is a state vector or the variable that was calculated.
α is a vector that contains the physical characteristics of the system, including cross sections, dimensions, decay data, ...

θ is a column vector denoting the non homogeneous source terms. It may have a nonlinear dependence on the system's parameters.

Let Θ be a system response (usually k_{eff}), which is contingent upon multiple parameters: $(\alpha_1, \alpha_2, \ldots, \alpha_N)$. These parameters may be characterized as random variables adhering to a normal distribution, contingent upon their nominal or mean values (α_i^0) and their deviations or standard deviations $(\Delta\alpha_i)$. In this formulation, the relevant responses to the issue are specified as follows:

$$\Theta = \Theta(\alpha_1, \alpha_2, \ldots, \alpha_E) = \Theta(\alpha_1^0 + \Delta\alpha_1, \alpha_2^0 + \Delta\alpha_2, \ldots, \alpha_E^0 + \Delta\alpha_E). \quad (2.2)$$

Using a Taylor series that revolves around the nominal values of the parameters, this response may be enlarged up to the following:

$$\begin{aligned}
\Theta &= \Theta(\alpha_1, \alpha_2, \ldots, \alpha_E) \\
&= \Theta(\alpha_1^0 + \Delta\alpha_1, \alpha_2^0 + \Delta\alpha_2, \ldots, \alpha_E^0 + \Delta\alpha_E) \\
&= \Theta(\alpha^0) + \sum_{i_1=1}^{E} \left(\frac{\partial\Theta}{\partial\alpha_{i_1}}\right)_{\alpha^0} \Delta\alpha_{i_1} \\
&+ \frac{1}{2!} \sum_{i_1,i_2=1}^{E} \left(\frac{\partial^2\Theta}{\partial\alpha_{i_1}\partial\alpha_{i_2}}\right)_{\alpha^0} \Delta\alpha_{i_1}\Delta\alpha_{i_2} \\
&+ \ldots \\
&+ \frac{1}{n!} \sum_{i_1,i_2\ldots,i_n=1}^{E} \left(\frac{\partial^n\Theta}{\partial\alpha_{i_1}\partial\alpha_{i_2}\ldots\partial\alpha_{i_n}}\right)_{\alpha^0} \Delta\alpha_{i_1}\Delta\alpha_{i_2}\ldots\Delta\alpha_{i_n}.
\end{aligned} \quad (2.3)$$

It is possible to eliminate the nonlinear elements of the Taylor expansion, as a general rule, since a response is a linear function of the parameters:

$$\begin{aligned}
\Theta(\alpha_1, \alpha_2, \ldots, \alpha_E) &= \Theta(\alpha^0) + \sum_{i_1=1}^{E} \left(\frac{\partial\Theta}{\partial\alpha_i}\right)_{\alpha^0} \Delta\alpha_i \\
&= \Theta(\alpha^0) + \sum_{i_1=1}^{E} S_i\Delta\alpha_i.
\end{aligned} \quad (2.4)$$

In this equation, $\Theta(\alpha^0)$ represents the anticipated value of the response, which is the response when all parameters are set to their nominal values, and S_i denotes the sensitivity of the response Θ to the parameter α_i. The variation in the response is derived by calculating the second central

moment of Θ:

$$U^2(\Theta) = \sum_{i_1=1}^{E} S_i^2 U(\alpha_i) + 2 \sum_{i\#j\#1}^{E} S_i S_j . Covariance(\alpha_i, \alpha_j). \tag{2.5}$$

Specifically, in matrix form is:

$$U^2(\Theta) = \left| S^T . C_\alpha . S \right| . \tag{2.6}$$

In which:

$$\begin{aligned} S^T &= (S_1, S_2, \ldots, S_i) \\ S_i &= \left(\frac{\partial \Theta}{\partial \alpha_i} \right)_{\alpha^0} . \end{aligned} \tag{2.7}$$

It is possible to determine the uncertainty in a response that is due to the uncertainty input parameters using the equation (2.6), which is known as the *Sandwich Rule*. C_α stands for the covariance matrix within the input parameters, and S, a column vector, stands for the sensitivity coefficients.

2.5.2 *Direct perturbation sensitivity analysis*

The method referred to as the Direct Perturbation Sensitivity Analysis (DPSA) method is the least complicated. It involves manually causing perturbations in the system's parameters around a certain point. By using this method, a perturbed linear system is created as follows [52]

$$(\Psi^0 + \Delta\Psi).(\varphi^0 + \Delta\varphi) = (\theta^0 + \Delta\theta). \tag{2.8}$$

A novel approach to resolving the disturbed system is:

$$\chi_{new} = \chi^0 + \Delta\chi. \tag{2.9}$$

So, the new replacement response would be:

$$\Theta_{new} = (\eta^0 + \Delta\eta)\chi_{new} = \Theta^0 + \Delta\Theta. \tag{2.10}$$

When the perturbation only affects one parameter, it is possible to calculate the sensitivity coefficient of the response to that parameter by contrasting the results of the perturbed simulation with the results of the unperturbed simulation. The vector of sensitivity coefficients is produced each time each parameter is perturbed once as follows:

$$S_i = \left(\frac{\partial \Theta}{\partial \alpha_i} \right)_{\alpha^0} = \frac{[\Theta(\alpha_1^0 + \Delta\alpha_1, \alpha_2^0 + \Delta\alpha_2, \ldots, \alpha_E^0 + \Delta\alpha_E) - \Theta(\alpha^0)]}{\Delta\alpha_i}. \tag{2.11}$$

The DPSA method validates the efficacy of more complex implementations using simple cases. On the other hand, this method, despite its apparent simplicity, has three primary drawbacks, as follows:

In most cases, each parameter is disturbed by either a positive or negative value, necessitating n + 1 simulations, where n is the total number of input parameters. Instead of utilizing the nominal value of the parameters, it is possible to use central differences, which require 2n computations. Therefore, the DPSA method is effective when there are many replies and a small number of input parameters. However, this is not the case with reactor core simulators, which have many input parameters and a limited number of outputs.

When the perturbation is too small, computational round off errors may be significant. Conversely, if the perturbation is too high, linearity may be difficult. Selecting the appropriate perturbation requires experimentation and may depend on the parameters under consideration.

In order to solve the linear system in Equation 2.8, the DPSA method requires either calculating $(\Psi^0 + \Delta\Psi)^{-1}$ or solving the problem using an iterative method. This is done each time an element of $\Delta\Psi$ changes. Depending on the nature of the issue, it may not be feasible to perform the calculations multiple times.

2.5.3 *Forward sensitivity analysis*

A description of the Forward Sensitivity Analysis (FSA), which is a more advanced method for calculating the sensitivity coefficients of a problem, is based on the formulation presented in the research work of D.G. Cacuci [52, 52].

Consider the linear system written in equation 2.12, along with a response given in equation 2.13.

$$\Psi(\alpha).\varphi = \theta(\alpha). \tag{2.12}$$

$$\Theta = \eta(\alpha).\varphi. \tag{2.13}$$

The reaction is contingent upon the input parameters α and the computed variable φ. Conversely, Ψ, θ, and η are contingent upon the parameters

α, which possess uncertainty. That is, a perturbation in the parameters $\Delta\alpha$ will induce perturbations in the terms: $\Delta\Psi$, $\Delta\theta$, $\Delta\eta$, and $\Delta\varphi$.

FSA assesses how sensitive the response is to the system's parameters by first finding out how the state vector φ changes around its nominal value as a result of changes in the input parameters α. This is done to determine the system is sensitivity to the parameters. To phrase it another way, to determine the sensitivity of the response, it is necessary to first establish the relationship between the perturbations in φ and the perturbation in α.

The sensitivity of Θ is determined by the disturbances caused by variations in the parameters:

$$\Delta\Theta = \varphi^0.\Delta\eta + \eta^0.\Delta\varphi, \tag{2.14}$$

The first component of Equation 2.14, $\varphi^0.\Delta\eta$, is referred to as the direct effect, and it is possible to calculate it directly because it is only dependent on the nominal solution of the system and perturbations in η that can be obtained directly:

$$\Psi^0.\varphi^0 = \theta^0. \tag{2.15}$$

The second component of equation 2.14, $\eta^0.\Delta\varphi$ is classified as an indirect effect and may be computed by differentiating equation 2.12, resulting in a new linear system for $\Delta\varphi$.

$$\Psi^0(\Delta\varphi) + (\Delta\Psi).\varphi^0 = \Delta\theta, \tag{2.16}$$

$$\Psi^0(\Delta\varphi) = \Delta\theta - (\Delta\Psi).\varphi^0. \tag{2.17}$$

The forward sensitivity equation is shown in Equation 2.17 form. When it is solved, the perturbations in the solution reveal themselves as a function of the perturbations in the parameters that are being input. It is important to remember that the solution $\Delta\varphi$, the $\Delta\Psi$, and $\Delta\theta$ must be calculated each time an input parameter is altered. This means that a new system must be calculated for each sensitivity coefficient. When compared to the direct perturbation method, the fact that all systems are based on the creation of the same matrix Ψ^0 just once, directly.

The FSA is advantageous for scenarios with many responses and some input parameters. Conversely, it does not apply to transport or diffusion

issues, which include many input parameters, such as cross sections, and some responses, such as k_{eff}.

2.5.4 *Adjoint sensitivity analysis*

The sensitivity analysis techniques mentioned earlier have a significant restriction: many simulations must be conducted, with one simulation for each input parameter. The Adjoint Sensitivity Analysis (ASA) method circumvents this problem because it only requires two calculations for each response to obtain all the sensitivities. This is accomplished by using an adjoint system, allowing its solution to mitigate perturbations in the response sensitivity of the solution [52, 55].

The linear system described in equation 2.18 and a response structured as given in equation 2.19 are both aspects that we will consider.

$$\Psi(\alpha).\varphi = \theta(\alpha), \tag{2.18}$$

$$\Theta = \eta(\alpha).\varphi. \tag{2.19}$$

In the same manner that it is done with the FSA, the sensitivity of the reaction is specified in the following way:

$$\Delta\Theta = \varphi^0.\Delta\eta + \eta^0.\Delta\varphi. \tag{2.20}$$

Once again, the first component, which is the direct effect, is computed directly from the nominal solution, and the second term, which is the indirect effect, may be mathematically expressed as follows:

$$\Psi^0(\Delta\varphi) = \Delta\theta - (\Delta\Psi).\varphi^0. \tag{2.21}$$

At this point, an a priori unknown, arbitrary function Ω is presented, which defines the scalar product as follows:

$$\langle\Omega, \Psi^0(\Delta\varphi)\rangle = \langle\Omega, \Delta\theta - (\Delta\Psi).\varphi^0\rangle. \tag{2.22}$$

By using the definition and characteristics of the adjoint function, the left side is transposed, with the superscript "+" indicating transposition, resulting in:

$$\langle\Delta\varphi, (\Psi^0)^+\ \Omega\rangle = \langle\Omega, \Delta\theta - (\Delta\Psi).\varphi^0\rangle. \tag{2.23}$$

At this point in time, vector Ω is still considered arbitrary. The left side of Equation 2.23 is identified with the second, or indirect, term on the

right side of Equation 2.20, which indicates that it is defined:

$$\left(\Psi^0\right)^+ \Omega = \eta^0. \tag{2.24}$$

At this point, vector Ω can be recognized as the solution of the adjoint system, which is the source of the adjoint sensitivity equations, specifically Equation 2.24. In the case of reactor core simulators, the function referred to here is the adjoint flux solution of the adjoint diffusion or transport equations.

The definition of the sensitivity in the response Θ is as follows:

$$\Delta\Theta = \varphi^0.\Delta\eta + \eta^0.\Delta\varphi = \varphi^0.\Delta\eta + \langle\Omega, \Delta\theta - (\Delta\Psi).\varphi^0\rangle. \tag{2.25}$$

The adjoint solution is employed to evaluate the sensitivity of a response to variations in input parameters. Importantly, the adjoint equations need to be solved only once for each response in order to obtain the corresponding adjoint function (or adjoint flux), as this function is independent of perturbations in the input parameters. However, since the adjoint equations are formulated with respect to a specific response of interest, a distinct adjoint system must be constructed and implemented for each response, a process that is often nontrivial. As a result, the adjoint sensitivity analysis (ASA) technique is particularly efficient for sensitivity studies in systems characterized by a large number of input parameters but a relatively small number of response quantities.

2.5.5 *Sensitivity and uncertainty analysis methods*

In full core reactor simulations, computational codes based on transport equations that operate with continuous energy cross section data, rather than multigroup data, are generally preferred for sensitivity and uncertainty analyses. Among the most advanced tools for performing three dimensional sensitivity and uncertainty studies using continuous energy nuclear data are TSUNAMI-3D, a module within the SCALE code package [49], MCNP [49], and SERPENT [50]. These codes enable the calculation of sensitivities of reactor responses with respect to nuclear reaction cross section data. The resulting sensitivity profiles can subsequently be combined with nuclear data covariance matrices, typically using the sandwich rule, to quantify the uncertainties in the reactor parameters of interest [49].

This thesis employs the MCNP code to perform transport calculations using stochastic methods for sensitivity and uncertainty analysis of the three dimensional full core model of the DNRR. The analysis is conducted in two main stages. In the first stage, sensitivity coefficients are computed to quantify the response's dependence on variations in different reaction cross sections. In the second stage, the uncertainties of reactor responses are evaluated by propagating the uncertainties of input nuclear data parameters. This is achieved by applying the sensitivity coefficients within the framework of the sandwich rule, as described in the following sections.

Using a first order approximation framework, based on the research of Cacuci and the adjoint sensitivity analysis (ASA) method, the sensitivity and uncertainty evaluations presented in this thesis have been performed [52, 55]. Within this approach, the relative sensitivity profile of the effective multiplication factor (k_{eff}) with respect to a neutron cross section parameter associated with a specific nuclear reaction in a defined set of energy groups ($E_1, \ldots, E_N$) is expressed as follows:

$$\overrightarrow{\mathrm{S}_{\alpha}^{\mathrm{k_{eff}}}} = \left(\frac{\alpha_{E_1}}{k_{eff}} \frac{\partial k_{eff}}{\partial \alpha_{E_1}}, \frac{\alpha_{E_2}}{k_{eff}} \frac{\partial k_{eff}}{\partial \alpha_{E_2}}, \ldots, \frac{\alpha_{E_N}}{k_{eff}} \frac{\partial k_{eff}}{\partial \alpha_{E_N}} \right). \tag{2.26}$$

The estimation of the sensitivity of β_{eff} in this thesis is based on Bretscher's prompt method [5], in combination with the adjoint sensitivity analysis procedure (ASAP) [52]. This approach enables a comprehensive evaluation of the sensitivity of individual reaction components using the first-order perturbation theory [5, 8, 11, 16, 107].

$$\overrightarrow{\mathrm{S}_{\alpha}^{\beta_{\text{eff}}}} = \left(\frac{\alpha_{E_1}}{\beta_{eff}} \frac{\partial \beta_{eff}}{\partial \alpha_{E_1}}, \frac{\alpha_{E_2}}{\beta_{eff}} \frac{\partial \beta_{eff}}{\partial \alpha_{E_2}}, \ldots, \frac{\alpha_{E_N}}{\beta_{eff}} \frac{\partial \beta_{eff}}{\partial \alpha_{E_N}} \right). \tag{2.27}$$

From Equation (2.46), the corresponding components of Equation (2.27) can be identified as follows:

$$\begin{aligned}\frac{\alpha_{E_N}}{\beta_{eff}}\frac{\partial\beta_{eff}}{\partial\alpha_{E_N}} &= \frac{\alpha_{E_N}}{\beta_{eff}}\left(\frac{k_p\partial k}{k^2\partial\alpha_{E_N}} - \frac{\partial k_p}{k\partial\alpha_{E_N}}\right) \\ &= \frac{k_p}{k-k_p}\left(\frac{\alpha_{E_N}\partial k}{k\partial\alpha_{E_N}} - \frac{\alpha_{E_N}\partial k_p}{k_p\partial\alpha_{E_N}}\right) \\ &= \frac{k_p}{k-k_p}\left(S^k_{\alpha_{E_N}} - S^{k_p}_{\alpha_{E_N}}\right).\end{aligned} \tag{2.28}$$

Equation (2.5.5) can be presented in the following form:

$$\frac{\alpha_{E_N}}{\beta_{eff}}\frac{\partial\beta_{eff}}{\partial\alpha_{E_N}} = \frac{(1-\beta_{eff})}{\beta_{eff}}\left(S^k_{\alpha_{E_N}} - S^{k_p}_{\alpha_{E_N}}\right), \tag{2.29}$$

where, $S^k_{\alpha_{E_N}}$ and $S^{k_p}_{\alpha_{E_N}}$ are the sensitivities of k and k_p, respectively, obtained from the linear perturbation theory. In which, k is the eigenvalue for all neutrons and k_p is the eigenvalue for prompt neutrons only.

The covariance matrix $C_{\alpha,\alpha'}$ derived from nuclear data via the NJOY computer code is as follows [76]:

$$C_{\alpha,\alpha'} = \begin{bmatrix} c_{\alpha_1,\alpha'_1} & c_{\alpha_1,\alpha'_2} & \dots & c_{\alpha_1,\alpha'_N} \\ c_{\alpha_2,\alpha'_1} & c_{\alpha_2,\alpha'_2} & \dots & c_{\alpha_2,\alpha'_N} \\ \vdots & \vdots & \ddots & \vdots \\ c_{\alpha_N,\alpha'_1} & c_{\alpha_N,\alpha'_2} & \dots & c_{\alpha_N,\alpha'_N} \end{bmatrix}. \tag{2.30}$$

It is possible to calculate the uncertainty in the response of the input parameter by using the sandwich rule as follows [51, 52, 107, 108]:

$$U^2 = \left|S^T_{\alpha'} \cdot C_{\alpha,\alpha'} \cdot S_\alpha\right|, \tag{2.31}$$

In which: $S^T_{\alpha'}$ is the transpose of the vector $S_{\alpha'}$.

It can be seen from Equation (2.31) that the uncertainty in k_{eff} or β_{eff} associated with a given isotope depends separately on both the sensitivity matrix and the covariance matrix.

Equation (2.31), known as the sandwich rule, provides a means for calculating the uncertainty in a response due to uncertainties in the input

parameters. It can be observed that the uncertainty in k_{eff} or β_{eff} associated with a given isotope depends on both the sensitivity matrix and the covariance matrix. The resulting uncertainty is significant when both the sensitivity and covariance matrices exhibit large values within the same energy range.

2.6 Estimation of the effective multiplication factor

In the MCNP code, the criticality eigenvalue of the effective multiplication factor (k_{eff}) is defined as follows [67]:

$$\begin{aligned} k_{eff} &= \frac{fission \quad neutrons \quad in \quad generation \quad i+1}{fission \quad neutrons \quad in \quad generation \quad i} \\ &= \frac{\rho_a \int_V \int_0^\infty \int_E \int_\Gamma v\sigma_f \Phi dV dt dE d\Gamma}{\int_V \int_0^\infty \int_E \int_\Gamma \bigtriangledown . J dV dt dE d\Gamma + \rho_a \int_V \int_0^\infty \int_E \int_\Gamma (\sigma_c + \sigma_f + \sigma_m)\Phi dV dt dE d\Gamma}, \end{aligned} \tag{2.32}$$

where: t, E, r and Γ are the time, energy, position, and direction phase-space variables.

ρ_a is atom sensity $(atoms/barn.cm)$,

Φ is neutron flux,

J is total current crossing a surface,

σ is microscopic cross section for capture, fission, multiplicity (n,xn) terms.

According to neutron balance, the total loss equals the total source; in a k-eigenvalue calculation, the multiplicity term is:

$$\begin{aligned} &\rho_m \int_V \int_0^\infty \int_E \int_\Gamma \sigma_m \Phi \, dV \, dt \, dE \, d\Gamma \\ &= \rho_a \int_V \int_0^\infty \int_E \int_\Gamma \sigma_{n,2n} \Phi \, dV \, dt \, dE \, d\Gamma - 2\rho_a \int_V \int_0^\infty \int_E \int_\Gamma \sigma_{n,2n} \Phi \, dV \, dt \, dE \, d\Gamma \\ &+ \rho_a \int_V \int_0^\infty \int_E \int_\Gamma \sigma_{n,3n} \Phi \, dV \, dt \, dE \, d\Gamma \\ &- 3\rho_a \int_V \int_0^\infty \int_E \int_\Gamma \sigma_{n,3n} \Phi \, dV \, dt \, dE \, d\Gamma + \cdots , \end{aligned} \tag{2.33}$$

This definition of k_{eff} derives from the Boltzmann transport equation after integrating over time without any external source term,

$$\begin{aligned}\int_V \int_0^\infty \int_E \int_\Gamma \nabla\cdot\mathbf{J}\, dV\, dt\, dE\, d\Gamma \quad &+ \rho_a \int_V \int_0^\infty \int_E \int_\Gamma \sigma_t \Phi\, dV\, dt\, dE\, d\Gamma \\ = \frac{1}{k_{\text{eff}}}\, \rho_a \int_V \int_0^\infty \int_E \int_\Gamma \nu\sigma_f \Phi\, dV\, dt\, dE\, d\Gamma \\ + \rho_a \int_V \int_0^\infty \int_E \int_\Gamma \sigma_s \Phi\, dV\, dt\, dE\, d\Gamma,\end{aligned} \tag{2.34}$$

Equivalently, the expression can be written in the canonical k_{eff} form,

$$\begin{aligned}&\int_V \int_0^\infty \int_E \int_\Gamma \nabla\cdot\mathbf{J}\, dV\, dt\, dE\, d\Gamma \\ &+ \rho_a \int_V \int_0^\infty \int_E \int_\Gamma \big(\sigma_c + \sigma_f + \sigma_{n,2n} + \sigma_{n,3n} + \cdots\big)\Phi\, dV\, dt\, dE\, d\Gamma \\ &= \frac{1}{k_{\text{eff}}}\, \rho_a \int_V \int_0^\infty \int_E \int_\Gamma \nu\sigma_f \Phi\, dV\, dt\, dE\, d\Gamma \\ &+ \rho_a \int_V \int_0^\infty \int_E \int_\Gamma \big(2\sigma_{n,2n} + 3\sigma_{n,3n} + \cdots\big)\Phi\, dV\, dt\, dE\, d\Gamma.\end{aligned} \tag{2.35}$$

The loss processes are on the left; the production processes are on the right. For eigenvalue criticality calculations, we usually normalize the source to one. If the number of fission neutrons produced in a given generation equals that of the previous one, the system is critical; if it is higher, the system is supercritical; if it is lower, subcritical.

2.7 Methods for kinetic parameter evaluation

2.7.1 *Effectively delayed neutron fraction*

The kinetic parameters of a nuclear reactor, particularly the β_{eff} and Λ, play a fundamental role in reactor kinetics, safety analysis, and the control of the fission chain reaction [109, 110]. The parameter β_{eff} represents the fraction of delayed neutrons relative to the total neutron population in the reactor core. These delayed neutrons originate from the radioactive decay of fission-product precursors formed during fission, including iodine and

bromine isotopes. Although delayed neutrons account for less than approximately 1% of the total neutron population, they significantly enhance reactor controllability by introducing a time delay in the neutron population response. This delayed contribution provides an essential margin for reactor control and safety systems. Consequently, accurate determination of kinetic parameters such as β_{eff} and Λ is crucial for reliable reactor analysis and safe operation [10].

The intensity of delayed neutrons and their influence on reactor behavior vary over time, depending on the half lives of the associated radionuclides. Based on these half lives, delayed neutron precursors are conventionally categorized into six groups, each corresponding to a characteristic range of decay times. The delayed neutron fraction for a given precursor group, denoted as β_i, is defined as the ratio of delayed neutrons produced by that group to the total number of neutrons generated in a fission event. The β_{eff} is determined as the sum of the delayed neutron fractions from all six precursor groups. In this study, β_{eff} was evaluated using two distinct approaches: the adjoint weighted method and the prompt method.

The adjoint weighted method:

The formulation of point reactor kinetics equations can be derived from the time dependent neutron transport equation in the absence of an external source. Based on this approach, the point kinetics equations are expressed as follows [111, 112]:

$$\frac{dn}{dt} = \frac{\rho - \beta}{\Lambda} n(t) + \sum_{i=1}^{6} \lambda_i c_i(t), \tag{2.36}$$

$$\frac{dc_i}{dt} = \beta_i n(t) - \lambda_i c_i(t), \quad i = 1, ..., 6. \tag{2.37}$$

The above equations characterize the temporal behavior of the neutron population n and the delayed neutron precursor concentrations c_i within a nuclear reactor. By assuming that spatial and temporal variables are separable, these equations are applicable under the framework of point reactor kinetics. In this context, ρ denotes the reactor reactivity, which is determined

according to the following expression:

$$\rho = \frac{k_{eff} - 1}{k_{eff}}. \tag{2.38}$$

where k_{eff} represents the fundamental eigenvalue or the effective multiplication factor of the system as section 2.6.

The β_i represents the effective fraction of precursors of type i, and λ_i is the corresponding decay constant. From the deduction, the equations 2.36, 2.37 for calculating the β_{eff} by the adjoint weighted method is written as follows [107, 112]:

$$\beta_{eff} = \frac{\langle \phi^+, \mathbf{B}\phi \rangle}{\langle \phi^+, \mathbf{F}\phi \rangle}, \tag{2.39}$$

where, ϕ and ϕ^+ are the forward and adjoint neutron fluxes, respectively; $\mathbf{B}$ is the delayed neutron operator; $\mathbf{F}$ is the fission term operator; $\langle . \rangle$ is the integration over space and energy.

The terms in the numerator and denominator of Equation (2.39) may be elaborated as follows [8, 113]:

$$\begin{aligned} \langle \phi^+, \mathbf{B}\phi \rangle = \int \phi^+(\vec{r}, E, \vec{\Gamma}) \Sigma_f(\vec{r}, E') \upsilon_d(E') \chi_d(E', \vec{\Gamma'} \rightarrow \\ E, \vec{\Gamma}) \phi(\vec{r}, E', \vec{\Gamma'}) dE' d\vec{\Gamma'} dE d\vec{\Gamma} d\vec{r}. \end{aligned} \tag{2.40}$$

and

$$\begin{aligned} \langle \phi^+, \mathbf{F}\phi \rangle = \int \phi^+(\vec{r}, E, \vec{\Gamma}) \Sigma_f(\vec{r}, E') \upsilon(E') \chi(E', \vec{\Gamma'} \rightarrow \\ E, \vec{\Gamma}) \phi(\vec{r}, E', \vec{\Gamma'}) dE' d\vec{\Gamma'} dE d\vec{\Gamma} d\vec{r}. \end{aligned} \tag{2.41}$$

where: $\upsilon(E')$ and $\upsilon_d(E')$ are the average of total neutron and only delayed neutron at energy E' generate per fission, respectively. $\chi(E', \vec{\Gamma'} \rightarrow E, \vec{\Gamma})$ and $\chi_d(E', \vec{\Gamma'} \rightarrow E, \vec{\Gamma})$ are spectrum of energy and angular distribution $(E, \vec{\Gamma})$ of the total and delayed neutrons produced by incoming neutrons with $(E', \vec{\Gamma'})$, respectively. Σ_f is the macroscopic fission cross section. $\vec{r}$ is the neutron position. E is neutron energy, and $\vec{\Gamma}$ is neutron direction.

From equations (2.39, 2.40, 2.41), the β_{eff} can be estimated by equation as follows:

$$\begin{aligned}\beta_{eff} =& \frac{\int \phi^{+}(\vec{r},E,\vec{\Gamma})\Sigma_f(\vec{r},E^{'})\upsilon_d(E^{'})\chi_d(E^{'},\vec{\Gamma^{'}}\rightarrow E,\vec{\Gamma})}{\int \phi^{+}(\vec{r},E,\vec{\Gamma})\Sigma_f(\vec{r},E^{'})\upsilon(E^{'})\chi(E^{'},\vec{\Gamma^{'}}\rightarrow E,\vec{\Gamma})} \\ & \times \frac{\phi(\vec{r},E^{'},\vec{\Gamma^{'}})dE^{'}d\vec{\Gamma^{'}}dEd\vec{\Gamma}d\vec{r}}{\phi(\vec{r},E^{'},\vec{\Gamma^{'}})dE^{'}d\vec{\Gamma^{'}}dEd\vec{\Gamma}d\vec{r}}.\end{aligned} \tag{2.42}$$

In order to simplify the equation 2.42, the operator $\langle . \rangle$ might be used to carry out an integration over all of the spatial, angular, and energy variables. This integration may be expressed as follows using simplification:

$$\beta_{eff} = \frac{\langle \phi^{+}\upsilon_d\chi_d\Sigma_f\phi\rangle}{\langle \phi^{+}\upsilon\chi\Sigma_f\phi\rangle} \approx \frac{\langle \chi_d\upsilon_d\rangle}{\langle \chi\upsilon\rangle}. \tag{2.43}$$

Spriggs reformulated the β_{eff} from the equation to concentrate only on quantifying the delayed neutron fraction; hence, the *kratio* is subsequently introduced as follows [8, 114]:

$$\beta_{eff} \approx \frac{\langle \chi_d\upsilon\rangle}{\langle \chi_d\upsilon\rangle}\frac{\langle \chi_d\upsilon_d\rangle}{\langle \chi\upsilon\rangle} \approx \frac{\langle \chi_d\upsilon_d\rangle}{\langle \chi_d\upsilon\rangle}\frac{\langle \chi_d\upsilon\rangle}{\langle \chi\upsilon\rangle} \approx \beta_0\frac{\langle \chi_d\upsilon\rangle}{\langle \chi\upsilon\rangle} \approx \beta_0\frac{k_d}{k}. \tag{2.44}$$

Calculating β_0 using the MCNP code is straightforward. It may be accomplished by counting the total and delayed neutrons generated during fission events, whereas k_d is derived from the delayed neutron energy spectrum.

Prompt method:

From equation 2.43 can rewrite the expression for the β_{eff} as follows [8]:

$$\begin{aligned}\beta_{eff} &\approx \frac{\langle \chi_d\upsilon_d\rangle}{\langle \chi\upsilon\rangle} \\ &= 1 - \frac{\langle \chi\upsilon - \chi_d\upsilon_d\rangle}{\langle \chi\upsilon\rangle} \\ &= 1 - \frac{\langle \chi\upsilon_d - (\chi_d - \chi)\upsilon_d\rangle}{\langle \chi\upsilon\rangle} \\ &\cong 1 - \frac{\langle \chi_d\upsilon_d\rangle}{\langle \chi\upsilon\rangle}.\end{aligned} \tag{2.45}$$

The estimation in the final phase is founded on the subsequent rationale. The term $(\chi_d - \chi)\upsilon_d$ is two orders of magnitude less than the one with

$\chi\upsilon_d$ because υ_d is two orders of magnitude smaller than ν_p. Due to the same rationale, the shape of χ is almost equal to that of χ_p.

At this point, an important step is carried out. The β_{eff} can be estimated as follows [115, 116]:

$$\frac{\langle \chi_p \upsilon_p \rangle}{\langle \chi \upsilon \rangle} = \frac{k_p}{k} \rightarrow \beta_{eff} \approx 1 - \frac{k_p}{k}, \tag{2.46}$$

where, k is the eigenvalue for all neutrons and k_p is the eigenvalue for prompt neutrons only.

2.7.2 *Neutron generation and prompt neutron lifetime*

The adjoint weighted method:

The β_{eff}, Λ, and l_p are key kinetic parameters that govern the dynamic response of a nuclear reactor. The values of β_{eff} and Λ are essential for assessing reactor controllability and stability under transient conditions, while l_p reflects the average lifetime of prompt neutrons before absorption or leakage. These parameters may vary as the reactor fuel composition changes due to burnup. Accurate determination of these quantities requires accounting for the neutron importance, typically through the calculation of the adjoint neutron flux or time dependent neutron transport. Monte Carlo neutron transport codes, such as MCNP, are widely employed to perform these evaluations with high fidelity [67, 113, 117].

The l_p is a fundamental parameter of nuclear reactors, as it directly influences the reactor's kinetic behavior during all transient conditions. The l_p represents the average time interval between the emission of a prompt neutron from a fission event and its subsequent removal from the neutron population through absorption processes, such as radiative capture, fission, or leakage from the reactor core [118].

Based on the adjoint weighted method, the Λ and l_p can be derived from the point kinetics formalism. The governing expressions for these quantities are written as follows [107, 112]:

$$\Lambda = \frac{\left\langle \phi^+, \frac{1}{v}\phi \right\rangle}{\langle \phi^+, \mathbf{F}\phi \rangle}, \tag{2.47}$$

and

$$l_p = \frac{\left\langle \phi^+, \frac{1}{v}\phi \right\rangle k_{eff}}{\langle \phi^+, \mathbf{F}\phi \rangle}, \tag{2.48}$$

In which:

$$\left\langle \phi^+, \frac{1}{v}\phi \right\rangle = \int \phi^+(\vec{r}, E, \vec{\Gamma}) \frac{1}{\upsilon(E)} \phi(\vec{r}, E', \vec{\Gamma'}) dE' d\vec{\Gamma'} dE d\vec{\Gamma} d\vec{r}. \tag{2.49}$$

where, k_{eff} is the effective multiplication factor.

From equations (2.41, 2.47, 2.49), the Λ can be estimated by equation as follows:

$$\Lambda = \frac{\int \phi^+(\vec{r}, E, \vec{\Gamma}) \frac{1}{\upsilon(E)} \phi(\vec{r}, E', \vec{\Gamma'}) dE' d\vec{\Gamma'} dE d\vec{\Gamma} d\vec{r}}{\int \phi^+(\vec{r}, E, \vec{\Gamma}) \Sigma_f(\vec{r}, E') \upsilon(E') \chi(E', \vec{\Gamma'} \to E, \vec{\Gamma}) \phi(\vec{r}, E', \vec{\Gamma'}) dE' d\vec{\Gamma'} dE d\vec{\Gamma} d\vec{r}}, \tag{2.50}$$

From equations (2.41, 2.48, 2.49), the prompt neutron lifetime (l_p) can be estimated by equation as follows:

$$l_p = \frac{k_{eff}. \int \phi^+(\vec{r}, E, \vec{\Gamma}) \frac{1}{\upsilon(E)} \phi(\vec{r}, E', \vec{\Gamma'}) dE' d\vec{\Gamma'} dE d\vec{\Gamma} d\vec{r}}{\int \phi^+(\vec{r}, E, \vec{\Gamma}) \Sigma_f(\vec{r}, E') \upsilon(E') \chi(E', \vec{\Gamma'} \to E, \vec{\Gamma}) \phi(\vec{r}, E', \vec{\Gamma'}) dE' d\vec{\Gamma'} dE d\vec{\Gamma} d\vec{r}}, \tag{2.51}$$

Where, k_{eff} is the effective multiplication factor; v is the neutron speed.

The prompt neutron lifetime l_p was determined using the adjoint weighted method [110]. The adjoint weighted method has been implemented in the KOPTS card of the MCNP code.

The Λ is defined as the average time between a prompt neutron emission and a capture that results only in fission. It is important to note that the l_p is not the same as Λ. This is due to the fact that the Λ only takes into account neutron absorptions that result in fission events and not others [118].

The $1/v$ absorber insertion method:

The prompt neutron lifetime l_p was calculated using the $1/v$ absorber insertion method [7, 110]. The $1/v$ absorber insertion method involved introducing a small addition of B-10 as a perturbation in the core materials. The

appearance of the absorber content results in a negative change in reactivity. The negative reactivity insertion is calculated as follows:

$$\rho = \frac{\Delta k}{k} = \frac{1}{k_{eff,u}} - \frac{1}{k_{eff,p}}. \tag{2.52}$$

Where, the $k_{eff,u}$ is the effective multiplication factor without the B-10 addition (unperturbed);

The $k_{eff,p}$ is the effective multiplication factor with additional B-10 content (perturbed).

The $k_{eff,p}$ is calculated by changing the B-10 content added to the core materials. The reactivity insertion due to the addition of the B-10 content is:

$$-\frac{\Delta k}{k} = N.\sigma_0.v_0.l_p^{'}. \tag{2.53}$$

Where, N is the atomic density of the B-10 absorber $(atoms/(b.cm))$; σ_0 is the thermal neutron absorption cross section of the absorber; v_0 is the speed of thermal neutrons; $l_p^{'}$ is the prompt neutron lifetime when B-10 absorber is added.

The prompt neutron lifetime l_p is calculated when the B-10 content approaches zero:

$$l_p = \lim_{N\to 0}(l_p^{'}) = \lim_{N\to 0}\left(-\frac{\Delta k}{k}.\frac{1}{N.\sigma_0.v_0}\right). \tag{2.54}$$

In the present work, the B-10 content was added uniformly to all core materials with the concentration from 4.0×10^{-9} to $15.0\times10^{-9} atoms/(b.cm)$. The $k_{eff,p}$ value was then calculated at each step of the B-10 contents for determining the linear dependence of the reactivity with the B-10 content. The l_p is obtained when the B-10 content approaches zero.

This chapter develops the DNRR model, computational methods, and nuclear data. The next chapter offers an in depth discussion of the core's neutronic analysis, including evaluations of criticality, sensitivity, and the uncertainty of the main reactions. This analysis emphasizes the connections between the neutron properties of the DNRR reactor and the evaluated nuclear data libraries.

Chapter 3 RESULTS AND DISCUSSION

3.1 Introduction

This chapter presents the validation results of the DNRR model with 92 LEU fuel bundles using the MCNP6 code and experimental data. It also includes S/U analyses for the DNRR in relation to the latest nuclear data libraries, which are ENDF/B-VIII.0, JENDL-5, JEFF-3.3, and CENDL-3.2. The MCNP6 calculations were performed for 500 cycles, including 50 inactive cycles, to examine the convergence of both k_{eff} and the fission source distribution using Shannon entropy and 10^6 neutron histories per cycle. The goal was to achieve a statistical error of less than 6 pcm in the standard deviation of k_{eff} and to ensure that the Figure of Merit (FOM) remains roughly constant as a function of the number of histories for each tally [67].

In thermal nuclear reactor analysis, the thermal neutron flux is very important; therefore, the 44 group cross section library contains 22 energy groups below 3 eV that are used to analyze the sensitivity and uncertainty of the DNRR. Additionally, it includes covariances derived from high fidelity nuclear data evaluations, and it is utilized for uncertainty analyses [69]. The S/U analyses are performed for k_{eff} and β_{eff} for 44 group structures, and the results are compared among four of the latest nuclear data libraries (ENDF/B-VIII.0, JENDL-5, JEFF-3.3, and CENDL-3.2). Furthermore, the most important reaction channels, including (n, elastic), (n, inelastic), (n, 2n), (n, fission), and (n, gamma), are also analyzed and evaluated.

To support the operation of the DNRR, several codes based on both Monte Carlo and deterministic methods have been deployed for core physics, safety analysis and in core fuel management, such as WIMSD/CITATION [20], the SRAC code system [22], MCNP5 [22], MCNP6.2 [23], Serpent and PARCS [24]. A previous work reported the S/U analysis of the DNRR with HEU fuel using MCNP6.2 and the data libraries of ENDF/B-VII.1, ENDF/B-VIII.0, JENDL-4.0 and JENDL-5 [23]. Criticality analysis for 49 criticality configurations indicated that the largest discrepancy of the k_{eff}, calculated with the data libraries was within -300 pcm in comparison with the measurements [23]. The isotopes with major contribution to positive sensitivities were

U-235, H-1, C-12, Be-9, Al-27 and O-16. While, negative sensitivities were significantly contributed by the captures of H-1, U-235, Al-27, U-238, B-10, Be-9, Fe-56, O-16 and C-12. The uncertainties in the k_{eff} prediction caused by the data libraries were found within the range of 379–535 pcm. Whereas, JENDL-5 was noticed as the most reliable data library for neutronic analysis of the DNRR with HEU fuel [23]. Attention was recommended for the elastic scattering and capture of H-1, and the capture and fission of U-235. However, the S/U analyses of k_{eff} and β_{eff} in DNRR have not been investigated. Therefore, further evaluation of S/U for k_{eff} and β_{eff} in the latest libraries for the current core of the DNRR using LEU fuel is essential.

This chapter also presents the results of kinetic parameters in some operational conditions and the S/U analyses for the DNRR in relation to the newest nuclear data libraries, which are ENDF/B-VIII.0, JENDL-5, JEFF-3.3, and CENDL-3.2. Several studies were conducted to estimate the kinetic parameters of various research reactors using continuous energy Monte Carlo transport codes [10, 44, 78–80, 83]. Kinetic parameters of the 20 MW D_2O moderated research reactor (NBSR) were estimated using the MCNP5 code and the ENDF/B-VII library, which yielded the most accurate estimates for the delayed neutron fraction and the prompt neutron lifetime [110]. Assessment of the kinetic parameters was conducted for the initial core of the Indonesian 30 MW Multipurpose Research Reactor using continuous energy Monte Carlo codes (MVP3 and MCNP-6.2) and the nuclear data libraries of JENDL-4.0, ENDF/B-VII.0 and ENDF/B-VII.1. The results indicated that the MVP3 calculations with the ENDF/B-VII.0 library agreed well with those obtained using the MCNP-6.2 (JENDL-4.0, ENDF/B-VII.0, and ENDF/B-VII.1) and the MVP3 (JENDL-4.0) results [119]. Kinetic parameters were estimated for the Ghana Research Reactor 1 (GHARR-1) after 19 years of operation using MCNP5. The results aligned closely with the initial Safety Analysis Report [12]. Kinetic parameters based on burnup were investigated to improve the performance of a research reactor. It was reported that the β_{eff} decreased with burnup, while the l_p exhibited an inversal tendency [80]. The core physics of the DNRR has been studied [20, 23, 24]; however, its kinetic

parameters have not yet been reported. Therefore, it is essential to evaluate these kinetic parameters using LEU fuel. This work also evaluates the kinetic parameters of the DNRR with LEU fuel and their sensitivities to the reactor operating parameters using the MCNP6 code and the ENDF/B-VIII.0, JENDL-5. The operating parameters include fuel burnup, fuel temperature, and the positions of control rods (CRs).

3.2 Criticality, sensitivity and uncertainty analysis

3.2.1 Criticality calculations and comparison with measurements

This part shows how the critical calculation results of the DNRR core model, which has 92 LEU fuel bundles as shown in Section 2.3.2, compare with the experimental results. These criticality calculations are based on changes in the positions of the control rods in the reactor core according to the measured results of the experiments. To evaluate the impact of beryllium poisoning in the reactor core, this study considers the accumulation of neutron absorber isotopes, such as He-3 and Li-6, produced by neutron interactions with beryllium in the beryllium rods, which were accounted for in the reactor model. The uncertainty of the measured results is estimated to be less than 1% [23].

The first critical configuration of the DNRR with LEU fuel was attained with 92 fuel bundles, including 80 fresh and 12 partially burnt bundles with the burnup rates of about 1.5–3.5% (percent loss of U-235). Additionally, the core consisted of twelve beryllium blocks and a neutron trap located at the core's center as shown in Figure 2.1. The critical conditions were established with the complete withdrawal of the two SR rods, the partial insertion of four ShR rods, and the adjustment of the AR rod positions. The process of the critical measurements was monitored using two neutron detectors (He-3) located at two beam ports, and three fission chambers (the IC1 type operating in pulse mode) of the control system located inside the reactor pool. The control system's detectors were located in waterproof aluminum tubes in the dry channels of the water reflection area between the graphite reflector and the reactor tank. These detectors were featured with gamma compensation, encased in electromagnetic shields, and contained in gas tight

enclosures filled with dry high purity nitrogen gas. The control system's detectors were linked to a current neutron display for monitoring reactor power. The initial counts of the five detectors were recorded as N01, N02, N03, N04, and N05, respectively. While adjusting the position of the AR rod, at each step of the AR rod movement, the counts of the the five neutron detectors were recorded as N1, N2, N3, N4, and N5. The count ratios of N01/N1, N02/N2, N03/N3, N04/N4 and N05/N5 were then determined. The critical condition was achieved when the ratios approached zero.

Table 3.1 provides the detailed control rod positions, i.e., the four ShR rods and the AR rod, corresponding to the thirty critical conditions of the DNRR with LEU. The critical conditions were experimentally established during the core conversion to LEU fuel. The experimental criticality establishment were monitored by three neutron detectors located at the beam ports [22]. In this work, calculations were performed for the thirty critical conditions of the DNRR using MCNP6 and the four latest data libraries. Comparison among the data libraries and with the experiments was presented.

Table 3.1: Control rod position corresponding to the criticality conditions of the DNRR with LEU fuel established experimentally.

No.	Rod insertion (mm)					No.	Rod insertion (mm)				
	ShR1	ShR2	ShR3	ShR4	AR		ShR1	ShR2	ShR3	ShR4	AR
1	430	430	430	430	390	16	514	310	514	514	254
2	420	420	420	420	530	17	420	420	420	650	255
3	431	431	431	431	430	18	416	416	650	416	253
4	435	435	435	435	375	19	650	650	102	650	650
5	438	438	438	438	310	20	464	464	360	464	267
6	442	442	442	442	225	21	477	477	330	477	267
7	390	460	460	460	256	22	493	493	300	493	255
8	358	477	477	477	259	23	510	510	270	510	259
9	325	498	498	498	253	24	530	530	239	530	256
10	290	527	527	527	252	25	558	558	205	558	263
11	250	545	545	545	259	26	398	650	398	398	262
12	424	424	424	424	650	27	505	505	505	260	259
13	463	384	463	463	265	28	471	471	471	335	262
14	477	360	477	477	261	29	457	457	457	374	247
15	494	335	494	494	254	30	650	397	397	397	254

Table 3.2 presents the k_{eff} prediction for the three cases corresponding to the critical, supercritical and subcritical conditions of the DNRR core with

92 LEU fuel bundles using MCNP6 and the four latest libraries of ENDF/B-VIII.0, JEFF-3.3, JENDL-5 and CENDL-3.2. The experimental measurements were also done in all cases. The critical condition in Case 1 established experimentally corresponds to the positions of AR = 390 mm and four ShR = 430 mm. Case 2 is the supercritical condition with the assumption of the complete withdrawal of all control rods. Whereas, Case 3 corresponds to the subcritical condition with the assumption of the complete insertion of the AR and four ShR rods. The two SR rods were completely withdrawn in all cases. In the critical condition, the k_{eff} values were evaluated with the discrepancies less than 162 pcm for all data libraries compared to the experimental value ($k_{eff} = 1.0$). In case 2 (all CRs out), the calculations with the four data libraries of ENDF/B-VIII.0, JEFF-3.3, JENDL-5 and CENDL-3.2 gave the k_{eff} values of 1.07708, 1.07692, 1.07851 and 1.07626, respectively. Compared to ENDF/B-VIII.0, the discrepancies are -14.9, 132.8 and -76.1 pcm for JEFF-3.3, JENDL-5 and CENDL-3.2, respectively. The discrepancies between these calculated values and the experimental value ($k_{eff} = 1.07643$) were found to be less than 208 pcm for all libraries, demonstrating a high degree of consistency with experimental data. Whereas, in Case 3 (all CRs in), the calculation with ENDF/B-VIII.0 obtained the k_{eff} of 0.97032, and the discrepancies in the k_{eff} prediction with the other libraries compared to ENDF/B-VIII.0 are 47.4, 165.9 and -89.7 pcm, respectively. Additionally, compared to the experimental value ($k_{eff} = 0.97276$), the discrepancies were less than 331 pcm. The k_{eff} values obtained with JEFF-3.3 agree well with ENDF/B-VIII.0 and the experimental results within 47.4 pcm and 20 pcm, respectively, in all three cases. The values obtained with JENDL-5 tend to be greater than that obtained with ENDF/B-VIII.0. The tendency is inverse with CENDL-3.2.

Table 3.2: The k_{eff} of the DNRR core with 92 LEU fuel bundles at critical, supercritical and subcritical conditions calculated using the MCNP6 code and the four data libraries.

Case	Reactor condition	Configuration	ENDF/B-VIII.0	JEFF-3.3	JENDL-5	CENDL-3.2
1	Critical	Experiment[a]	1.00021 ± 0.00005	1.00020 ± 0.00005	1.00162 ± 0.00005	0.99929 ± 0.00005
		–		(-1.0 pcm)[b]	(141.0 pcm)	(-92.0 pcm)
2	Supercritical	All CRs out	1.07708 ± 0.00005	1.07692 ± 0.00005	1.07851 ± 0.00005	1.07626 ± 0.00005
		–		(-14.9 pcm)	(132.8 pcm)	(-76.1 pcm)
3	Subcritical	All CRs in	0.97032 ± 0.00005	0.97078 ± 0.00005	0.97193 ± 0.00005	0.96945 ± 0.00005
		–		(47.4 pcm)	(165.9 pcm)	(-89.7 pcm)

[a]Rod insertion of the experimental criticality: 4 ShR = 430 mm, AR = 390 mm.

[b] Discrepancy compared to ENDF/B-VIII.0.

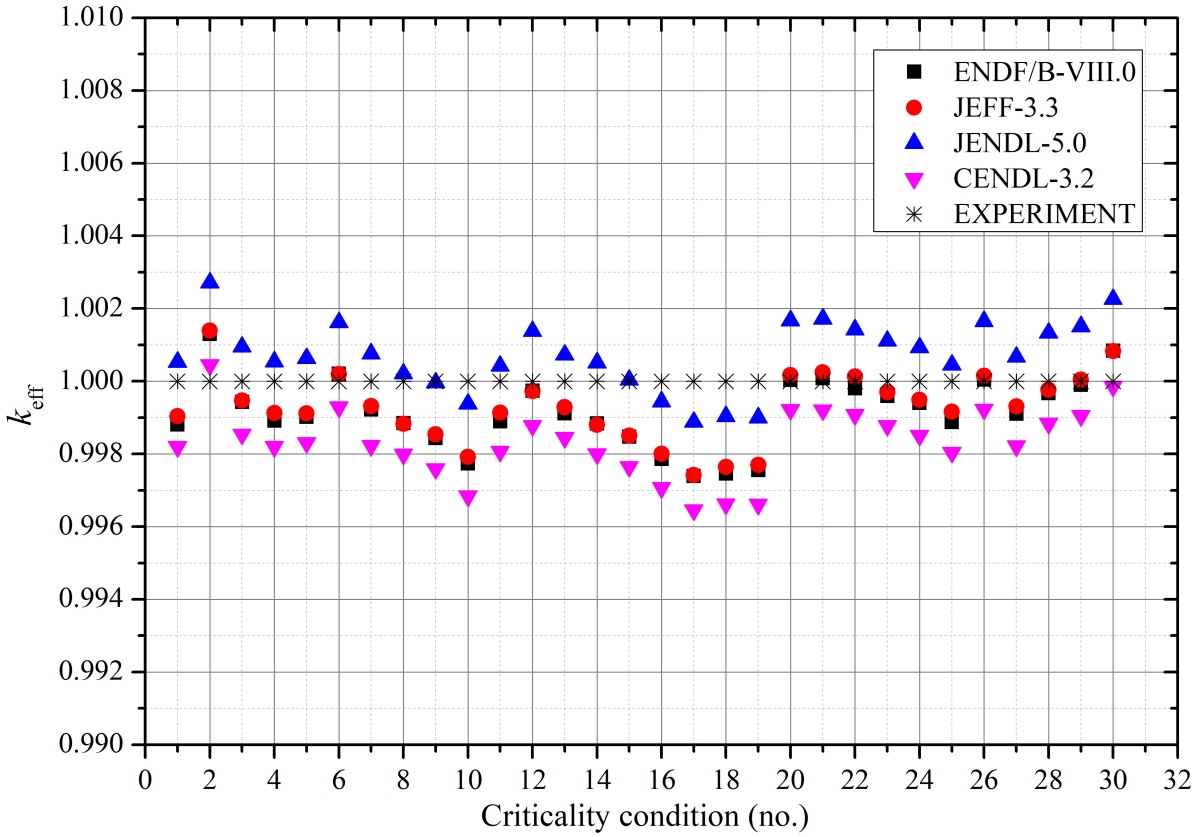

Figure 3.1: The k_{eff} values of 30 critical conditions of the DNRR with 92 LEU fuel bundles obtained with the four nuclear data libraries.

Figure 3.1 and Table 3.3 present the calculation results of the thirty criticality conditions of the DNRR core corresponding to various positions of the CR system using MCNP6 and the four latest data libraries. As described in the previous section, the reactor's critical configuration was established based on the counting rates measured by five neutron detectors. The ratio

of the initial counting rate to that at the critical state (N_0/N) approaches zero as the reactor reaches criticality. In this study, the effective multiplication factor (k_{eff}) corresponding to the critical condition is assumed to be one, with an estimated uncertainty of less than 1%. In critical experiments, experimental uncertainties primarily originate from factors such as detector counting statistics, reactor power and temperature stability, control rod positioning accuracy, and instrument calibration. These uncertainties have been quantified to validate computational models and ensure reliable comparison between experimental and calculated results. The largest discrepancy of the k_{eff} prediction is -354 pcm compared to the experiments, which indicates a good agreement between the calculations and the experiments. As shown in Figure 3.1, JENDL-5 tends to provide greater values of the k_{eff}, while CENDL-3.2 tends to predict the lower values. Again, one can see that the k_{eff} values of all cases obtained with ENDF/B-VIII.0 and JEFF-3.3 have a good agreement with the largest discrepancy of about 140 pcm. Comparing among the four latest libraries, the discrepancy in the k_{eff} prediction is less than 172 pcm. The k_{eff} values obtained with JENDL-5 tend to be greater than that obtained with ENDF/B-VIII.0 with the largest discrepancy of 10 pcm. While the k_{eff} values obtained with CENDL-3.2 are smaller than that obtained with ENDF/B-VIII.0.

3.2.2 Sensitivity analysis of the effective multiplication factor

3.2.2.1 *Sensitivity coefficients*

Sensitivity analysis allows to evaluate the effect of the changes in input parameters on the reactor core responses. Nuclear data, such as fission, capture, elastic and inelastic scattering cross sections, and so on, are among the significant input parameters in neutronic analysis. Whereas, the k_{eff} is the most significant response of the reactor core. To determine the sensitivity coefficients of the k_{eff} to the multigroup macroscopic cross sections, the adjoint sensitivity procedure (ASAP) is used [52]. The sensitivity coefficient of the k_{eff} to the parameter α, denoted as $S_{k,\alpha}$, is defined as [107]:

$$S_{k,\alpha} = \frac{\alpha}{k_{eff}} \frac{\partial k_{eff}}{\partial \alpha}. \tag{3.1}$$

Table 3.3: Criticality analysis of the DNRR with 92 LEU fuel bundles using the MCNP6 code and the four data libraries.

No.	k_{eff}				ρ (pcm)			
	ENDF/B-VIII.0	JEFF-3.3	JENDL-5	CENDL-3.2	ENDF/B-VIII.0	JEFF-3.3	JENDL-5.0	CENDL-3.2
1	1.00021	1.00020	1.00162	0.99929	21	20	162	-71
2	1.00130	1.00140	1.00271	1.00045	130	140	271	45
3	0.99943	0.99947	1.00095	0.99854	-57	-53	95	-146
4	0.99892	0.99913	1.00054	0.99820	-108	-87	54	-180
5	0.99902	0.99912	1.00063	0.99831	-98	-88	63	-169
6	0.99881	0.99904	1.00053	0.99820	-119	-96	53	-180
7	0.99922	0.99932	1.00076	0.99823	-78	-68	76	-177
8	0.99885	0.99883	1.00021	0.99799	-115	-117	21	-201
9	0.99844	0.99854	0.99996	0.99759	-156	-146	-4	-241
10	0.99774	0.99792	0.99938	0.99684	-226	-208	-62	-316
11	0.99890	0.99914	1.00042	0.99807	-110	-86	42	-193
12	0.99974	0.99973	1.00138	0.99878	-26	-27	138	-122
13	0.99912	0.99929	1.00073	0.99845	-88	-71	73	-155
14	0.99884	0.99880	1.00051	0.99800	-116	-120	51	-200
15	0.99848	0.99850	1.00004	0.99765	-152	-150	4	-235
16	0.99786	0.99801	0.99944	0.99707	-214	-199	-56	-293
17	0.99739	0.99742	0.99888	0.99646	-261	-258	-112	-354
18	0.99746	0.99764	0.99904	0.99662	-254	-236	-96	-338
19	0.99756	0.99770	0.99900	0.99661	-244	-230	-100	-339
20	1.00004	1.00017	1.00167	0.99922	4	17	167	-78
21	1.00008	1.00025	1.00172	0.99921	8	25	172	-79
22	0.99981	1.00013	1.00142	0.99908	-19	13	142	-92
23	0.99960	0.99970	1.00111	0.99878	-40	-30	111	-122
24	0.99940	0.99949	1.00093	0.99851	-60	-51	93	-149
25	0.99888	0.99916	1.00045	0.99804	-112	-84	45	-196
26	1.00005	1.00015	1.00165	0.99923	5	15	165	-77
27	0.99911	0.99931	1.00067	0.99822	-89	-69	67	-178
28	0.99967	0.99977	1.00133	0.99884	-33	-23	133	-116
29	0.99990	1.00005	1.00151	0.99905	-10	5	151	-95
30	1.00084	1.00083	1.00226	0.99986	84	83	226	-14

The KSEN mode of MCNP6, based on linear perturbation theory using adjoint weighting, was used to determine the sensitivity coefficients of the k_{eff} to nuclear cross section data [1]. The KSEN mode provides the list of reaction numbers. It deploys the iterated fission probability approach to obtain the adjoint weighted integrals for the sensitivity coefficients. The sensitivity profiles are discretized either with respect to energy or with respect to space. The sensitivity coefficients in the 44 group energies are organized in a matrix form denoted as S_k. To determine the uncertainty of the k_{eff} due to the uncertainty of the cross section data, the sensitivity coefficients are included in a sandwich rule in conjunction with the covariance matrix of the multigroup homogenized constants. The covariance matrix C_α in form of 44 energy groups was produced using the NJOY2021 code [76]. The uncertainty of the k_{eff}, denoted as U_{kk}, is estimated from the sensitivity coefficients and

the covariance matrix as [76, 107]:

$$U_{kk} = |(S_k)^T.C_\alpha.S_k|^{1/2}. \tag{3.2}$$

where, $(S_k)^T$ is the transpose of the vector S_k. Since the covariance matrices are not available in the CENDL-3.2 library, in the present work the uncertainties were only computed for the ENDF/B-VIII.0, JEFF-3.3 and JENDL-5 libraries.

3.2.2.2 *Sensitivity profiles*

To evaluate the effect of the nuclear reaction cross section data on the criticality prediction, sensitivity analysis was conducted based on the first criticality condition in Table 3.1. Sensitivity coefficients of major nuclides and reaction cross sections were analyzed and classified into the positive and negative effects. Table 3.4 presents the positive sensitivity coefficients obtained with the libraries of ENDF-VIII.0, JEFF-3.3, JENDL-5 and CENDL-3.2. Only significant sensitivity coefficients with the absolute values greater than 0.1% were shown. It can be seen that the orders of magnitudes of the sensitivities almost agree among the four libraries as shown in Table 3.4.

Table 3.4: Positive sensitivities of the k_{eff}, listed in descending order of magnitude according to the ENDF/B-VIII.0 library*.

Isotope	Reaction	ENDF/B-VIII.0 ($\times 10^{-1}$)	JEFF-3.3 ($\times 10^{-1}$)	JF3/E8	JENDL-5.0 ($\times 10^{-1}$)	J5/E8	CENDL-3.2 ($\times 10^{-1}$)	C3/E8
U-235	total ν	9.9354	9.9350	1.00	9.9352	1.00	9.9348	1.00
U-235	fission	3.3662	3.3681	1.00	3.3697	1.00	3.3757	1.00
H-1	elastic	2.7696	2.7831	1.00	2.7733	1.00	2.7842	1.01
C-nat	elastic	0.7207	0.7014	0.97	0.6760	0.94	0.7098	0.98
Lwtr $S(\alpha,\beta)$	inelastic	0.6830	0.6655	0.97	0.7007	1.03	–	–
O-16	elastic	0.3948	0.3604	0.91	0.3752	0.95	0.3900	0.99
Al-27	elastic	0.3648	0.3481	0.95	0.3489	0.96	0.3664	1.00
Be-9	elastic	0.3045	0.2907	0.95	0.3009	0.99	0.3075	1.01
Be-9	n-2n	0.1569	–	–	0.1589	1.01	0.1593	1.02
Al-27	inelastic	0.1117	0.1122	1.00	0.1026	0.92	0.1067	0.96
C-nat $S(\alpha,\beta)$	inelastic	0.0783	0.0775	0.99	0.0884	1.13	–	–
U-238	total ν	0.0547	0.0548	1.00	0.0547	1.00	0.0551	1.01
C-nat $S(\alpha,\beta)$	elastic	0.0511	0.0858	1.68	0.0655	1.28	–	–
U-238	elastic	0.0508	0.0512	1.01	0.0524	1.03	0.0497	0.98
U-238	fission	0.0371	0.0374	1.01	0.0371	1.00	0.0373	1.00
U-238	inelastic	0.0219	0.0231	1.06	0.0225	1.03	0.0222	1.02
Fe-56	elastic	0.0217	0.0195	0.90	0.0218	1.01	0.0217	1.00

* Absolute value $> 0.1\%$.

The U-235 (total-ν) and (n,fission) reactions yield the greatest positive sensitivity coefficients (0.994 and 0.337) compared to other reactions.

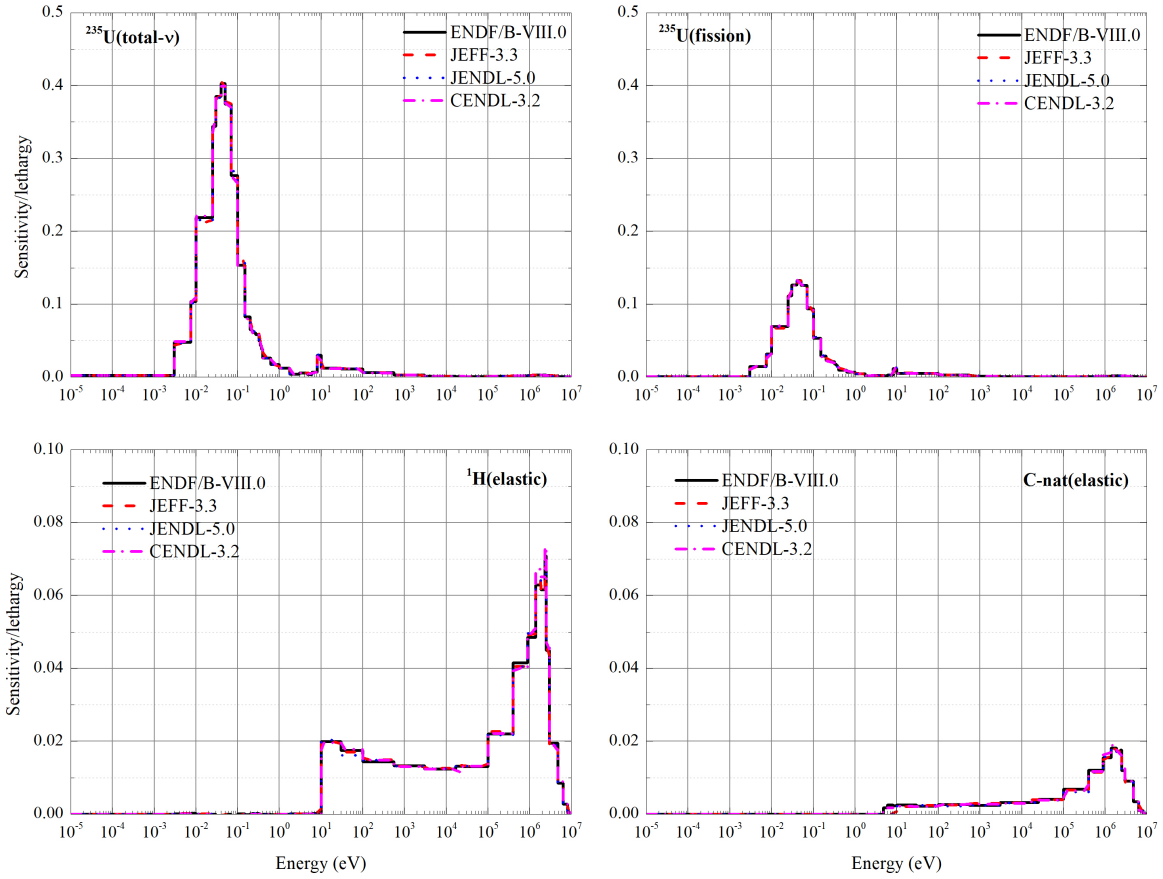

Figure 3.2: Energy dependent sensitivities of the k_{eff} to U-235, H-1, and C-nat in the increasing direction.

The positive sensitivities are subsequently due to the elastic scatterings of H-1, C-nat, O-16, Al-27 and Be-9 as shown in Table 3.4. Figure 3.2 displays the energy dependent sensitivity profiles of U-235 (total-ν) and (n,fission), H-1 (elastic) and C-nat (elastic). The sensitivity profiles are indicative of the relationship between sensitivity coefficients, the cross sections, and the neutron spectrum. The thermal energy of 0.001–1.0 eV exhibits distinct peaks in the positive sensitivity of U-235 (total-ν) and (n,fission). Whereas, Figures 3.2 and 3.3 indicate that H-1, C-nat, O-16, Al-27 and Be-9 exhibits significant positive sensitivities for elastic scatterings in the fast energy of 0.5–1.0 MeV. These results reflect the underlying physical processes governing the neutron balance in the reactor core. The large positive sensitivities of U-235 (total-ν) and (n,fission) mainly originate from the thermal energy region, where the fission cross section of U-235 is high and dominates neutron production in

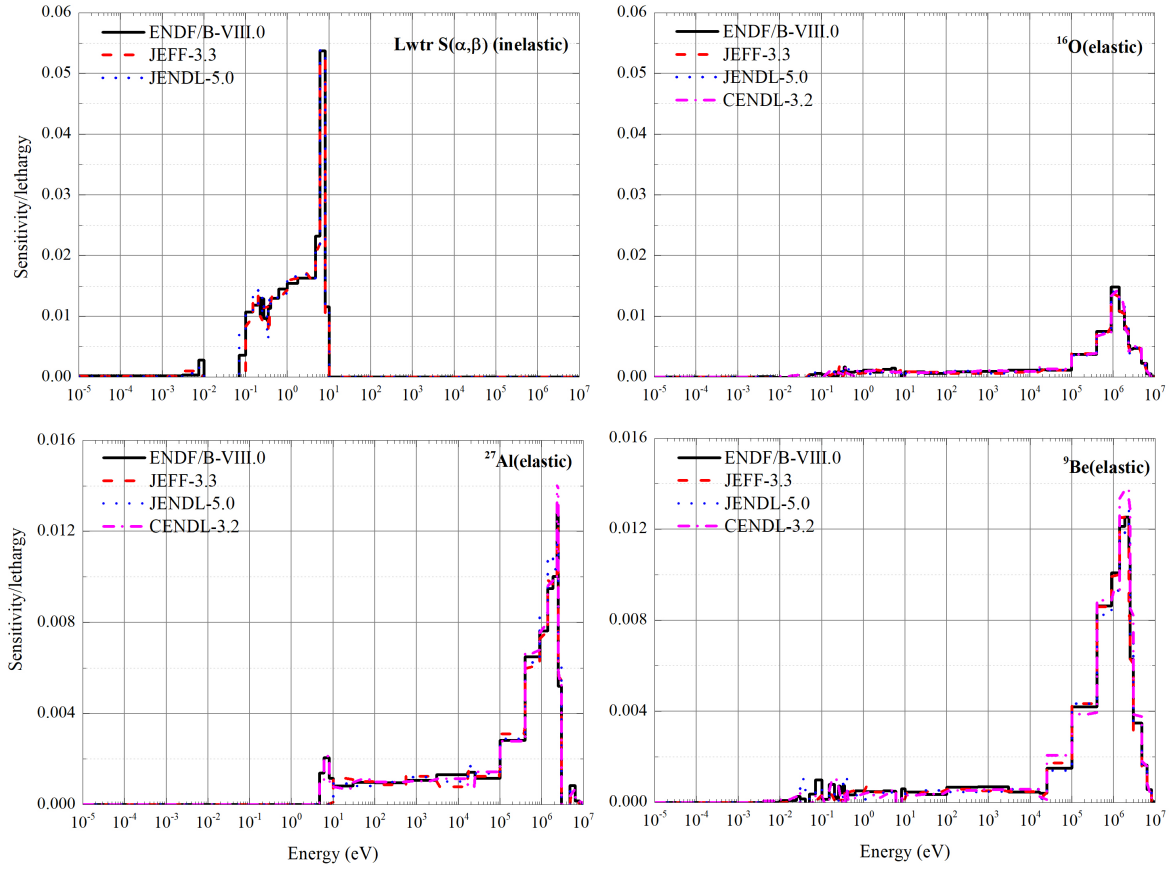

Figure 3.3: Energy dependent sensitivities of the k_{eff} to Lwtr S(α, β), O-16, Be-9, and Al-27 in the increasing direction.

the chain reaction. In contrast, the positive sensitivities of elastic scattering reactions of H-1, C-nat, O-16, Al-27, and Be-9 are mainly observed in the fast energy region. These scattering reactions play an important role in neutron moderation, slowing down fast neutrons toward the thermal energy range, where the probability of U-235 fission becomes significantly higher.

Table 3.5 shows the negative sensitivity coefficients obtained with the libraries of ENDF-VIII.0, JEFF-3.3, JENDL-5 and CENDL-3.2. It is noticed that the main factors contributing to the negative sensitivities are the capture reactions of H-1, U-235, Al-27, U-238 and B-10 (n,alpha). The values, determined with the ENDF/B-VIII.0 library, are -0.145, -0.128, -0.046, -0.039 and -0.010, respectively, as presented in Table 3.5. Figures 3.4 and 3.5 illustrate the energy dependent sensitivities of the capture reactions of H-1, U-235, Al-27, U-238. H-1, Be-9 and Al-27 induce the negative sensitivities due to

Table 3.5: Negative sensitivities of the k_{eff}, listed in descending order of magnitude according to the ENDF/B-VIII.0 library*.

Isotope	Reaction	ENDF/B-VIII.0 ($\times 10^{-1}$)	JEFF-3.3 ($\times 10^{-1}$)	JF3/E8	JENDL-5.0 ($\times 10^{-1}$)	J5/E8	CENDL-3.2 ($\times 10^{-1}$)	C3/E8
H-1	n,γ	-1.3930	-1.3928	1.00	-1.3988	1.00	-1.4064	1.01
U-235	n,γ	-1.2794	-1.2730	0.99	-1.2782	1.00	-1.2747	1.00
Al-27	n,γ	-0.4994	-0.4993	1.00	-0.4869	0.98	-0.5046	1.01
U-238	n,γ	-0.3963	-0.3954	1.00	-0.3972	1.00	-0.3995	1.01
B-10	n,α	-0.1361	-0.1373	1.01	-0.1357	1.00	-0.1367	1.00
Be $S(\alpha,\beta)$	elastic	-0.0705	-0.0575	0.82	-0.0676	0.96	–	–
Be-9	n,α	-0.0474	-0.0448	0.95	-0.0456	0.96	-0.0490	1.03
Be-9	n,γ	-0.0366	-0.0326	0.89	-0.0312	0.85	-0.0322	0.88
U-234	n,γ	-0.0227	-0.0228	1.00	-0.0221	0.97	-0.0227	1.00
O-16	n,α	-0.0150	-0.0106	0.71	-0.0143	0.95	-0.0108	0.72
C-nat	n,γ	-0.0147	-0.0145	0.98	-0.0152	1.04	-0.0130	0.88
Fe-56	n,γ	-0.0145	-0.0143	0.99	-0.0144	1.00	-0.0146	1.01

* Absolute value $> 0.1\%$.

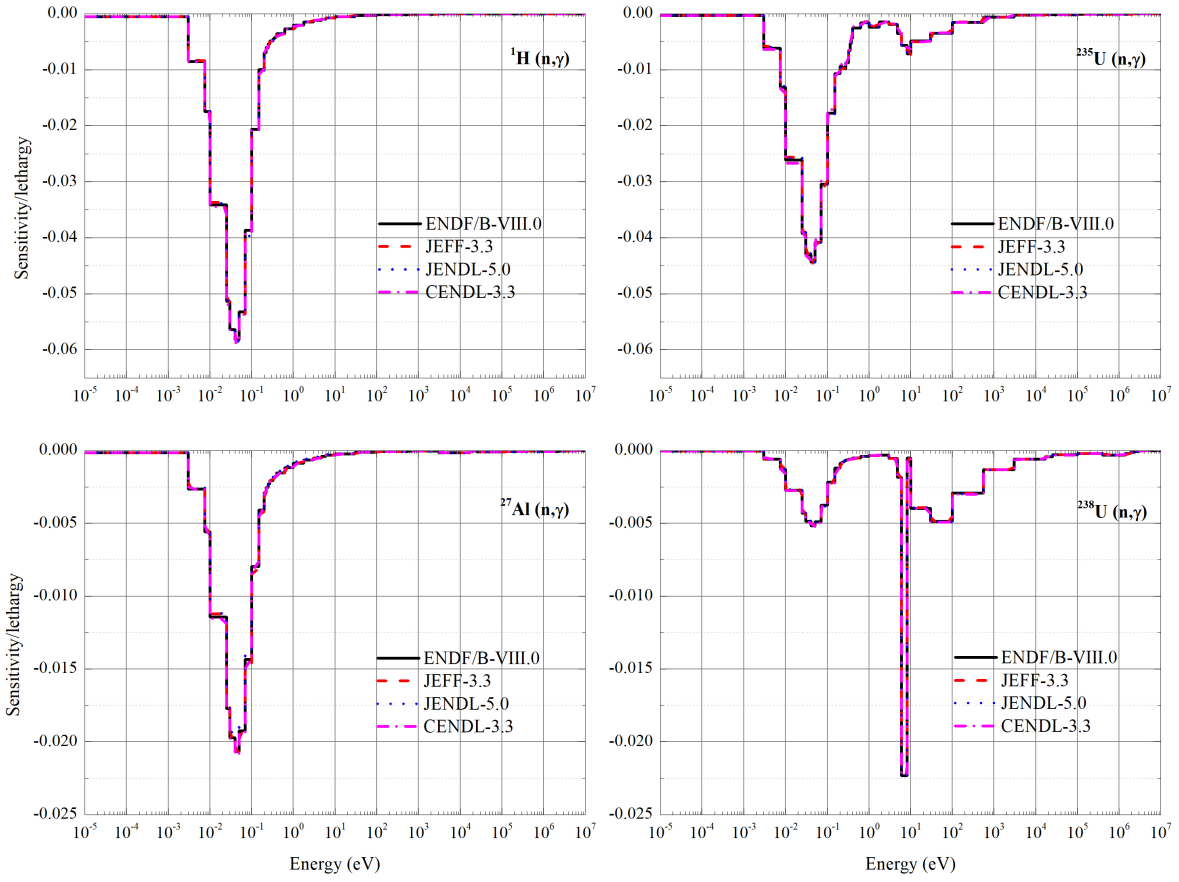

Figure 3.4: Energy dependent sensitivities of the k_{eff} to H-1, U-235, Al-27, and U-238 in the decreasing direction.

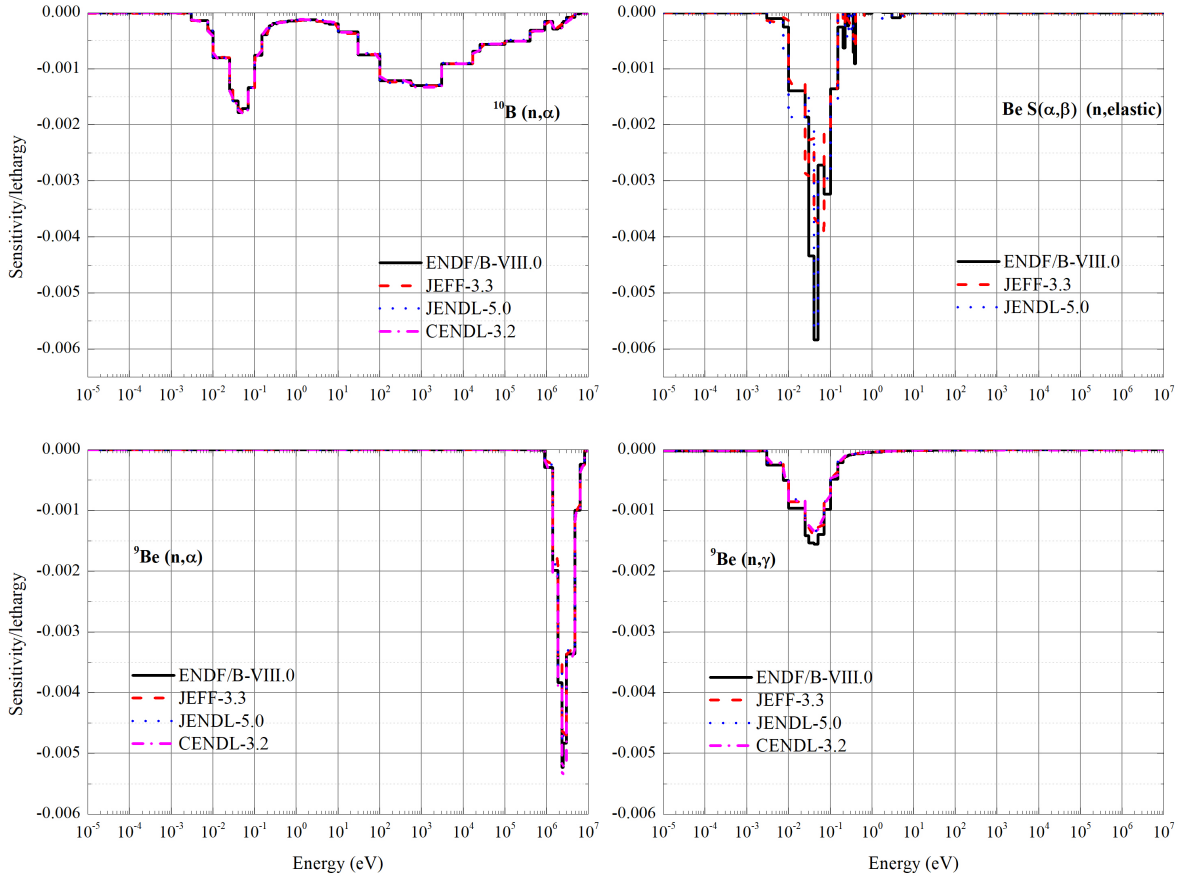

Figure 3.5: Energy dependent sensitivities of the k_{eff} to B-10, Be S(α, β), and Be-9 in the decreasing direction.

the capture reactions at the thermal energy of 0.0075–0.025 eV. These isotopes demonstrate a concave sensitivity at 0.01 eV, resulting in the negative sensitivities of -1.39×10^{-1} (H-1), -4.99×10^{-2} (Al-27) and -1.36×10^{-3} (Be-9). The neutron capture reactions of H-1, U-235 and Al-27 exhibit significantly negative sensitivities in the energy range of 0.01–0.1 eV as shown in Figure 3.4. The negative sensitivities associated with the capture reactions of H-1, U-235, Al-27, and U-238 indicate that these processes remove neutrons from the fission chain without producing additional neutrons. Consequently, an increase in the capture cross sections of these isotopes leads to a reduction in the neutron population and therefore decreases k_{eff}. The strong negative sensitivities observed in the thermal energy region (0.01–0.1 eV) are consistent with the reactor spectrum, where most neutrons are thermalized. In this

energy range, neutron capture by moderator and structural materials competes directly with U-235 fission. As a result, absorption reactions involving H-1, Al-27, and other materials represent important neutron-loss mechanisms in the thermal spectrum, which explains their significant negative sensitivity coefficients.

3.2.3 Uncertainty analysis of the effective multiplication factor

Table 3.6 shows the uncertainties of the k_{eff} for the DNRR with LEU fuel calculated with the ENDF/B-VIII.0, JEFF-3.3 and JENDL-5 libraries. The total uncertainties obtained with the libraries are 415.7, 588.0 and 363.0 pcm, respectively. Compared to the uncertainties obtained for the DNRR core of HEU fuel with ENDF/B-VIII.0 and JENDL-5 (466.6 and 379.1 pcm) in a previous work, the uncertainty values for the LEU core are smaller by about 12.2% and 4.4%, respectively [23]. One of the reasons is that the amount of U-235 in the LEU fuel is significantly less than that in the HEU fuel, which leads to the smaller uncertainty of the LEU core. The uncertainties obtained for the DNRR core with LEU fuel are also smaller than the value of 600 pcm of the RSG GAS research reactor reported by [14]. Compared to ENDF/B-VIII.0, the uncertainty obtained with JEFF-3.3 is greater by about 30%, while that obtained with JENDL-5 is smaller by 12%. It is noticed that the covariance data are not available in JENDL-5 for some isotopes, e.g., Al-27, Be-9 and C-12, thus, the uncertainties with respect to the capture and elastic scattering of Al-27, Be-9 and C-12 are not available. This may cause the smaller uncertainty (363.0 pcm) compared to ENDF/B-VIII.0.

The reactions contribute mostly to the uncertainties of the k_{eff} are H-1 (n,γ), U-235 (n,fission) and H-1 (elastic) with the uncertainty values of 288.1, 153.2 and 143.0 pcm, respectively, determined with ENDF/B-VIII.0. For H-1 (n,γ) and U-235 (n,fission) reactions, since the similarity in 44 group structured sensitivities are observed for the three libraries, difference in covariance matrices is the main reason to cause the difference in uncertainty values. To look closely to the difference of the covariance matrices of reactions with the largest uncertainties, the covariance matrices of U-235 (n,f),

Table 3.6: The k_{eff} uncertainties for the reactions of the primary isotopes are listed in order of decreasing magnitude based on the ENDF/B-VIII.0 dataset.

Isotope	Reaction	ENDF/B-VIII.0 (pcm)	JEFF-3.3 (pcm)	JF3/E8	JENDL-5 (pcm)	J5/E8
Total	-	415.7	588.0	1.41	363.0	0.87
H-1	n,γ	288.1	355.6	1.23	289.3	1.00
U-235	fission	153.2	215.2	1.40	153.2	1.00
H-1	elastic	143.0	203.7	1.42	142.6	1.00
Al-27	elastic	127.6	167.8	1.32	-	-
Al-27	n,γ	116.4	232.4	2.00	-	-
Al-27	inelastic	84.7	56.4	0.67	-	-
Be-9	n,2n	48.4	-	-	-	-
C-nat	elastic	37.5	39.0	1.04	-	-
U-238	n,γ	35.9	35.8	1.00	35.9	1.00
U-235	n,γ	34.1	195.2	5.73	33.9	1.00
Be-9	elastic	32.3	-	-	-	-
Be-9	n,α	22.8	-	-	-	-
Be-9	n,γ	18.2	-	-	-	-
O-16	elastic	15.0	66.2	4.41	11.4	0.76
U-238	elastic	12.5	10.9	0.88	13.2	1.06
U-238	total ν	12.3	13.3	1.08	5.5	0.45
O-16	n,α	9.1	2.6	0.28	6.2	0.68
B-10	n,α	7.9	1.5	0.19	7.9	1.00
Fe-56	n,γ	6.9	4.0	0.59	16.2	2.35
U-238	inelastic	6.3	15.3	2.42	21.0	3.33
U-234	n,γ	4.9	5.0	1.00	24.4	4.93
U-238	fission	4.5	10.2	2.26	3.7	0.81
C-nat	n,γ	4.4	4.3	0.98	-	-
Fe-56	elastic	2.3	9.2	3.96	7.7	3.31

H-1 (n,γ) and H-1 (elastic) are plotted in Figures B.1–B.3. With the highest covariance matrices, especially in the low energy range where the sensitivity coefficients are dominant, JEFF-3.3 has the greatest uncertainty of k_{eff}, greater than that obtained with ENDF/B-VIII.0 by 20-42% as shown in Table 3.16. Compared to the previous version, ENDF/B-VII.0, the covariance data of H-1 of ENDF/B-VIII.0 were updated and JENDL-5 adopted the data of ENDF/B-VIII.0 for H-1 [27]. The identical covariance matrices of H-1 (n,γ) and H-1 (elastic) are illustrated in Appendix section B, Figures B.2 and B.3. Thus, the uncertainties of H-1 (n,γ) and H-1 (elastic) reactions obtained by JENDL-5 and ENDF/B-VIII.0 indicate a good agreement as listed in Table 3.16. The resemblance in covariance data below 103 eV of JENDL-5 and ENDF/B-VIII.0 leads to the same uncertainty value of 153.2 pcm.

The third significant contributor to the total uncertainty of the k_{eff} is Al-27 with three reactions of elastic, (n,γ) and inelastic. This is because aluminum is a major core structural material. The uncertainty values correspond to the reactions are 127.6, 116.4 and 84.7 pcm, respectively. Subsequently, isotopes with remarkable contribution to the uncertainty are Be-9, C-nat, U-238 and O-16 as listed in Table 3.16. Based on the uncertainty analysis, JENDL-5 is noticed the relevant library for the DNRR analysis with the smallest uncertainty. Since U-235 and H-1 are the most contributors to the uncertainty of the DNRR with LEU fuel, the cross section data of the isotopes in thermal energy range need to be paid attention to improve the core physics analysis of the DNRR.

Significant positive sensitivities are observed with U-235, H-1, C-nat, O-16, Be-9 and Al-27 and U-238. Negative sensitivities are significantly contributed by H-1, U-235, Al-27, U-238, B-10, Be-9, C-nat. The uncertainty is found with the capture and elastic scattering of H-1, and the fission of U-235. Subsequently, Al-27 elastic, capture, and inelastic contributions significantly contribute to the uncertainty of the k_{eff}. Other nuclides contribute to remarkable uncertainties of the k_{eff} are Be-9, C-nat and U-238. The total uncertainties of the k_{eff} obtained with ENDF/B-VIII.0, JENDL-5 and JEFF-3.3 are 415.7, 363.0 and 588.0 pcm, respectively. Regarding the uncertainty analysis, ENDF/B-VIII.0 and JENDL-5 are considerably the most reliable for the core analysis of the DNRR with LEU fuel. Attention is recommended on the capture and elastic of H-1 and the fission of U-235 to improve the reliability of the core analysis for the DNRR. The results provide valuable feedback for nuclear data developers to improve cross section evaluations, particularly for H-1, U-235, Al-27, and Be-9. Enhancements in these data would increase the reliability of core simulations for research reactors, improving both safety and efficiency. By identifying main nuclides that significantly affect uncertainty, reactor analysts can enhance nuclear safety margins and improve predictability. Specifically, emphasis should be placed on the capture and elastic scattering of H-1 and the fission of U-235 to further

improve the accuracy of reactor calculations. Since ENDF/B-VIII.0 demonstrated lower uncertainties, they should be prioritized for future core calculations and safety evaluations of the DNRR and similar reactors. Additionally, further benchmarking studies using experimental data are recommended to validate the nuclear data libraries under different reactor conditions, thereby enhancing confidence in their predictive capabilities.

3.3 Evaluation of kinetic parameters

3.3.1 Influence of operational parameters on kinetic parameters

3.3.1.1 *Kinetic characteristics*

To investigate the impact of operational parameters on reactor kinetics, evaluations were conducted to quantify their effects on the kinetic parameters, using the first criticality condition shown in Table 3.1. Table 3.7 provides a comparative assessment of the β_{eff} calculated using two distinct methodologies: the adjoint weighted method and the prompt method. The analysis incorporates four evaluated nuclear data libraries, namely ENDF/B-VIII.0, JEFF-3.3, JENDL-5, and CENDL-3.2. Generally, the adjoint weighted method has slightly higher β_{eff} values than the prompt method, except for the JEFF-3.3 library, where the prompt method predicts a higher value (762 pcm) compared to the adjoint weighted result (753 pcm). In contrast, the ENDF/B-VIII.0 library has the lowest values, with 735 pcm for the adjoint weighted method and 731 pcm for the prompt method. The JENDL-5 and CENDL-3.2 libraries produce identical β_{eff} results (738 pcm) with the adjoint weighted method. The observed differences between the two computational methods remain within 1.2%, indicating strong methodological consistency. Furthermore, the inter library variation in β_{eff} predictions is confined to within 4.0%, reflecting a reasonable level of agreement across the evaluated nuclear data libraries.

Table 3.7: Comparison of the β_{eff} calculated by the adjoint weighted method and prompt method.

Methods	ENDF/B-VIII.0 (pcm)	JEFF-3.3 (pcm)	JENDL-5.0 (pcm)	CENDL-3.2 (pcm)
Adjoint weighted method	735 ± 5	753 ± 5	738 ± 5	738 ± 5
Prompt method	731 ± 6	762 ± 6	731 ± 6	745 ± 6

Table 3.8 summarizes the kinetic parameters, namely the β_{eff}, Λ, and l_p calculated using the adjoint weighted and $1/v$ absorber insertion method. The estimated β_{eff} values span from 735 to 753 pcm, exhibiting modest variation among the libraries. The highest value is obtained with the JEFF-3.3 library (753 pcm), while ENDF/B-VIII.0 has the lowest (735 pcm), corresponding to a relative difference of approximately 2.5%. Notably, JENDL-5 and CENDL-3.2 produce identical β_{eff} estimates of 738 pcm, suggesting strong consistency between these two libraries. The Λ ranges from 80.88 μs to 81.77 μs. The CENDL-3.2 library provides the highest Λ value (81.77 μs), whereas JEFF-3.3 yields the lowest (80.88 μs). The predictions from ENDF/B-VIII.0 (80.96 μs) and JENDL-5 (81.01 μs) differ by merely 0.05 μs, indicating close agreement. Overall, the variation in Λ values across all libraries remains within 1.1%. Similarly, the l_p varies from 80.90 μs to 81.72 μs. Compared to the results of the $1/v$ absorber insertion method, the results of the adjoint weighted method for Λ and l_p are at most 0.3% larger, with a minimum of 0.12%.

Table 3.8: Comparison of the kinetic parameters calculated by the adjoint weighted and the $1/v$ absorber insertion method.

Parameters	ENDF/B-VIII.0	JEFF-3.3	JENDL-5	CENDL-3.2
The adjoint weighted method				
β_{eff} (pcm)	735 ± 5	753 ± 5	738 ± 5	738 ± 5
Λ (μs)	80.96 ± 0.10	80.88 ± 0.10	81.01 ± 0.10	81.77 ± 0.10
l_p (μs)	80.98 ± 0.10	80.90 ± 0.10	81.15 ± 0.10	81.72 ± 0.10
The $1/v$ absorber insertion method				
Λ (μs)	80.76 ± 0.14	80.64 ± 0.15	80.87 ± 0.11	81.67 ± 0.15
l_p (μs)	80.78 ± 0.17	80.66 ± 0.18	81.01 ± 0.15	81.62 ± 0.19

Table 3.9 presents the six group delayed neutron parameters evaluated using the adjoint weighted method, including the group wise delayed neutron yield fractions (β_i) and decay constants (λ_i). These parameters characterize the temporal behavior of delayed neutron emission and are essential for accurately modeling reactor kinetics. Across all evaluated nuclear data libraries, Group 4 contributes the highest fraction of delayed neutrons, with β_4 values ranging from 280 to 293 pcm. Groups 2 and 3 also exhibit significant contributions, with β_i values between 127 and 183 pcm. Notably, JEFF-3.3 yields the highest fractional yields in both Group 2 and Group 3. In contrast, Groups 5 and 6 contribute the least, with Group 6 providing the lowest yield, ranging from 31 to 51 pcm. The decay constant λ_i denotes the rate at which delayed neutron precursors decay, with larger values indicating shorter precursor half lives and, consequently, more rapid neutron emission. Group 1 consistently exhibits the lowest decay constants across all libraries, with λ_1 ranging from 0.012 to 0.013 s^{-1}, corresponding to the longest lived precursors. Conversely, Group 6 displays the highest decay rates, with λ_6 values between 2.857 and 3.555 s^{-1}, reflecting more quick neutron emission. Among the data libraries, JEFF-3.3 predicts the highest decay constant for Group 6 (3.555 s^{-1}). Additionally, JENDL-5 reports the highest decay constant for Group 5 (1.143 s^{-1}). In contrast, ENDF/B-VIII.0 and CENDL-3.2 provide closely aligned decay constants across most groups, with only minor

discrepancies observed in Groups 5 and 6. Group 4 exhibits consistent decay constants across all libraries, with λ_4 values falling within the range of 0.292–0.304 s^{-1}.

Table 3.9: Six group delayed neutron parameters calculated by the adjoint weighted method.

Group	ENDF/B-VIII.0		JEFF-3.3		JENDL-5		CENDL-3.2	
i	β_i (pcm)	λ_i (s^{-1})	β_i (pcm)	λ_i (s^{-1})	β_i (pcm)	λ_i (s^{-1})	β_i (pcm)	λ_i (s^{-1})
1	27 ± 1	0.013	28 ± 1	0.012	25 ± 1	0.012	26 ± 1	0.013
2	132 ± 2	0.033	141 ± 3	0.028	161 ± 3	0.031	131 ± 3	0.033
3	128 ± 2	0.121	183 ± 3	0.133	143 ± 3	0.112	127 ± 3	0.121
4	280 ± 3	0.303	287 ± 4	0.292	293 ± 4	0.302	285 ± 4	0.304
5	118 ± 2	0.851	66 ± 2	0.666	84 ± 2	1.143	118 ± 3	0.862
6	51 ± 1	2.857	48 ± 2	3.555	31 ± 1	3.037	51 ± 2	2.877
Total	735 ± 5	-	753 ± 5	-	738 ± 5	-	738 ± 5	-

Table 3.10: Comparison of kinetic parameters derived from MCNP6 with those obtained from the Serpent 2 code** using ENDF/B-VIII.0.

Parameters	Meulekamp	Chiba	Nauchi	IFP	Perturbation	MCNP6
β_{eff} (pcm)	733.83 ± 0.57	734.07 ± 0.82	732.87 ± 0.61	736.13 ± 2.02	735.36 ± 0.40	735 ± 5
Λ (μs)	-	-	81.92 ± 0.02	81.08 ± 0.05	81.62 ± 0.01	80.96 ± 0.10
l_p (μs)	-	-	81.96 ± 0.02	81.12 ± 0.05	81.66 ± 0.01	80.98 ± 0.10

** The methods presented in Appendix section A.1

The kinetic parameters obtained with the methods are compared to those obtained using MCNP6 as shown in Table 3.10, where β_{eff} is 735 pcm. Compared to this value, the Meulekamp, Chiba, and Nauchi methods produce slightly lower results, with deviations of –0.16%, –0.13%, and –0.29%, respectively. In contrast, the IFP and perturbation methods show higher results, with deviations of +0.15% and +0.05%, respectively. For the Λ, MCNP6 yields a value of 80.96 μs. In comparison, the Nauchi method produces 81.92 μs, which is a relative difference of +1.19%. The perturbation method gives 81.62 μs (+0.81%), while the IFP method reports 81.08 μs, with the smallest deviation of +0.15%. For the l_p, the MCNP6 result is 80.98 μs.

Compared to this, the Nauchi, IFP, and perturbation methods yield values of 81.96 μs, 81.12 μs, and 81.66 μs, corresponding to relative deviations of +1.21%, +0.17%, and +0.84%, respectively. Overall, the IFP method aligns most closely with MCNP6 results across all kinetic parameters. The high consistency of β_{eff}, Λ, and l_p across different methods, with deviations well below 1%, provides strong confidence in the reliability of the simulations and ensures that the derived kinetic parameters can be reliably applied in reactor safety and dynamic analyses. Figure 3.6 shows a comparison of kinetic parameters obtained from MCNP6 with those from the methods of the Sepent 2 code.

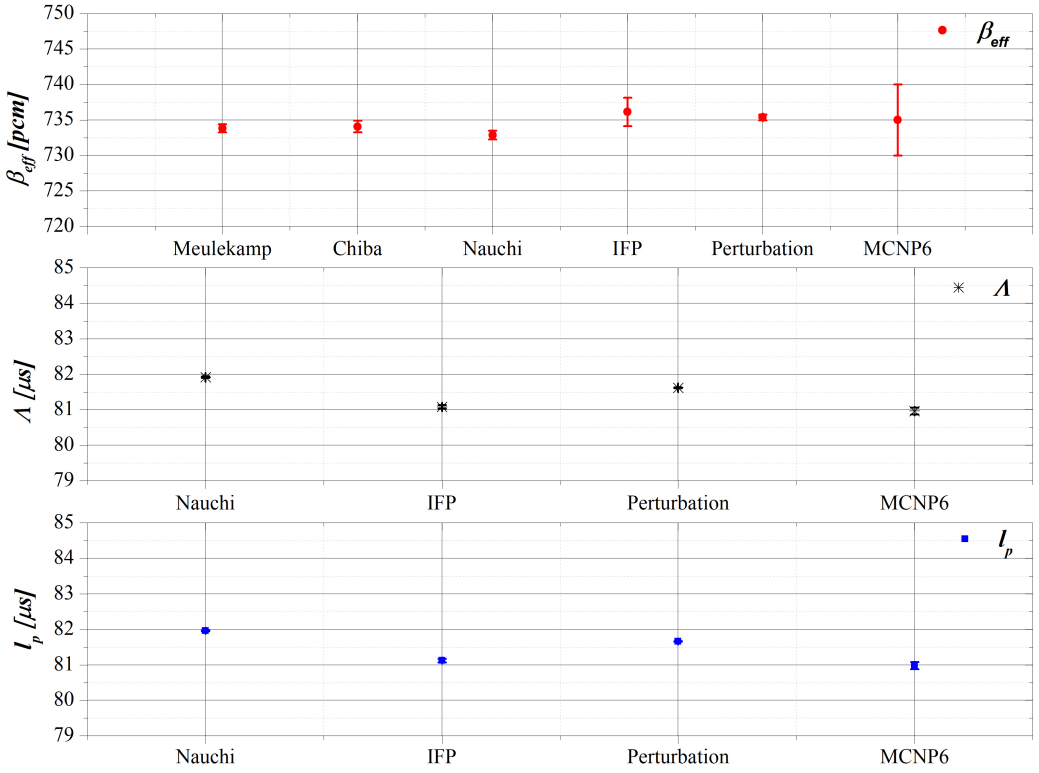

Figure 3.6: Comparison of kinetic parameters calculated using MCNP6 with various methods in the Serpent 2 code.

3.3.1.2 *Dependence of kinetic parameters on fuel burnup using ENDF/B-VIII.0*

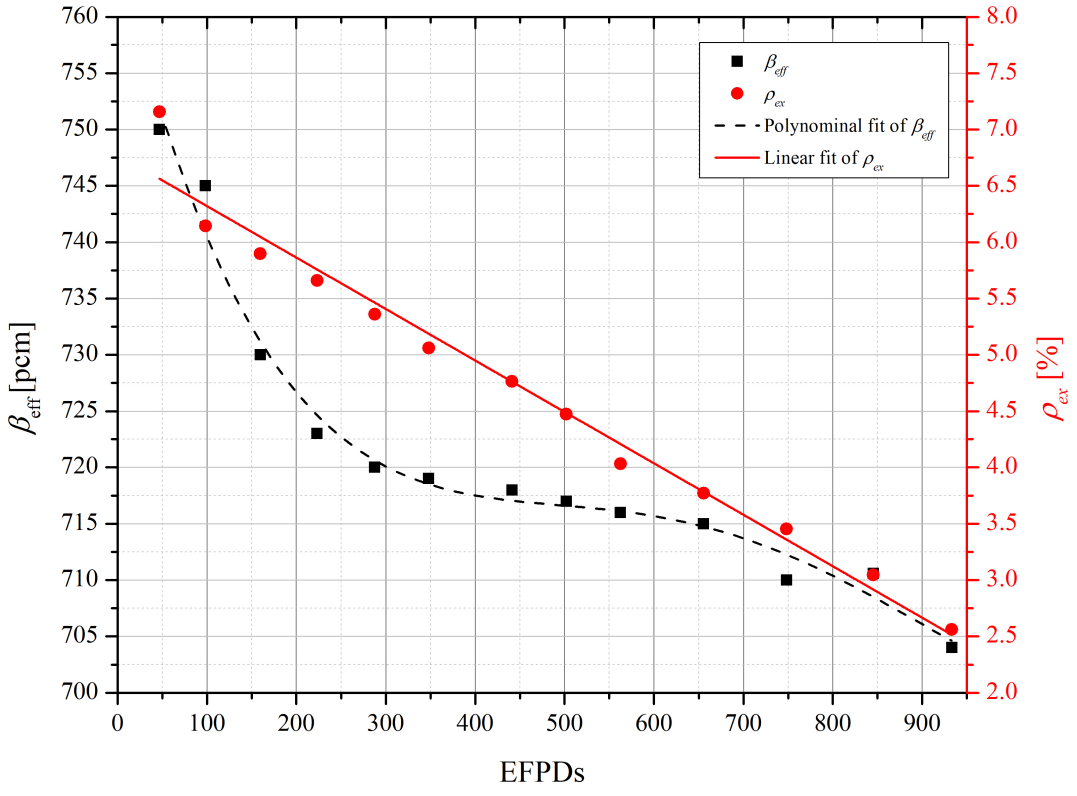

(a) β_{eff} and ρ_{ex}

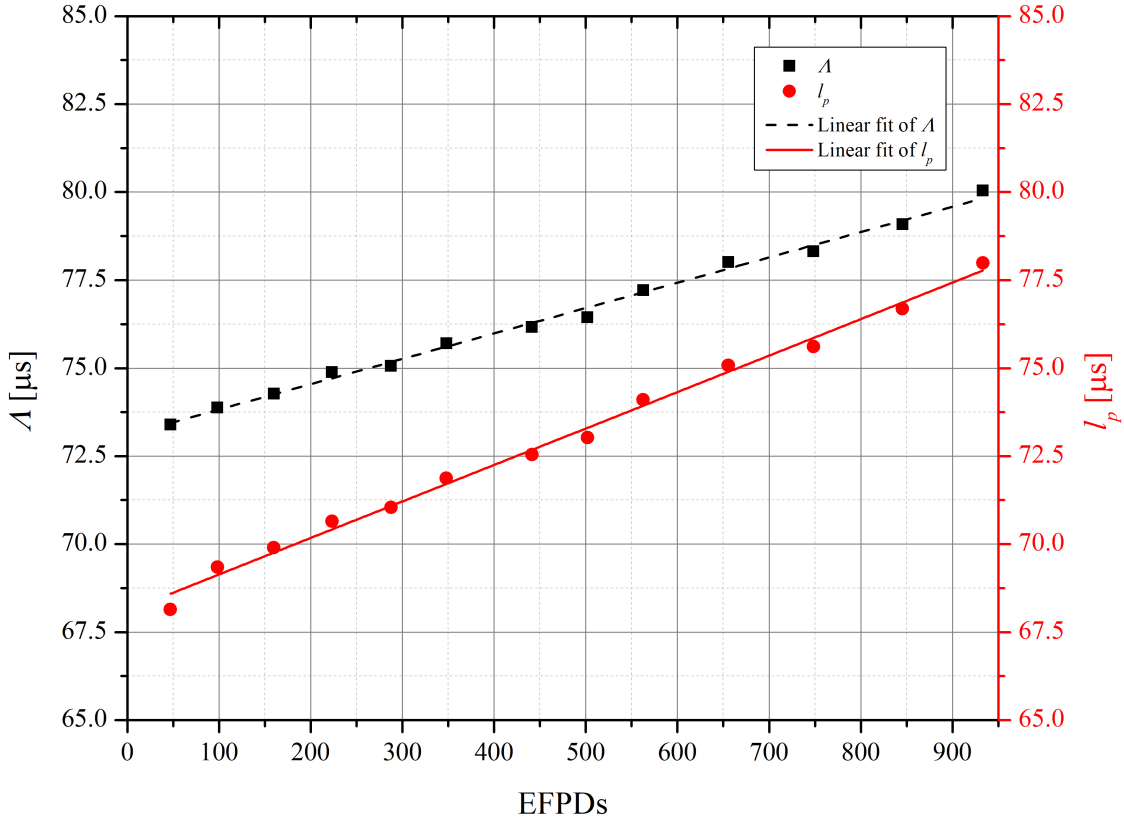

(b) Λ and l_p

Figure 3.7: Variation of the kinetic parameters as functions of burnup.

The study assessed the influence of operational parameters affect reactor kinetics, using simulations with all control rods outside the core. Figure 3.7 displays the kinetic parameters of the DNRR as functions of fuel burnup. Since all uncertainties in evaluating the kinetic parameters are less than 0.7%, individual error values will not be displayed as ranges on the all of figures and will be applied throughout this study. Both the excess reactivity (ρ_{ex}) and the β_{eff} exhibit decreasing trends with burnup, as demonstrated in Figure 3.7(a). The ρ_{ex} decreases linearly with burnup, while the β_{eff} follows a polynomial decline from 750 pcm at the beginning of cycle (BOC) to 704 pcm at the end of cycle (EOC). The decrease in β_{eff} is most pronounced in the early burnup stage (within 250 effective full power days (EFPDs)), followed by a gradual decline in the later burnup stage. This trend is attributed to the reduction of U-235 fissile material, which has a relatively high delayed neutron fraction, and the accumulation of Pu-239, Pu-240, and Pu-241, which have smaller delayed neutron fractions compared to U-235 in the latter burnup stage, along with the effects of neutron spectral hardness as detailed in Appendix section C. The decrease in β_{eff} with burnup implies a larger proportion of fission neutrons being prompt, resulting in a faster kinetic response of the DNRR. Figure 3.7(b) depicts a linear increase in both the Λ and l_p with burnup. The values at the BOC are 73.39 μs and 68.14 μs, while at the EOC, they increase to 80.04 μs and 77.99 μs, respectively. These trends indicate a progressive lengthening of neutron lifetimes due to fuel burnup.

3.3.1.3 *Kinetic parameters versus control rod positions using ENDF/B-VIII.0*

Figure 3.8 illustrates the influence of control rod positions on the kinetic parameters. The reactor remains subcritical with control rod withdrawal of less than 33.5% and becomes supercritical beyond 34.5%. Figure 3.8(a) shows that the β_{eff} decreases slightly from 741 pcm to 722 pcm as the control rods move from full insertion to complete withdrawal.

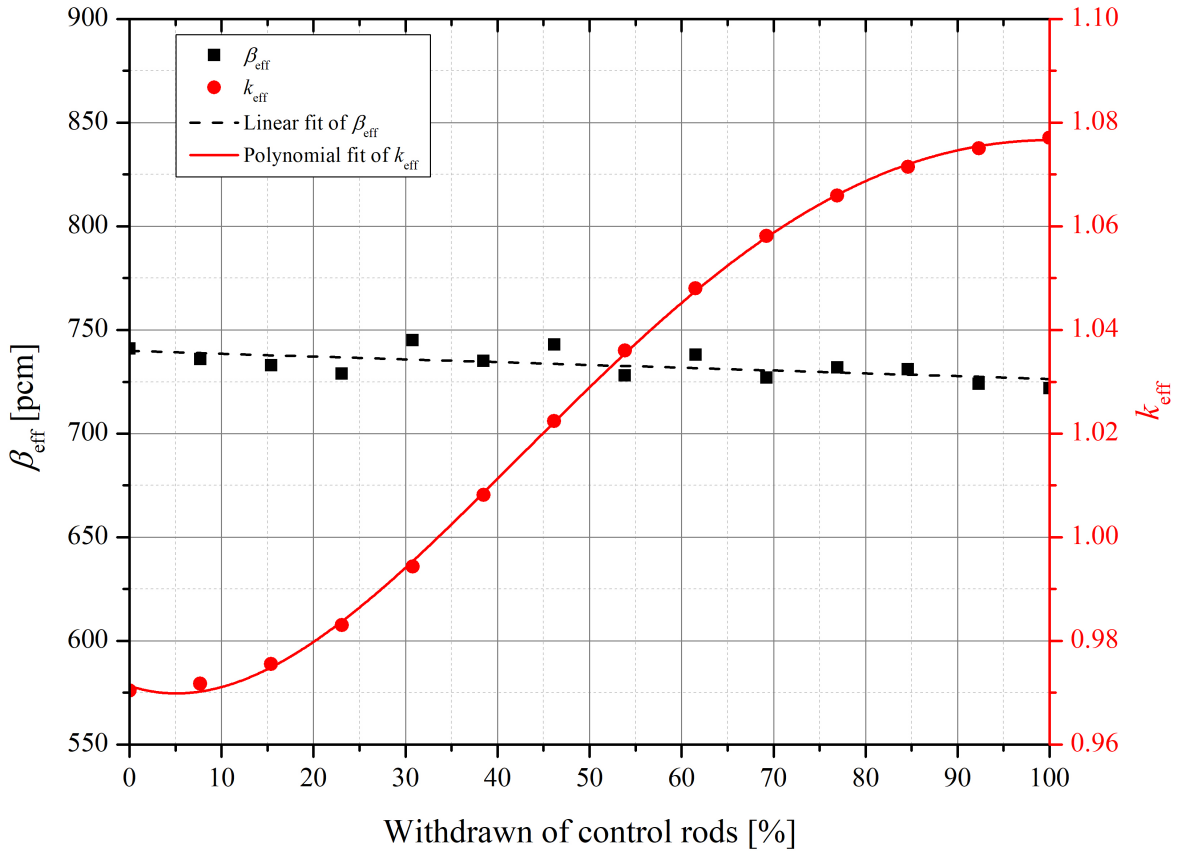

(a) β_{eff} and k_{eff}

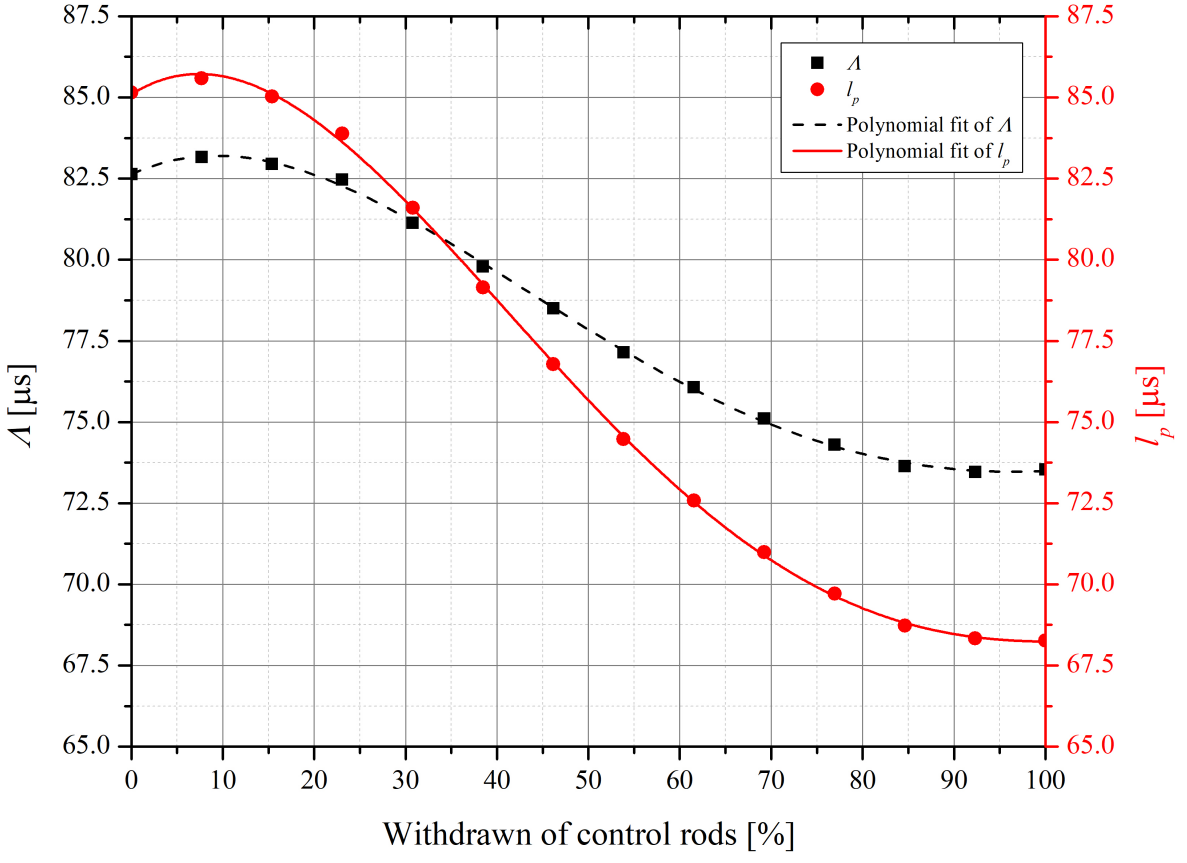

(b) Λ and l_p

Figure 3.8: Variation of the kinetic parameters with respect to control rod positions.

The Λ and l_p decrease similarly with control rod withdrawal. Figure 3.8(b) shows that Λ decreases from 82.63 μs to 73.54 μs, while the l_p decreases from 85.16 μs to 68.27 μs. This pattern illustrates the effective integral characteristic shape of the control rods. Withdrawing the control rods from the core reduces the average prompt neutron lifetime, indicating an increase in fast fission contributions and a reduction in thermal fission. Consequently, this leads to a decrease in the prompt neutron generation time.

3.3.1.4 *Dependence of kinetic parameters on fuel temperature using ENDF/B-VIII.0*

The impact of operational parameters on kinetic behavior was analyzed, referencing the first criticality condition presented in Table 3.1. During the operation of the DNRR, the fuel temperature varies from 20 to 95^oC. Thus, the effect of fuel temperature on the kinetic parameters was evaluated. Figure 3.9 illustrates the lesser effect of fuel temperature on the kinetic parameters. The k_{eff} steadily declines with the increase of fuel temperature due to the Doppler effect. This corresponds to a negative reactivity insertion. Figure 3.9(a) and Figure 3.9(b) indicate that the kinetic parameters are almost unaffected by the change in fuel temperature. Table 3.11 summarizes the kinetic parameters of the DNRR at different reactor operating conditions.

Table 3.11: Summary of the kinetic parameters of the DNRR with 92 LEU fuel bundles.

Parameters	Values	β_{eff} (pcm)	Λ (μs)	l_p (μs)
Fuel burnup	BOC	750	73.39	68.14
	EOC	704	80.04	77.99
CR positions	all CRs in	741	82.63	85.16
	all CRs out	722	73.54	68.27
Fuel temperature	20^oC	738	80.78	80.78
	95^oC	727	80.67	80.55

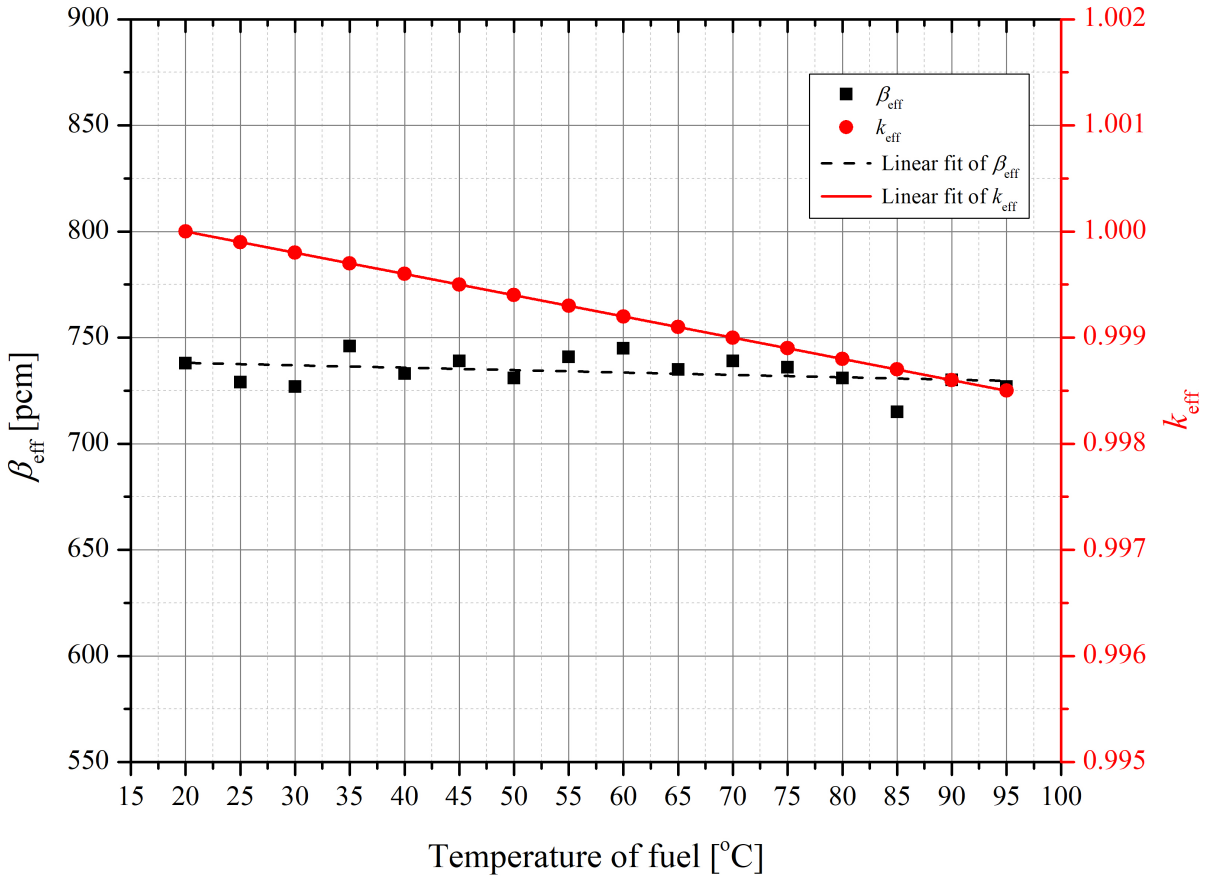

(a) β_{eff} and k_{eff}

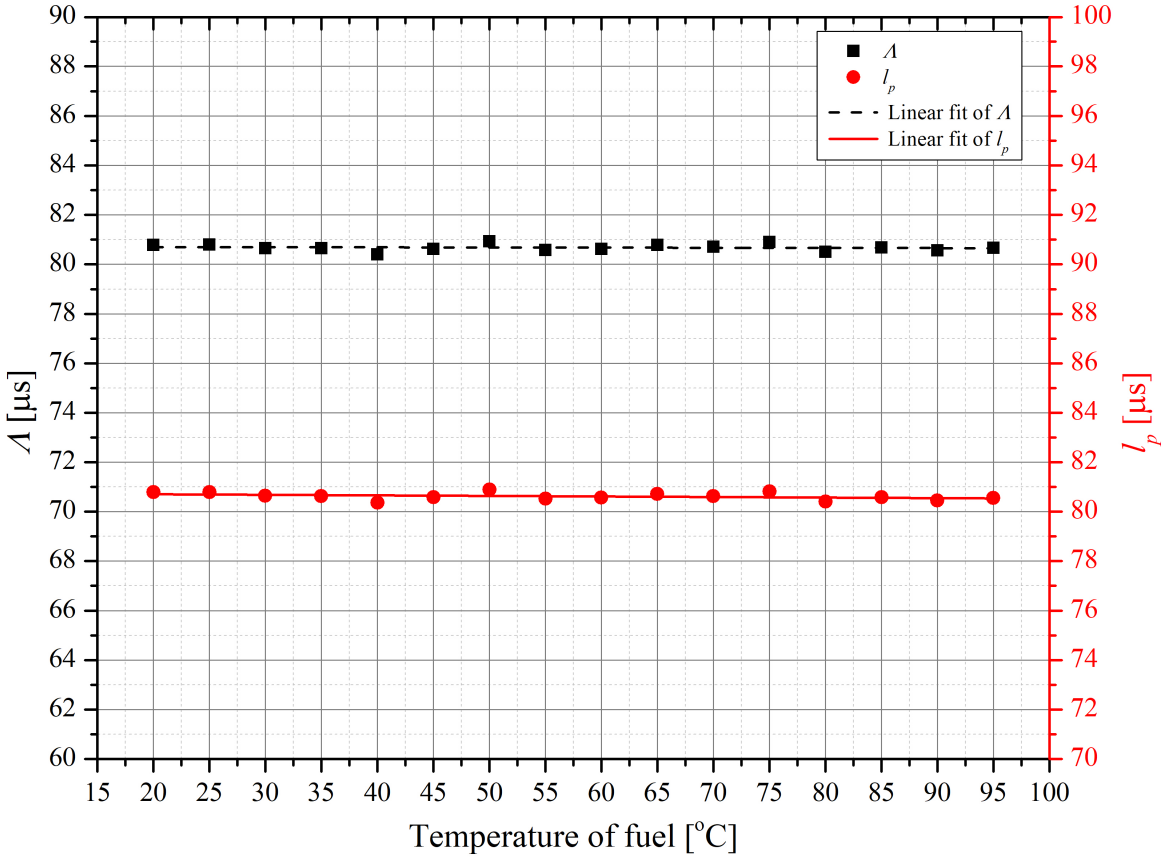

(b) Λ and l_p

Figure 3.9: Variation of the kinetic parameters with respect to the change of fuel temperature.

3.3.1.5 *Dependence of kinetic parameters on burnup using JENDL-5*

The study assessed the influence of operational parameters on reactor kinetics through simulations with all control rods fully withdrawn from the core. The MCNP6 calculations were set up to estimate the k_{eff} of the DNRR with 92 LEU fuel bundles, with the standard deviation (1σ) of 15–21 pcm. Figure 3.10(a) depicts the dependence of the β_{eff} as a function of burnup obtained from the adjoint weighted method. It can be seen that the β_{eff} decreases rapidly in the first 200 effective full power days (EFPD), which is then followed by a gradual decline. The β_{eff} decreases from the BOC to the EOC (800 EFPD) by about 52 pcm. The adjoint weighted method predicts the β_{eff} values of 760 pcm at the BOC and 708 pcm at the EOC, respectively. The excess reactivity ρ_{ex} decreases approximately linearly with the EFPDs. At the BOC, ρ_{ex} is about 6.1%, and it gradually decreases as fuel burnup increases, reaching approximately 1.9% at the EOC. This reduction is mainly attributed to the depletion of U-235 and the accumulation of neutron absorbing fission products during reactor operation, which reduce the neutron economy of the core. The observed trend reflects the progressive consumption of excess reactivity with fuel burnup, which is a typical behavior in research reactor core operation such as the DNRR.

Figure 3.10(b) presents the l_p as a function of burnup obtained from the adjoint weighted method. The l_p increases linearly with burnup due to the decrease of the production rate. The l_p values at the BOC and the EOC are 79.01 and 82.76 µs, respectively.

Table 3.12: The β_{eff} calculated by the adjoint weighted method and the prompt method.

Parameter	Adjoint weighted		Prompt	
	BOC	EOC	BOC	EOC
β_{eff} (pcm)	760 ± 4	708 ± 21	748 ± 9	700 ± 18

Table 3.12 shows the β_{eff} values of the DNRR core at the BOC and the EOC in comparison between the adjoint weighted method and the prompt method. The prompt method estimated the β_{eff} lower than those from the

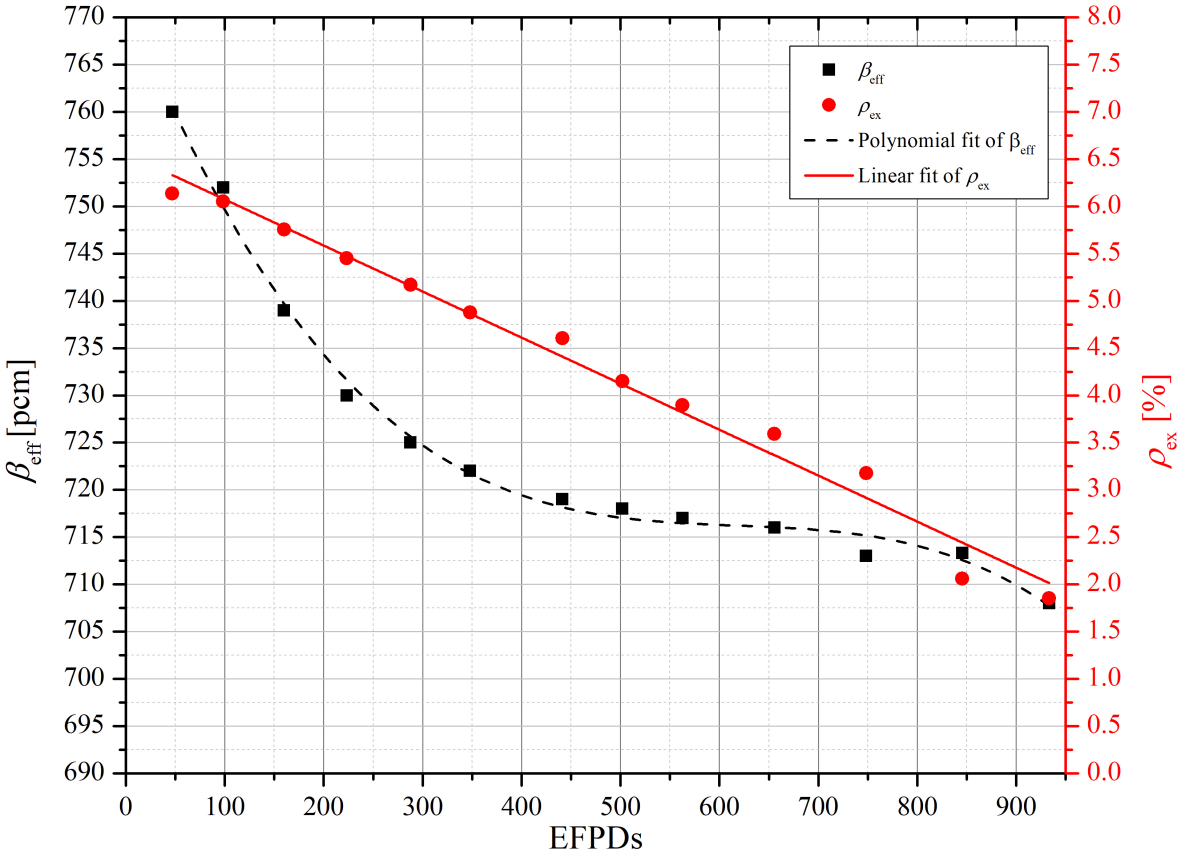

(a) β_{eff} and ρ_{ex}

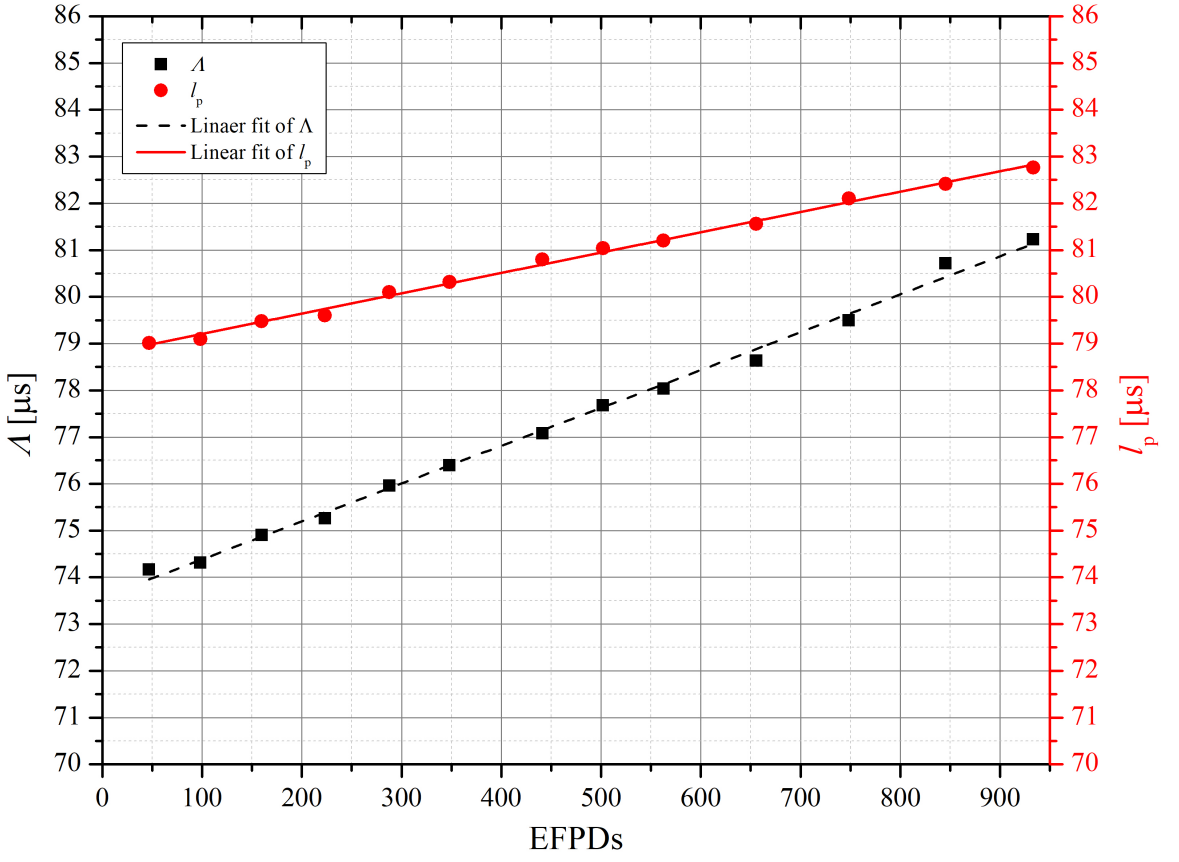

(b) Λ and l_p

Figure 3.10: Variation of the kinetic parameters as functions of burnup.

adjoint weighted method by about 8–12 pcm. Comparing between the two methods, a good agreement was found with the discrepancy less than 1.6%.

Compared to other research reactors, the β_{eff} of the first core of the RSG GAS using MVP3 and MCNP6.2 with various data libraries was reported to be approximately 738.3 pcm [119]. The β_{eff} of the TRIGA Mark II reactor was 800 pcm for a small core (43 fuel rods) and 750 pcm for a full core (90 fuel rods), respectively [120]. Thus, the β_{eff} values obtained for the DNRR are approximate to those of other research reactors.

Table 3.13: The Λ and l_p calculated by the adjoint weighted and the $1/v$ insertion methods.

Parameter	Adjoint weighted		$1/v$ insertion	
	BOC	EOC	BOC	EOC
Λ (µs)	74.16 ± 0.11	81.22 ± 0.15	74.83 ± 0.35	81.44 ± 0.20
l_p (µs)	79.01 ± 0.11	82.76 ± 0.15	79.72 ± 0.45	82.98 ± 0.19

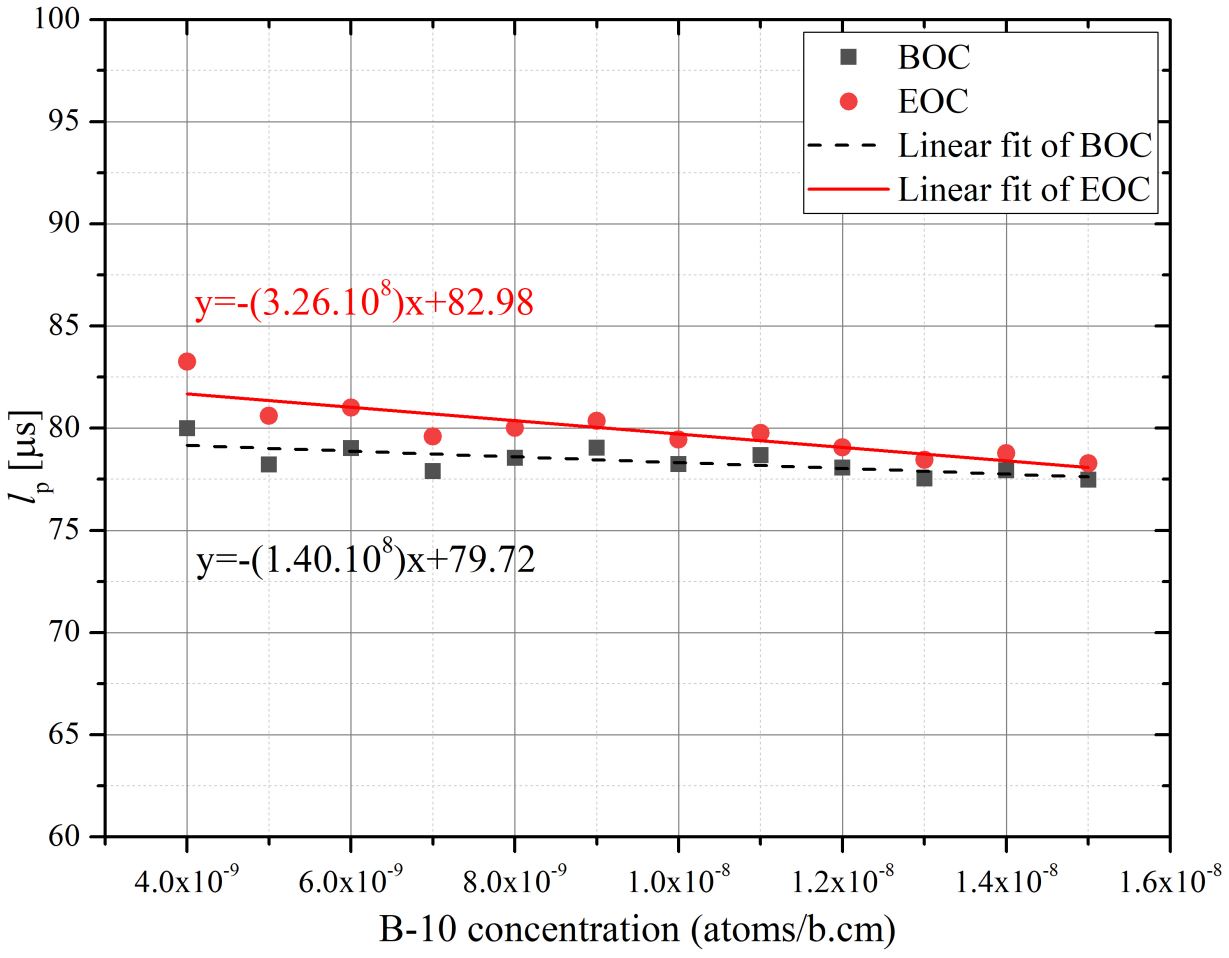

Figure 3.11: The l_p as a function of B-10 concentration at the BOC and the EOC obtained from the $1/v$ absorber insertion method.

Table 3.13 presents the calculated values of the Λ and l_p using the adjoint weighted and $1/v$ insertion methods. The values of Λ at the BOC and the EOC obtained by using the adjoint weighted method and the JENDL-5 library are 86.99 and 82.41 µs, respectively.

Figure 3.11 depicts the determination of the l_p values using the $1/v$ absorber insertion method by varying the B-10 concentration from 4.0×10^{-9} to 1.5×10^{-8} atoms/(b·cm). The l_p values at the BOC and the EOC are 79.72 and 82.98 µs, respectively. Comparing between the two methods, the discrepancy of the l_p values is within 1%.

3.3.2 Sensitivity analysis of the effectively delayed neutron fraction

The sensitivity analysis of β_{eff} was conducted using the same core configuration as that employed for the k_{eff} analysis in Section 3.2.2.2. Tables 3.14 and 3.15 present a comprehensive sensitivity analysis of the β_{eff} for various nuclear reaction channels of key isotopes. The analysis was performed using four evaluated nuclear data libraries: ENDF/B-VIII.0, JEFF-3.3, JENDL-5, and CENDL-3.2. To ensure clarity and relevance, only the most significant sensitivity coefficients defined as those with an absolute value exceeding 0.1% in the ENDF/B-VIII.0 are reported and arranged in descending order. The tables include the relative sensitivity coefficients (in percentage), which quantify the impact of perturbations in specific nuclear reaction cross sections on the calculated value of β_{eff}. Furthermore, inter library comparisons are provided in the form of ratios denoted as JF3/E8, J5/E8, and C3/E8 that represent the sensitivity coefficients from each library normalized to the ENDF/B-VIII.0 results.

The delayed neutron yield reaction (delayed ν) of U-235 exhibits the highest positive sensitivity among all nuclear reactions analyzed in the study, with values ranging from approximately 96% to 98% across the evaluated nuclear data libraries. Specifically, CENDL-3.2 yields the lowest sensitivity coefficient at 96.16%, whereas JENDL-5 reports the highest at 98.48%. The inter library sensitivity ratios, which are JF3/E8, J5/E8, and C3/E are found to be 0.98, 1.00, and 0.98, respectively. The dominant sensitivity of the U-235

Table 3.14: Positive sensitivities of the β_{eff}, listed in descending order of magnitude according to the ENDF/B-VIII.0 library*.

Isotope	Reaction	ENDF/B-VIII.0 ($\times 10^{-1}$)	JEFF-3.3 ($\times 10^{-1}$)	JF3/E8	JENDL-5.0 ($\times 10^{-1}$)	J5/E8	CENDL-3.2 ($\times 10^{-1}$)	C3/E8
U-235	delayed ν	98.13	96.65	0.98	98.48	1.00	96.16	0.98
Lwtr $S(\alpha,\beta)$	inelastic	29.64	71.12	2.40	21.02	0.71	–	–
Al-27	elastic	10.09	-4.65	-0.46	20.51	2.03	-8.09	-0.80
C-nat $S(\alpha,\beta)$	inelastic	5.23	-7.34	-1.40	6.20	1.19	–	–
Al-27	total	5.10	-11.31	-2.22	15.71	3.08	-9.83	-1.93
Be $S(\alpha,\beta)$	inelastic	1.88	-1.04	-0.55	20.09	10.69	–	–
Fe-56	elastic	1.68	-1.94	-1.16	-2.20	-1.31	-2.36	-1.41
U-235	elastic	1.35	0.95	0.71	2.22	1.65	1.51	1.12
U-238	delayed ν	1.30	1.30	1.00	1.36	1.05	1.38	1.06
Fe-56	total	1.13	-2.05	-1.82	-2.34	-2.07	-2.24	-1.98
Be-9	(n,α)	0.60	0.39	0.66	0.25	0.42	0.60	0.99
U-238	(n,γ)	0.60	-0.07	-0.11	0.87	1.45	0.50	0.83
Be-9	(n,γ)	0.58	0.72	1.23	0.37	0.64	0.74	1.27
U-238	fission	0.50	-0.44	-0.87	-0.39	-0.79	0.50	0.99
U-238	total ν	0.30	-0.59	-1.93	-0.59	-1.93	0.32	1.07
O-16	(n,γ)	0.25	1.13	0.51	0.03	0.14	0.11	0.44
O-16	(n,α)	0.24	0.173	0.52	0.04	0.15	0.11	0.45
U-235	inelastic	0.14	0.38	2.77	-0.62	-4.50	0.54	3.91
U-234	inelastic	0.11	-0.07	-0.66	0.05	0.47	0.01	0.10

* Absolute value $> 0.1\%$.

(delayed ν) reaction can be explained by the fact that β_{eff} is directly governed by the delayed neutron yield produced during U-235 fission. Consequently, any variation in the delayed neutron yield data leads to a corresponding change in β_{eff}, resulting in the very large positive sensitivity observed in this study.

The thermal inelastic scattering of light water, represented through the $S(\alpha,\beta)$, exhibits the second highest sensitivity concerning the β_{eff}, yet demonstrates considerable variation across the evaluated nuclear data libraries. Specifically, JEFF-3.3 predicts a pronounced impact with a sensitivity coefficient of 71.12%, in stark contrast to the lower values reported by ENDF/B-VIII.0 (29.64%) and JENDL-5 (21.02%). The CENDL-3.2 library does not have available data for this reaction channel. The calculated inter library sensitivity ratio, JF3/E8, is 2.40, indicating that JEFF-3.3 assigns 2.4 times greater influence to thermal scattering in light water than ENDF/B-VIII.0. This behavior reflects the important role of light water as the neutron moderator in the reactor core. The $S(\alpha,\beta)$ thermal scattering data determine the energy redistribution of neutrons in the thermal region, thereby shaping the neutron spectrum.

Table 3.15: Negative sensitivities of the β_{eff}, listed in descending order of magnitude according to the ENDF/B-VIII.0 library*.

Isotope	Reaction	ENDF/B-VIII.0 ($\times 10^{-1}$)	JEFF-3.3 ($\times 10^{-1}$)	JF3/E8	JENDL-5.0 ($\times 10^{-1}$)	J5/E8	CENDL-3.2 ($\times 10^{-1}$)	C3/E8
U-235	prompt ν	-98.21	-95.91	0.98	-97.73	1.00	-96.25	0.98
H-1	total	-50.51	31.12	-0.62	-51.64	1.02	-47.39	0.94
H-1	elastic	-49.99	26.17	-0.52	-49.65	0.99	-47.46	0.95
O-16	total	-49.66	-24.29	0.49	12.33	-0.25	17.17	-0.35
O-16	elastic	-49.63	-24.28	0.49	12.29	-0.25	16.88	-0.34
Be $S(\alpha,\beta)$	elastic	-27.07	-32.15	1.19	-2.42	0.09	–	–
Be $S(\alpha,\beta)$	total	-25.19	-33.19	1.32	17.67	-0.70	–	–
Be-9	elastic	-24.86	6.54	-0.26	9.17	-0.37	8.77	-0.36
Be-9	total	-24.52	5.27	-0.21	8.39	-0.34	8.77	-0.36
C-nat	total	-19.19	1.62	-0.08	26.04	-1.36	10.67	-0.56
C-nat	elastic	-19.01	1.90	-0.10	25.93	-1.36	10.94	-0.58
C-nat $S(\alpha,\beta)$	elastic	-7.89	-0.73	0.09	14.38	-1.82	–	–
U-235	fission	-7.40	-2.78	0.38	-0.48	0.06	0.72	-0.10
U-235	total	-7.37	-1.96	0.27	0.25	-0.03	2.92	-0.40
Al-27	inelastic	-4.18	-7.03	1.68	-3.55	0.85	-2.10	0.50
C-nat $S(\alpha,\beta)$	total	-2.65	-8.07	3.04	20.58	-7.76	–	–
U-235	(n,γ)	-1.54	-0.57	0.37	-0.72	0.47	0.11	-0.07
U-238	elastic	-1.36	4.72	-3.46	-4.44	3.26	5.74	-4.21
U-238	prompt ν	-1.00	-1.88	1.89	-1.95	1.96	-1.05	1.05
B-10	total	-0.92	-0.14	0.15	0.57	-0.62	-0.64	0.69
Al-27	(n,γ)	-0.91	0.22	-0.25	-1.16	1.27	0.29	-0.32
U-238	total	-0.87	5.23	-6.01	-2.55	2.92	5.83	-6.69
B-10	(n,α)	-0.80	-1.27	1.58	0.53	-0.66	-0.69	0.87
B-10	(n,γ)	-0.78	-1.26	1.62	0.53	-0.69	-0.69	0.88
U-238	inelastic	-0.67	0.91	-1.37	1.38	-2.08	-1.02	1.53
H-1	(n,γ)	-0.52	4.92	-9.44	-1.98	3.80	0.05	-0.10
Fe-56	inelastic	-0.33	0.13	-0.40	-0.42	1.27	-0.13	0.40
O-16	inelastic	-0.28	-0.15	0.54	-0.01	0.04	0.16	-0.60
Fe-56	(n,γ)	-0.22	-0.24	1.13	0.28	-1.29	0.27	-1.25
U-234	elastic	-0.21	0.02	-0.10	-0.47	2.20	0.13	-0.63
B-10	elastic	-0.21	1.12	-5.27	0.13	-0.61	0.04	-0.21
C-nat	(n,γ)	-0.11	0.12	-1.07	-0.13	1.19	-0.02	0.14
U-235	total ν	-0.11	0.77	-7.06	0.54	-5.06	-0.14	1.29

* Absolute value $> 0.1\%$.

Al-27, C-nat ($S(\alpha,\beta)$), and Be ($S(\alpha,\beta)$) showcase next sensitivity contributions in both elastic and inelastic reactions in ENDF/B-VIII.0, particularly in JENDL-5, which predicts a 20.51% sensitivity for Al-27 elastic scattering, in contrast to -4.65% in JEFF-3.3 and -8.09% in CENDL-3.2. This emphasizes that structural and moderator materials significantly affect the sensitivity of β_{eff}. The ratio of J5/E8 in Be ($S(\alpha,\beta)$) is 10.69, so JENDL-5 predicts an effect that is 10 times stronger than ENDF/B-VIII.0, and the ratio of J5/E8 in Al-27 total reaction is 3.08, so JENDL-5 is three times greater than ENDF/B-VIII.0. U-235 (prompt ν) reaction has a strong negative sensitivity (-96% to -98%). JEFF-3.3 has a slightly weaker negative

impact (-95.91%) than ENDF/B-VIII.0 (-98.21%). Elastic scattering of H-1 and O-16 shows strong negative sensitivities in ENDF/B-VIII.0 (-49.99% and -49.63%). JEFF-3.3, however, predicts a positive contribution for H-1 (26.17%), whereas CENDL-3.2 reports a negative value (-47.46%). This suggests significant differences in how neutron scattering in hydrogen is across libraries.

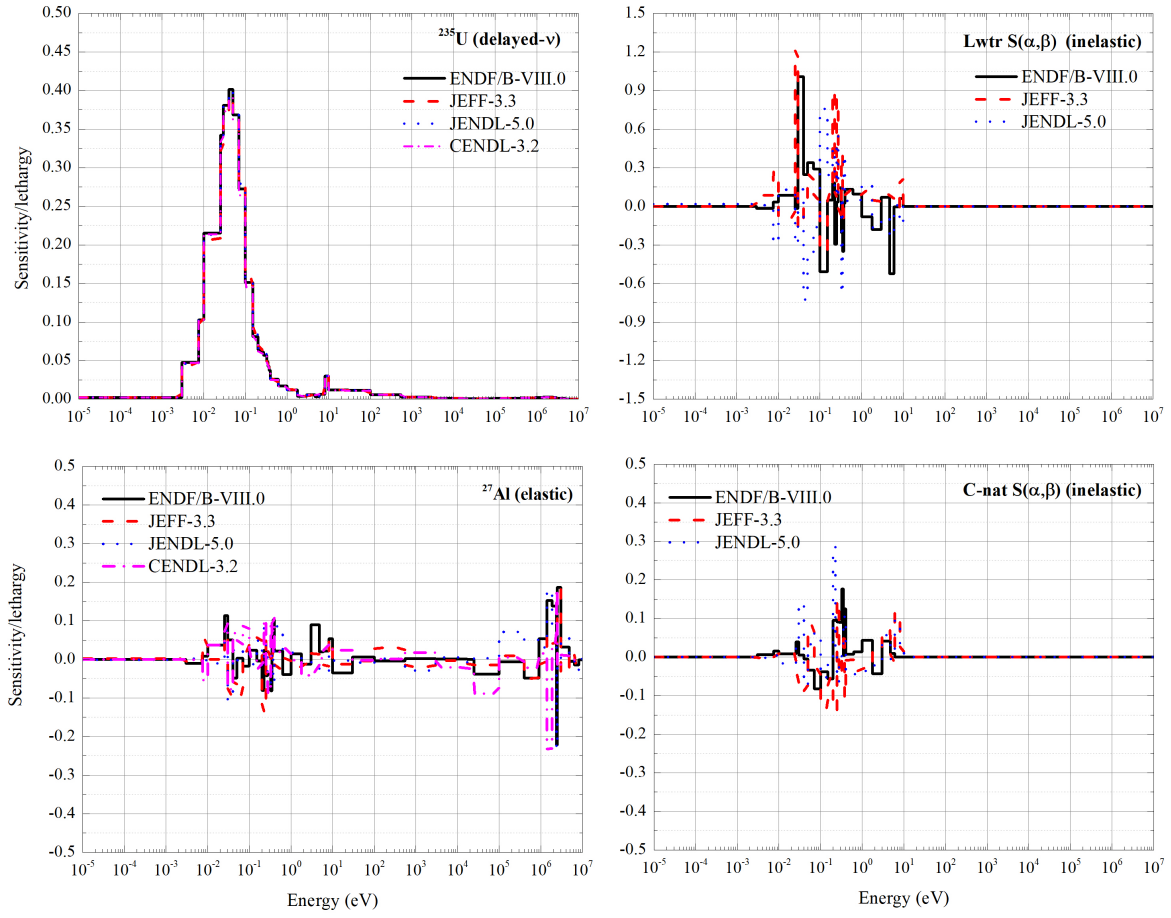

Figure 3.12: Energy dependent sensitivities of the β_{eff} of U-235, Lwtr-S(α, β), Al-27, and C-nat-S(α, β)

Figure 3.12 presents the energy dependent sensitivities of cross sections impacting the β_{eff} for four main reactions across different nuclear data libraries. The U-235 (delayed ν) reaction shows a significant positive sensitivity peak occurring between 10^{-2} and 10^{-1} eV, corresponding to the thermal energy region. The sensitivity decreases to nearly zero at higher neutron energies (above 1 MeV), indicating that fast fission contributes very little to

delayed neutron production. Lwtr $S(\alpha, \beta)$ inelastic and C-nat $S(\alpha, \beta)$ inelastic scattering exhibit sensitivity fluctuations in the thermal region from 10^{-2} to 10^{1} eV. Al-27 (elastic scattering) demonstrates low but fluctuating sensitivity across the neutron energy spectrum.

Figure 3.13 illustrates the energy dependent sensitivities of cross sections affecting the β_{eff} for four isotopes: Al-27 (total), Be-$S(\alpha, \beta)$ (inelastic), Fe-56 (elastic), and U-235 (elastic). The reactions of Al-27 (total), Fe-56 (elastic), and U-235 (elastic) demonstrate variations in sensitivity across all energy ranges, while Be-$S(\alpha, \beta)$ inelastic scattering is mainly significant in the thermal energy range.

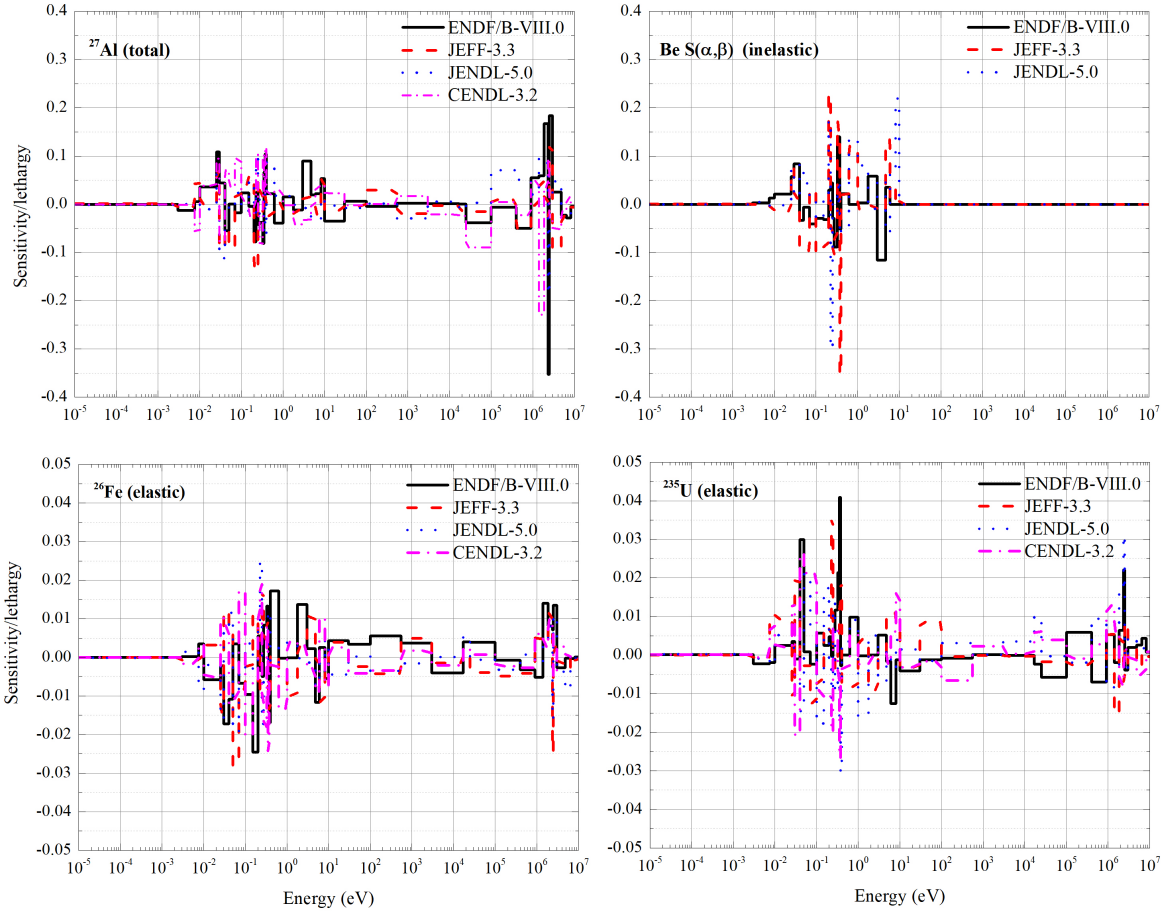

Figure 3.13: Energy dependent sensitivities of the β_{eff} of Al-27, Be-S(α, β), Fe-56, and U-235.

Figure 3.14 illustrates the energy dependent sensitivity cross sections

impacting the β_{eff} for U-235, H-1, and O-16 regarding the reactions of prompt-ν, total and elastic, and total, respectively. The U-235 (prompt-ν) reaction shows significant negative sensitivity, particularly in the low energy range (less than 10 eV). A more significant negative sensitivity is observed between 10^{-2} eV and 10^{-1} eV. This indicates that an increase in prompt neutron emission from U-235 affects a decrease in β_{eff}. The total and elastic H-1 reactions exhibit minor fluctuations in thermal and epithermal energies (less than 10^{1} eV) and more pronounced variations in the fast neutron region ($10^{3} - 10^{7}$ eV). The O-16 total reaction demonstrates relatively small yet noticeable fluctuations in sensitivity across all neutron energies.

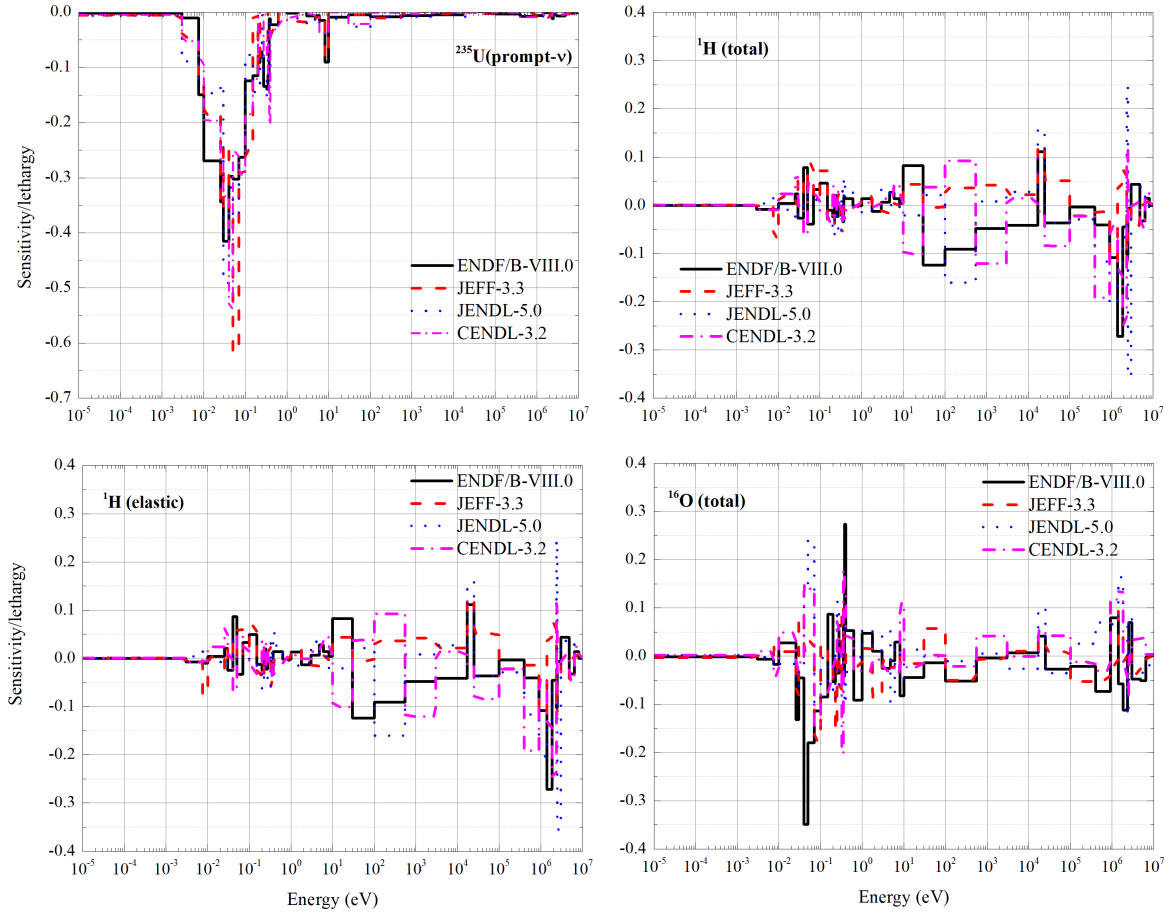

Figure 3.14: Energy dependent sensitivities of the β_{eff} of U-235, H-1, and O-16.

Figure 3.15 illustrates the energy dependent sensitivities of cross sections impacting the β_{eff} for four distinct reactions: the elastic scattering of O-16, the elastic scattering of Be-$S(\alpha, \beta)$, the total reaction of Be-$S(\alpha, \beta)$,

and the elastic scattering of Be-9. The O-16 elastic scattering demonstrates varying sensitivity across all neutron energy ranges. In the thermal and epithermal regions (below 10^{-2} eV), the sensitivity is nearly zero, indicating a minimal impact on β_{eff}. Be-$S(\alpha,\beta)$ elastic scattering and the total reaction show sensitivity across the low energy range ($10^{-2} - 1.0$ eV). CENDL-3.2 lacks data on thermal scattering of Be-$S(\alpha,\beta)$. The Be-9 elastic scattering exhibits energy dependent sensitivity to cross section effects on β_{eff} at high neutron energies ($10 - 10^{7}$ eV).

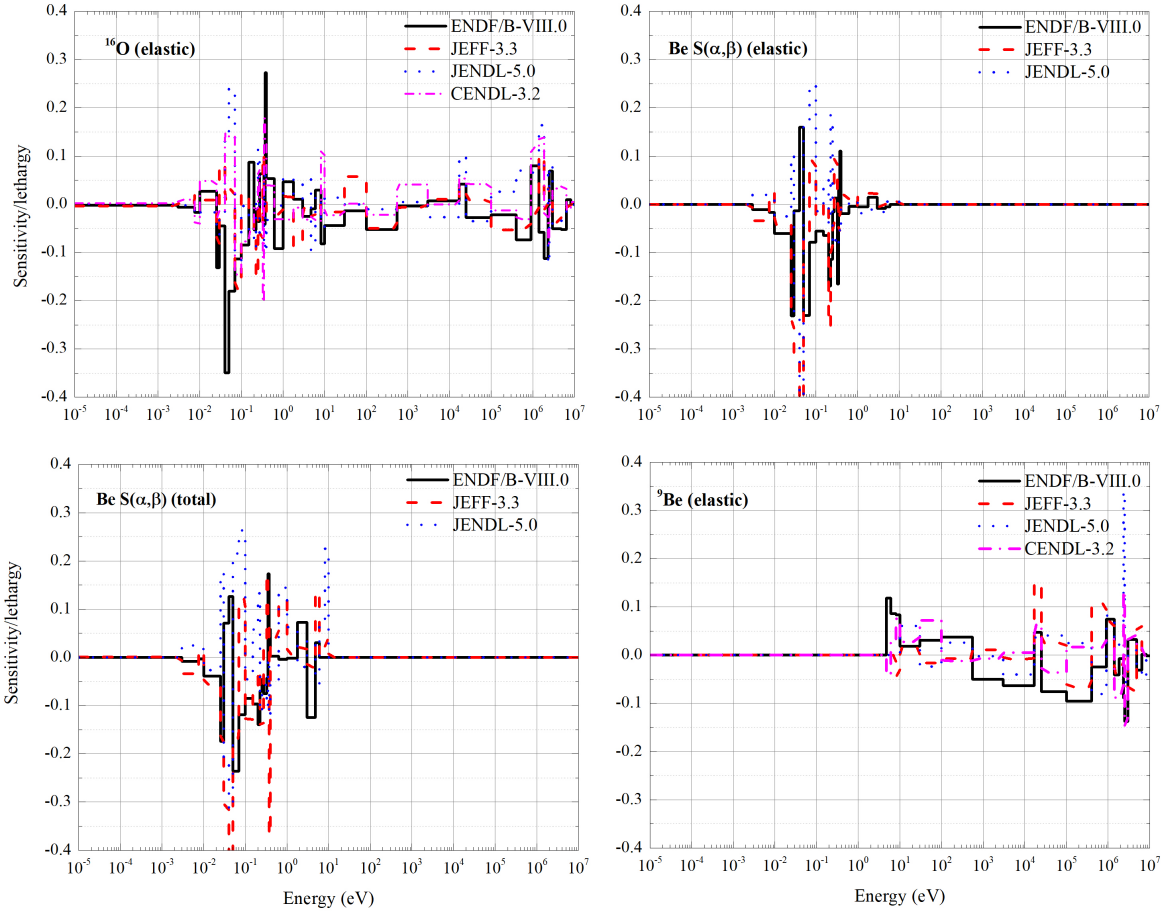

Figure 3.15: Energy dependent sensitivities of the β_{eff} of O-16, Be-S(α,β), and Be-9.

3.3.3 Uncertainty analysis of the effectively delayed neutron fraction

Table 3.16 presents the uncertainties in β_{eff} caused by variations in different nuclear reaction cross sections. These uncertainties correspond to

Table 3.16: The β_{eff} uncertainties for the reactions of the primary isotopes are listed in order of decreasing magnitude based on the ENDF/B-VIII.0 dataset.

Isotope	Reaction	ENDF/B-VIII.0 (pcm)	JEFF-3.3 (pcm)	JF3/E8	JENDL-5 (pcm)	J5/E8
Total	-	1312.2	1021.0	0.78	471.4	0.36
Al-27	elastic	811.2	617.7	0.8	-	-
Be-9	elastic	755.8	-	-	-	-
H-1	elastic	360.0	23.1	0.06	241.9	0.67
Al-27	inelastic	351.8	311.9	0.89	-	-
B-10	n,γ	344.7	530.9	1.54	209.2	0.61
Be-9	n,2n	194.3	-	-	-	-
O-16	elastic	124.8	450.4	3.61	48.7	0.39
O-16	n,γ	123.6	61.9	0.50	28.2	0.23
Be-9	n,γ	120.0	-	-	-	-
C-nat	elastic	109.0	48.3	0.44	-	-
U-238	elastic	93.5	135.6	1.45	242.0	2.59
O-16	inelastic	81.7	16.4	0.20	26.8	0.33
U-235	elastic	49.2	95.3	1.94	98.2	1.99
B-10	elastic	36.5	26.4	0.72	10.6	0.29
U-235	fission	34.0	114.7	3.37	41.6	1.22
Fe-56	inelastic	28.0	8.8	0.32	42.5	1.52
Be-9	n,α	27.7	-	-	-	-
U-238	inelastic	26.8	82.2	3.07	160.0	5.98
U-234	elastic	26.6	6.7	0.25	51.3	1.93
Fe-56	elastic	24.9	57.7	2.32	105.6	4.24
U-234	inelastic	19.8	17.4	0.88	10.8	0.55
U-235	inelastic	18.8	59.0	3.14	42.4	2.26
Al-27	n,γ	16.6	10.4	0.62	-	-
O-16	n,α	14.1	4.3	0.31	6.6	0.47
Fe-56	n,γ	11.2	6.9	0.62	30.7	2.74
H-1	n,γ	10.8	125.6	11.61	41.0	3.79
U-238	n,γ	8.7	10.2	1.17	12.0	1.38
B-10	n,α	7.0	1.2	0.18	2.6	0.37
C-nat	n,γ	6.7	3.4	0.51	-	-
U-238	fission	6.6	22.4	3.40	3.7	0.56
U-235	n,γ	5.6	11.5	2.06	9.4	1.67

three nuclear data libraries: ENDF/B-VIII.0, JEFF-3.3, and JENDL-5, along with their relative ratios JF3/E8 and J5/E8, which evaluate JEFF-3.3 and JENDL-5 in comparison to ENDF/B-VIII.0. The total uncertainties obtained with the libraries are 1312.2, 1021.0, and 471.4 pcm, respectively. Compared to ENDF/B-VIII.0, the uncertainties obtained with JEFF-3.3 and JENDL-5 are smaller by approximately 22.2% and 64.1%, respectively. It is

noted that the covariance data are not available in JEFF-3.3 and JENDL-5 for some isotopes, such as Al-27, Be-9, and C-12; thus, the uncertainties concerning the capture, (n,2n), (n,α), elastic, and inelastic scattering of Al-27, Be-9, and C-12 are not available. This reduces the uncertainties of JEFF-3.3 and JENDL-5 compared to ENDF/B-VIII.0, which are 1097.8 and 2393.1 pcm, respectively. Assuming that the uncertainties of the reactions involving missing isotopes from the libraries JEFF-3.3 and JENDL-5 are obtained from the library ENDF/B-VIII.0, the total uncertainties for the libraries ENDF/B-VIII.0, JEFF-3.3, and JENDL-5 are 1312.2, 1291.0, and 1280.8 pcm, respectively. These results indicate that JENDL-5 has the least uncertainty.

Figures B.4–B.7 in Appendix section B illustrate the data covariances for the reactions of Al-27 (n, elastic), H-1 (n, elastic), B-10 (n, capture), and O-16 (n, elastic). Figure B.4(a) of Appendix section B provides an example of the data covariances for the Al-27 (n, elastic) reactions from ENDF/B-VIII.0. The left plot displays the percent standard deviation in the Al-27 (n, elastic) cross section. The top plot presents the cross section for the Al-27 (n, elastic) reactions. The center plot depicts the correlations between the Al-27 (n, elastic) cross section at one energy and its values at other energies. Figure B.4 in Appendix section B illustrates the cross section for the Al-27 (n, elastic) reaction, indicating that ENDF/B-VIII.0 and JEFF-3.3 remain consistent across all energy ranges; however, the percentage standard deviation of this reaction differs, with a maximum difference of approximately 15% for ENDF/B-VIII.0 and about 9% for JEFF-3.3 at 10^4 eV. The covariance data for this reaction are not available in JENDL-5.

The reactions that primarily contribute to the uncertainties of the β_{eff} are the elastic reactions of Al-27, Be-9, and H-1, with corresponding uncertainty values of 811.2, 755.8, and 360.0 pcm, respectively, as determined by ENDF/B-VIII.0. The significant uncertainty contribution from Al-27 elastic scattering is 811.2 pcm in ENDF/B-VIII.0 and 617.7 pcm in JEFF-3.3, while it is not available in JENDL-5. Figure B.4 in Appendix compares the covariance data plots for the Al-27 (n, elastic) reaction from ENDF/B-VIII.0 and

JEFF-3.3. The correlation matrix illustrates both thermal and fast regions, revealing significant positive correlations within the thermal and resonance energy ranges. The uncertainty associated with Al-27 elastic cross sections is greater when using ENDF/B-VIII.0 covariances compared to JEFF-3.3 (15% versus 9% above 10^4 eV). Similarly, Be-9 elastic scattering contributes 755.8 pcm in ENDF/B-VIII.0, but it is not available from other libraries. Significant discrepancies are also observed in H-1 elastic scattering, where the uncertainty varies from 360.0 pcm (ENDF/B-VIII.0) to 23.1 pcm (JEFF-3.3) and 241.9 pcm (JENDL-5). Figure B.5 in Appendix illustrates the uncertainty related to the H-1 elastic cross sections, showing that it is lower when utilizing JEFF-3.3 covariances compared to ENDF/B-VIII.0 and JENDL-5 (0.4% versus 0.85% in the region below 10^4 eV).

In JEFF-3.3, the uncertainty associated with H-1 elastic scattering is significantly lower (23.1 pcm) when compared to the values for ENDF/B-VIII.0 and JENDL-5. In contrast, the corresponding value for B-10 (capture) is significantly higher at 530.9 pcm. Fission and inelastic scattering reactions, especially those involving U-235 and U-238, contribute to the overall uncertainty, though to a lesser extent. Other isotopes contributing to the uncertainty for β_{eff} include elastic and inelastic scattering, along with capture reactions involving B-10, O-16, C-nat, Fe-56, ... Figure B.6 in Appendix shows the uncertainty related to the B-10 capture cross sections by comparing the covariances from all regions of ENDF/B-VIII.0, JEFF-3.3, and JENDL-5, which are similar to about 40%. Figure B.7 in Appendix compares the covariance data plots for the O-16 (n, elastic) reaction from ENDF/B-VIII.0, JEFF-3.3, and JENDL-5. The uncertainty associated with the O-16 elastic cross sections is higher when using JEFF-3.3 covariances compared to ENDF/B-VIII.0 and JENDL-5 (2% versus 0.2-0.5% in the region below 10^5 eV). The differences in covariance matrices are the main reason for the variation in uncertainty values.

It is clear that both the elastic, inelastic, and capture properties of A-27, Be-9, H-1, B-10, and O-16 significantly affect the uncertainty of β_{eff}

the DNRR core, as these nuclides are essential components of the reactor core.

3.4 Conclusions

The criticality and sensitivity analyses of the DNRR core demonstrated high consistency among all evaluated nuclear data libraries, confirming the robustness of the computational approach. Nevertheless, systematic deviations were identified: JENDL-5 yielded the highest k_{eff}, CENDL-3.2 the lowest, while ENDF/B-VIII.0 and JEFF-3.3 showed nearly identical results lying in between. These differences arising from variations in evaluated neutron reaction data rather than modeling uncertainties constitute a key finding of this dissertation. They clearly demonstrate that the choice of nuclear data library significantly influences reactor criticality predictions, underscoring the essential role of accurate and consistent nuclear data in ensuring the reliability of analyses for research reactors such as the DNRR.

The uncertainty analysis revealed that the main contributors to the total uncertainty of k_{eff} are the capture and elastic scattering of H-1 and the fission of U-235, with a significant additional contribution from Al-27. Other important nuclides include Be-9, C-nat, and U-238. The total uncertainties from ENDF/B-VIII.0, JENDL-5, and JEFF-3.3 are 415.7, 363.0, and 588.0 pcm, respectively. These results indicate that differences among nuclear data libraries mainly arise from variations in evaluated cross sections, especially for H-1, U-235, and Al-27. The findings highlight the crucial need to improve elastic-scattering and fission data for key isotopes, thereby increasing the accuracy, safety, and predictive capabilities of reactor physics analyses for the DNRR.

In evaluating the kinetic parameters using the adjoint weighted method, the calculated β_{eff} values ranged from 735 to 753 pcm, with variations of less than 4% among the evaluated libraries, while the differences between computational methods remained below 1.2%. For the ENDF/B-VIII.0 library, the kinetic parameters were determined as β_{eff} of 732 pcm, Λ of 86.75 μs, and l_p of 86.75 μs. Comparisons with other methods implemented in Serpent 2 show good agreement.

The kinetic parameters were analyzed along with their sensitivity to operating conditions using ENDF/B-VIII.0. The effective delayed neutron fraction (β_{eff}) exhibits a marked reduction, decreasing from 750 pcm at the BOC to 704 pcm at the EOC. In contrast, both the neutron generation time (Λ) and the prompt neutron lifetime (l_p) increase as burnup proceeds, rising from 73.39 μs to 80.04 μs and from 68.14 μs to 77.99 μs, respectively. Control rod withdrawal produces a general reduction in the kinetic parameters, with decreases of approximately 2.6% for β_{eff}, 11% for Λ, and 19.8% for l_p when comparing the all rods in to all rods out configurations. An increase in fuel temperature results in a slight reduction of β_{eff}, while Λ and l_p remain essentially unaffected. With the JENDL-5 library, it's in the same direction. These results indicate that the kinetic parameters of the DNRR are heavily influenced by fuel burnup and control rod position, while they are only slightly affected by fuel temperature.

The sensitivity analysis of kinetic parameters identified that the delayed neutron yield of U-235 exerts the strongest positive influence on the β_{eff}, while the prompt neutron yield has the largest negative effect. However, notable discrepancies were observed among the evaluated nuclear data libraries, mainly due to differences in the treatment of delayed neutron data. The results demonstrate that neglecting the direct contribution of delayed neutrons (represented by k_p in Equation 2.5.5) leads to significant deviations in β_{eff} sensitivity. This constitutes an important finding of the dissertation, underscoring the need for improved and more consistent evaluation of delayed neutron parameters across nuclear data libraries.

The uncertainty analysis of the β_{eff} revealed total uncertainties of 1312.2, 1021.0, and 471.4 pcm for ENDF/B-VIII.0, JEFF-3.3, and JENDL-5, respectively. The dominant contributors to these uncertainties are the elastic scattering reactions of Al-27, Be-9, and H-1, with Al-27 alone accounting for about 38–40% of the total. Additional contributions above 100 pcm arise from B-10, O-16, and C-nat, from which the covariance data were identified as the primary source of uncertainty. These results constitute an important

finding of the dissertation, confirming that uncertainties in elastic scattering cross sections, particularly for Al-27, Be-9, and H-1 govern the overall accuracy of β_{eff} evaluation.

This dissertation shows that differences in evaluated nuclear data, rather than modeling uncertainties, are the main cause of the uncertainties in both k_{eff} and β_{eff} for the DNRR. The analysis emphasizes fission of ^{235}U, as well as elastic and inelastic scattering of H-1, Al-27, and Be-9, as the primary contributors to the uncertainties in criticality and kinetic parameters.

CONCLUSIONS, NEW CONTRIBUTIONS AND FUTURE WORKS

1. General conclusions

(1) Criticality and sensitivity/uncertainty (S/U) analyses were conducted for the DNRR core with 92 LEU fuel bundles. The largest difference in the k_{eff} prediction is -354 pcm compared to the experiments, indicating good agreement between the calculations and the experimental results. JENDL-5 tends to predict the highest values of k_{eff}, while CENDL-3.2 tends to predict the lowest. Among the four libraries, the difference in the k_{eff} predictions is less than 172 pcm. The k_{eff} values obtained with JENDL-5 generally exceed those from ENDF/B-VIII.0, with the largest difference being 160 pcm. Meanwhile, the k_{eff} values obtained with CENDL-3.2 are lower than those from ENDF/B-VIII.0. In uncertainty analyses, the results show that the main uncertainties in k_{eff} are primarily linked to the capture and elastic scattering reactions of H-1 and the fission reaction of U-235. Additionally, Al-27, Be-9, C-nat, and U-238 also significantly contribute to the uncertainty of k_{eff}. The total uncertainties obtained with ENDF/B-VIII.0, JENDL-5, and JEFF-3.3 are 415.7, 363.0, and 588.0 pcm, respectively. These findings emphasize the importance of improving cross section evaluations for key nuclides, especially H-1 and U-235. Among the evaluated libraries, ENDF/B-VIII.0 and JENDL-5 offer comparatively smaller uncertainties and are recommended for future core physics and safety analyses of the DNRR.

(2) A comprehensive assessment of the kinetic parameters and their associated β_{eff} uncertainties was carried out for the DNRR core. The β_{eff} values calculated using the adjoint weighted method show good consistency across the evaluated libraries, ranging from 735 to 753 pcm. Differences between the adjoint weighted and prompt methods are below 1.2%, while the variation between libraries is limited to around 4.0%.

For the reference ENDF/B-VIII.0 library, β_{eff}, Λ, and l_p were determined to be 735 pcm, 80.96 μs, and 80.90 μs, respectively. Furthermore, good agreement when compared to the Serpent 2 built in methods. The uncertainty analysis shows that the overall β_{eff} uncertainty is mainly influenced by elastic scattering reactions, with Al-27 being the largest contributor. Other significant contributors include B-10,O-16, and C-nat. The differences in β_{eff} uncertainties across the evaluated libraries are primarily due to variations in energy dependent sensitivity coefficients and covariance data. These results provide a valuable basis for safety analysis and transient modeling of the DNRR and emphasize the importance of using evaluated nuclear data libraries with comprehensive covariance information in future reactor studies.

(3) The sensitivity of kinetic parameters to the DNRR operating parameters was analyzed using the ENDF/B-VIII.0 library. The β_{eff} decreases dramatically from 750 pcm at the BOC to 704 pcm at the EOC. The values of Λ and l_p increase with burnup (from 73.39 μs to to 80.04 μs for Λ, and from 68.14 μs to 77.99 μs for l_p). The withdrawal of the control rods leads to a decrease in the kinetic parameters. The decrease of β_{eff}, Λ and l_p corresponding to all rods in and all rods out are about 2.6%, 11% and 19.8%, respectively. The increase of fuel temperature leads to a slight decrease of the β_{eff}, whereas the l_p and Λ remain unchanged.

2. New contributions

(1) The dissertation provides a comprehensive analysis on the sensitivity and uncertainty of nuclear data on kinetic and criticality parameters for the DNRR core consisting 92 LEU fuel bundles. The research employs the latest version of MCNP code (MCNP6.3) and the most recent released nuclear data libraries, including ENDF/B-VIII.0, JEFF-3.3, JENDL-5, and CENDL-3.2.

(2) In analyzing critical configurations, this study finds that k_{eff} estimates from JENDL-5 generally predict higher k_{eff} values compared to experimental results, while ENDF/B-VIII.0, JEFF-3.3, and CENDL-3.2 tend

to produce lower estimates. This confirms that JENDL-5 is suitable for analyzing the critical parameters of the reactor core.

(3) Through the sensitivity analysis of critical parameters, this thesis identifies the nuclear reactions that most significantly affect the effective multiplication factor (k_{eff}). Reactions that increase k_{eff} include the total and fission reactions of U-235, as well as the elastic scattering reactions of H-1, C-nat, O-16, Al-27, Be-9, and others. Conversely, reactions that tend to decrease k_{eff} are mainly the neutron capture reactions of H-1, U-235, Al-27, U-238, and others. These findings emphasize the importance of carefully considering these reactions in future studies to improve the accuracy and efficiency of reactor neutronic analyses.

(4) Through the uncertainty analysis of critical parameters, this thesis shows that the main sources of uncertainty in k_{eff} are related to the capture and elastic scattering of H-1, as well as the capture and fission of U-235. Additional significant contributions come from Al-27, Be-9, C-nat, and U-238. The total uncertainties of k_{eff} obtained with ENDF/B-VIII.0, JENDL-5, and JEFF-3.3 are 415.7, 363.0, and 588.0 pcm, respectively. Among these data libraries, JENDL-5 should be prioritized for future core physics and safety analyses of the DNRR and similar reactors because it demonstrates the smallest uncertainties.

(5) The kinetic parameters were estimated based on operation conditions, and this is the first time this research has been conducted on the DNRR. The research findings indicated that the β_{eff} decreases significantly, while the values of Λ and l_p increase with fuel burnup. The withdrawal of control rods results in a decrease in the kinetic parameters, whereas an increase in fuel temperature does not affect them. These findings will be considered for safety analysis and for enhancing the efficiency of the Dalat nuclear reactor.

(6) Through the sensitivity analysis of kinetic parameters parameters, this dissertation reveals that the delayed neutron yield reaction (delayed ν)

of U-235 has the most significant positive impact on the effective delayed neutron fraction β_{eff}, whereas the prompt neutron yield reaction (prompt ν) of U-235 contributes the most to its decrease. The sensitivity analysis results for the effective multiplication factor (k_{eff}) exhibited good agreement across all evaluated nuclear data libraries. In contrast, the effective delayed neutron fraction (β_{eff}) sensitivity analysis results did not demonstrate a similarly high level of agreement, a discrepancy attributable to the omission of delayed neutron effects in these sensitivity calculations.

(7) Through the uncertainty analysis of the kinetic parameters, this dissertation identifies the dominant contributors to the uncertainty of the effective delayed neutron fraction (β_{eff}) as the elastic scattering reactions of Al-27, Be-9, and H-1. Additional notable contributors include B-10, O-16, and C-nat. The covariance matrices are recognized as the primary sources of these uncertainties. Therefore, improving the cross section evaluations, particularly for Al-27, Be-9, and B-10 is essential to enhance the accuracy and reliability of reactor simulations. The total uncertainties of β_{eff} were determined to be 1312.2 pcm (ENDF/B-VIII.0), 1021.0 pcm (JEFF-3.3), and 471.4 pcm (JENDL-5), with JENDL-5 exhibiting the lowest overall uncertainty. These findings confirm that JENDL-5 provides a more reliable basis for analyzing the kinetic parameters of the reactor core.

3. Future works

(1) The S/U analysis will be expanded to include kinetic parameters such as Λ and l_p, as well as burnup scenarios, using the newly released libraries such as ENDF/B-VIII.1 and various software, including Serpent, under various operating and fuel cycle conditions.

(2) The methods developed for criticality and sensitivity/uncertainty (S/U) analysis will be applied to the Center for Nuclear Energy Science and Technology (CNEST) to enhance its design, operation, and safety evaluation.

(3) In the long term, the methodologies of criticality and nuclear data sensitivity/uncertainty (S/U) analysis developed for research reactors will be extended to small modular reactors (SMRs) and large-scale power reactors.

Publications used in this dissertation

1. **Duc-Tu Dau**, Nhi-Dien Nguyen, Ton-Nghiem Huynh, Quang-Huy Pham, Kien-Cuong Nguyen, Thoi-Nam Chu, Van-Khanh Hoang, Giang T.T. Phan, Huu-Tiep Nguyen, Thanh-Mai Vu, and Hoai-Nam Tran, "Criticality and sensitivity/uncertainty analysis of the DNRR with LEU fuel using MCNP6.3 and the latest data libraries", *Nuclear Engineering and Design* **442**, (2025), 114182. [SCIE, Q1]

2. **Duc-Tu Dau**, Nhi-Dien Nguyen, Kien-Cuong Nguyen, Quang-Huy Pham, Thoi-Nam Chu, Van-Khanh Hoang, Giang T. T. Phan, and Hoai-Nam Tran, "Kinetic parameters of the Dalat nuclear research reactor with LEU fuel using MCNP6 and JENDL-5 library", *Nuclear Technology and Radiation Protection* **40**, (2025), 1-9. [SCIE, Q3]

3. **Duc-Tu Dau**, Nhi-Dien Nguyen, Huu-Tiep Nguyen, Thoi-Nam Chu, and Hoai-Nam Tran, "Sensitivity of kinetic parameters to operation parameters of the Dalat nuclear research reactor with LEU fuel", *Journal of Physics: Conference Series* **3040**, (2025), 012020. [SCOPUS]

Other publications related to this dissertation

1. Thoi-Nam Chu, Giang T.T. Phan, Le Quang Linh Tran, Thi Hong Bui, Quang Binh Do, **Duc-Tu Dau**, Kien-Cuong Nguyen, Nhi-Dien Nguyen, Huu-Tiep Nguyen, Van-Khanh Hoang, Thanh Mai Vu, and Hoai-Nam Tran, "Sensitivity and uncertainty analysis of the first core of the DNRR using MCNP6 and new nuclear data libraries" *Nuclear Engineering and Design* 419, (2024), 112986.

2. **Duc-Tu Dau**, Nhi-Dien Nguyen, and Hoai-Nam Tran, "Evaluation of kinetic parameters of the Dalat nuclear research reactor with LEU fuel", *The 24th IEEE Real Time Conference - ICISE*, (2024), Quy Nhon, Vietnam.

3. **Duc-Tu Dau**, Nhi-Dien Nguyen, and Hoai-Nam Tran, "Sensitivity analysis of kinetic parameters to operation parameters of the Dalat nuclear research reactor", *PIAS Workshop*, (2024), Phenikaa Univesity.

4. **Duc-Tu Dau**, Nhi-Dien Nguyen, and Hoai-Nam Tran, "Evaluation of kinetic parameters of the Dalat nuclear research reactor using Monte Carlo method", *The 16th Vietnam Conference on Nuclear Science and Technology (VINANST-16)*, (2025), Da Nang, Vietnam.

5. **Duc-Tu Dau**, Nhi-Dien Nguyen, Thoi-Nam Chu and Hoai-Nam Tran, "Neutronic analysis of the NuScale-like Small Modular Reactor (SMR)", *Phenikaa International Physics Conference*, (2025), Phenikaa University.

6. **Duc-Tu Dau**, Nhi-Dien Nguyen, Thoi-Nam Chu and Hoai-Nam Tran, "Evaluation of kinetic parameters of the Dalat Nuclear Research Reactor with fuel burnup using a Continuous-Energy Monte Carlo method", *Phenikaa International Physics Conference*, (2025), Phenikaa University.

References

[1] Kulesza J. A., Adams T. R., Armstrong J. C., Bolding S. R., Brown F. B., Bull J. S., Burke T. P., Clark A. R., Forster R. A., Giron J. F., Grieve T. S., Josey C. J., Martz R. L., McKinney G. W., Pearson E., Rising M. E., Solomon C. J., Swaminarayan S., Trahan T. J., Wilson S. C., Zukaitis A. J., *"MCNP® Code Version 6.3.0 Theory and User Manual"*, Tech. Rep. LA-UR-22-30006, Rev. 1, Los Alamos National Laboratory, Los Alamos, NM, USA (2022).

[2] Nagaya Y., Okumura K., Sahurai T., Mori T., *"MVP/GMVP Version 3"*, Tech. rep., Japan Atomic Energy Agency (2016).

[3] Leppnen J., *"Serpent a Continuous-energy Monte Carlo Reactor Physics Burnup Calculation Code"*, Tech. rep., VTT Technical Research Centre of Finland 4.455 (2013) 2023-09.

[4] D'Auria F., Glaeser H., Lee S., Misak J., Modro M., Schultz R., *"Best etimate safety analysis for nuclear power plants: Uncertainty Evaluation"*, Tech. rep., STI/PUB/1306.IAEA (2008).

[5] Bretscher M. M., *"Evaluation of reactor kinetic parameters without the need for perturbation codes"*, Tech. rep., Argonne National Laboratory, IL (United States) (1998).

[6] Romero-Barrientos J., Damián J. M., Molina F., Zambra M., Aguilera P., López-Usquiano F., Parra B., Ruiz A., *"Calculation of kinetic parameters β_{eff} and Λ with modified open source Monte Carlo code OpenMC(TD)"*, Nuclear Engineering and Technology 54 (3) (2022) 811–816. doi:10.1016/j.net.2021.09.020.

[7] Hanson L. A., Ludewig H., Diamond D. J., *"Calculation of the Prompt Neutron Lifetime in the NBSR"*, Nuclear Science and Engineering 153 (1) (2006) 26–32. doi:10.13182/NSE06-4.

[8] Meulekamp R. K., Van S. C. D. M., *"Calculating the effective delayed neutron fraction with Monte Carlo"*, Nuclear science and engineering 152 (2) (2006) 142–148.

[9] Hosseini S., Vosoughi N., Ghofrani M., Gharib M., *"Calculation, measurement and sensitivity analysis of kinetic parameters of Tehran Research Reactor"*, Annals of Nuclear Energy 37 (4) (2010) 463–470. doi:10.1016/j.anucene.2010.01.018.

[10] Pinem S., Liem P. H., Luthfi W., Surbakti T., Hartanto D., *"Evaluation of Kinetic Parameters RSG-GAS Reactor Equilibrium Silicide Core Using Continuous-Energy Monte Carlo Serpent 2 Code"*, Nuclear Science and Engineering 198 (10) (2024) 1935–1949.

[11] Kodeli I.-A., *"Sensitivity and uncertainty in the effective delayed neutron fraction β_{eff}"*, Nuclear Instruments and Methods in Physics Research Section A: Accelerators, Spectrometers, Detectors and Associated Equipment 715 (2013) 70–78.

[12] Mweetwa B., Amoako E. A., Akaho E., Odoi C., *"Prediction of Neutronic and Kinetic Parameters of Ghana Research Reactor 1 (GHARR-1) after 19 Years of Operation Using Monte Carlo-N Particle (MCNP) Code"*, World Journal of Nuclear Science and Technology 8 (2018) 160–175.

[13] Makhloul M., Boukhal H., Chakir E., Bardouni T. E., Lahdour M., Kaddour M., Ahmed A., Arectout A., Yaakoubi H. E., *"Sensitivity and uncertainty quantification of neutronic integral data in the TRIGA Mark II research reactor"*, Nuclear Engineering and Technology 54 (2) (2022) 523–531.

[14] Liem P. H., Zuhair , Hartanto D., *"Sensitivity and uncertainty analysis on the first core criticality of the RSG GAS multipurpose research reactor"*, Progress in Nuclear Energy 114 (2019) 46–60.

[15] Ghione A., Noel B., Vinai P., Demazire C., *"Uncertainty and sensitivity analysis for the simulation of a station blackout scenario in the Jules Horowitz Reactor"*, Annals of Nuclear Energy 104 (2017) 28–41.

[16] Kodeli I. A., *"Beta-effective sensitivity and uncertainty analysis of MYRRHA reactor for possible use in nuclear data validation and improvement"*, Annals of Nuclear Energy 113 (2018) 425–435.

[17] Ahmed A., Boukhal H., Bardouni T. E., Makhloul M., Chakir E., Ouahdani S. E., *"Sensitivity and uncertainty analysis on $keff$ due to nuclear data in the KRITZ-2:19 - Comparison between JENDL-4.0 and ENDF/B-VII.1"*, Annals of Nuclear Energy 129 (2019) 308–315.

[18] Hartanto D., Liem P. H., *"Sensitivity and uncertainty analyses of a high temperature gas-cooled reactor by using a 44-group covariance library"*, Annals of Nuclear Energy 151 (2021) 107943.

[19] Ziani H., Bardouni T. E., Lahdour M., Barbari M. E., Yaakoubi H. E., Boulaich Y., *"Eigenvalue sensitivity and nuclear data uncertainty analysis for the Moroccan TRIGA Mark II research reactor using SCALE6.2 and MCNP6.2"*, Nuclear Engineering and Design 378 (2021) 111160.

[20] Phan T. T. G., Tran H. N., Nguyen K. C., Tran V. P., Hoang V. K., Pham N. V. H., Hoang A. T. K., *"Comparative analysis of the Dalat nuclear research reactor with HEU fuel using SRAC and MCNP5"*, Science and Technology of Nuclear Installations 2017 (1) (2017) 2615409.

[21] Phan T. T. G., Do Q. B., Ngo Q. H., Tran T. A., Tran H. N., *"Application of differential evolution algorithm for fuel loading optimization of the DNRR research reactor"*, Nuclear Engineering and Design 362 (2020) 110582.

[22] Do Q. B., Phan T. T. G., Nguyen K. C., Ngo Q. H., Tran H. N., *"Criticality and rod worth analysis of the DNRR research reactor using the SRAC and MCNP5 codes"*, Nuclear Engineering and Design 343 (2019) 197–209.

[23] Chu T. N., Phan T. T. G., Tran L. Q. L., Bui T. H., Do Q. B., Dau D. T., Nguyen K. C., Nguyen N. D., Nguyen H. T., Hoang V. K., Vu T. M., Tran H. N., *"Sensitivity and uncertainty analysis of the*

first core of the DNRR using MCNP6 and new nuclear data libraries", Nuclear Engineering and Design 419 (2024) 112986.

[24] Tran V. P., Nguyen K. C., Hartanto D., Tran H. N., Tran V. T., Hoang V. K., Pham N. V. H., *"Development of a PARCS/Serpent model for neutronics analysis of the Dalat nuclear research reactor"*, Nuclear Science and Techniques 32 (2) (2021) 15.

[25] Brown D., Chadwick M., Capote R., Kahler A., Trkov A., Herman M., Sonzogni A., *"ENDF/B-VIII. 0: the 8th major release of the nuclear reaction data library with CIELO-project cross sections, new standards and thermal scattering data"*, Nuclear Data Sheets 148 (2018) 1–142.

[26] Plompen A. J. M., Cabellos O., Jean C. D. S., Fleming M., Algora A., Angelone M., Archier P., *"The joint evaluated fission and fusion nuclear data library, JEFF-3.3"*, The European Physical Journal A 56 (7) (2020) 181.

[27] Osamu I., Nobuyuki I., Satoshi K., Futoshi M., Shinsuke N., *"Japanese evaluated nuclear data library version 5: JENDL-5"*, Journal of Nuclear Science and Technology 60 (1) (2023) 1–60.

[28] Ge Z., Xu R., Wu H., Zhang Y., Chen G., Jin Y., Shu N., Chen Y., Tao X., Tian Y., *"CENDL-3.2: The new version of Chinese general purpose evaluated nuclear data library"*, in: EPJ Web of Conferences, Vol. 239, EDP Sciences, 2020, p. 09001.

[29] Kolos K., Sobes V., Vogt R., Romano C. E., Smith M. S., Bernstein L. A., Brown D. A., Burkey M. T., Danon Y., Elsawi M. A., *"Current nuclear data needs for applications"*, Physical Review Research 4 (2) (2022) 021001.

[30] International Nuclear Data Evaluation Network , *"Nuclear Data Services"* (01.10.2024).
URL https://www-nds.iaea.org/INDEN/

[31] International Network of Nuclear Reaction Data Centers , *"Nuclear Data Services'* (01.10.2024).
URL https://www-nds.iaea.org/nrdc/

[32] US NNDC , *"National nuclear data center"* (01.10.2024).
URL https://www.nndc.bnl.gov./

[33] International Atomic Energy Agancy , *"Nuclear Data Services"* (01.10.2024).
URL https://www-nds.iaea.org/

[34] Cross Section Evaluation Working Group , *"National nuclear data center"* (01.10.2024).
URL https://www.nndc.bnl.gov/csewg/

[35] Nuclear Energy Agency (NEA) , *"Working Party on International Nuclear Data Evaluation Cooperation (WPEC)"* (01.10.2024).
URL https://www.oecd-nea.org/jcms/pl_23072/workingparty-on-international-nuclear-data-evaluation-co-operationwpec.

[36] Osamu I., Nobuyuki I., Keiichi S., Akira I., Satoshi K., Futoshi M., Shinsuke N., *"Status of JENDL"*, in: EPJ Web of Conferences, Vol. 239, EDP Sciences, 2020, p. 09002.

[37] Koning A., Forrest R., Kellett M., Mills R., Henriksson H., Rugama Y., Bersillon O., Bouland O., Courcelle A., Duijvestijn M., *"The JEFF-3.1 nuclear data library-JEFF report 21"*, Tech. rep., Organisation for Economic Co-Operation and Development, Nuclear Energy (2006).

[38] TALYS-based evaluated nuclear data library , *"TENDL"* (01.10.2024).
URL https://tendl.web.psi.ch/tendl_2023/tendl2023.html

[39] Russian Evaluated Nuclear Data Librar , *"BROND"* (01.10.2024).
URL https://www.oecd-nea.org/BROND31.

[40] IAEA , *"NDS Coordinated Research Projects"* (01.10.2024).
URL https://www.iaea.org/projects/coordinated-researchprojects?type=3720&status=5017&topics=3070

[41] US Nuclear Data Program , *"US NNDC"* (01.10.2024).
URL https://www.nndc.bnl.gov/usndp/

[42] International Network of Nuclear Structure and Decay Data Evaluators , *"Nuclear Data Services"* (01.10.2024).
URL https://www-nds.iaea.org/nsdd/

[43] Rochman D., Leray O., Hursin M., Ferroukhi H., Vasiliev A., Aures A., Bostelmann F., Zwermann W., Cabellos O., Diez C., *"Nuclear data uncertainties for typical LWR fuel assemblies and a simple reactor core"*, Nuclear Data Sheets 139 (2017) 1–76.

[44] Kiedrowski B. C., Brown F. B., *"Adjoint-based k-eigenvalue sensitivity coefficients to nuclear data using continuous-energy Monte Carlo"*, Nuclear science and Engineering 174 (3) (2013) 227–244.

[45] Broadhead B. L., Rearden B. T., Hopper C. M., Wagschal J. J., Parks C. V., *"Sensitivity- and Uncertainty-Based Criticality Safety Validation Techniques"*, Nuclear Science and Engineering 146 (3) (2004) 340–366.

[46] Romojaro P., Velarde Álvarez F., Kodeli I., Stankovskiy A., Díez C., Cabellos O., García-Herranz N., Heyse J., Schillebeeckx P., Van den Eynde G., Žerovnik G., *"Nuclear data sensitivity and uncertainty analysis of effective neutron multiplication factor in various MYRRHA core configurations"*, Annals of Nuclear Energy 101 (2017) 330–338.

[47] Chiba G., Tsuji M., Narabayashi T., *"Sensitivity and uncertainty analysis for reactor stable period induced by positive reactivity using one-point adjoint kinetics equation"*, Journal of Nuclear Science and Technology 50 (12) (2013) 1150–1160.

[48] Chiba G., Kawamoto Y., Tsuji M., Narabayashi T., *"Estimation of neutronics parameter sensitivity to nuclear data in random sampling-based uncertainty quantification calculations"*, Annals of Nuclear Energy 75 (2015) 395–403.

[49] Favorite J. A., Perkó Z., Kiedrowski B. C., Perfetti C. M., *"Adjoint-based sensitivity and uncertainty analysis for density and composition:*

A user's guide", Nuclear Science and Engineering 185 (3) (2017) 384–405.

[50] Aufiero M., Bidaud A., Hursin M., Leppänen J., Palmiotti G., Pelloni S., Rubiolo P., *"A collision history-based approach to sensitivity/perturbation calculations in the continuous energy Monte Carlo code SERPENT"*, Annals of Nuclear Energy 85 (2015) 245–258.

[51] Panizo S., Alfonso C., Jiménez-Carrascosa A., García-Herranz N., Bécares V., Romojaro P., Velarde Álvarez F., Cabellos O., Cuesta-Matesanz A., Fiorito L., Stankovskiy A., Eynde den G. V., *"Sensitivity and uncertainty analyses for advanced nuclear systems (ALFRED, ASTRID, ESFR and MYRRHA)"*, Progress in Nuclear Energy 172 (2024) 105207.

[52] Cacuci D. G., Ionescu B. M., Navon I. M., *"Sensitivity and uncertainty analysis, volume II: applications to large-scale systems"*, CRC press, (2005).

[53] Perez L. D. C., Lorenzi S., Cammi A., *"Sensitivity and uncertainty analysis of Triga mark II reactor using first order perturbation theory"*, The ^{28}th international conference nuclear energy for new Europe.

[54] Usachev L., *"Perturbation theory for the breeding ratio and for other number ratios pertaining to various reactor processes"*, Journal of Nuclear Energy. Parts A/B. Reactor Science and Technology 18 (10) (1964) 571–583.

[55] Gandini A., *"A generalized perturbation method for bi-linear functionals of the real and adjoint neutron fluxes"*, Journal of Nuclear Energy 21 (10) (1967) 755–765.

[56] Rochman D., Koning A., van der Marck S., Hogenbirk A., Sciolla C., *"Nuclear data uncertainty propagation: Perturbation vs. Monte Carlo"*, Annals of Nuclear Energy 38 (5) (2011) 942–952.

[57] Rochman D., Vasiliev A., Ferroukhi H., Zhu T., van der Marck S., Koning A., *"Nuclear data uncertainty for criticality-safety: Monte Carlo vs. linear perturbation"*, Annals of Nuclear Energy 92 (2016) 150–160.

[58] Han T. Y., Lee H. C., Noh J. M., *"Development of a sensitivity and uncertainty analysis code for high temperature gas-cooled reactor physics based on the generalized perturbation theory"*, Annals of Nuclear Energy 85 (2015) 501–511.

[59] Ao Q., *"Uncertainty analysis in Monte Carlo criticality computations"*, Nuclear Engineering and Design 241 (12) (2011) 4697–4703.

[60] International Atomic Energy Agency , *"History, development and future of TRIGA research reactors"*, Technical reports series, ISSN 0074–1914, 482 (2016).

[61] Pham D. H., Ngo Q. H., Vu H. L., Tran K. M., *"Report startup of nuclear research reactor"*, Tech. rep., Nuclear Research Institute, Vietnam Atomic Energy Commission (1984).

[62] Nguyen N. D., *"Safety Analysis Report for the Dalat Nuclear Research Reactor version 2018"*, Tech. rep., Dalat Nuclear Research Institute (2018).

[63] Nguyen N. D., Luong B. V., Le V. V., Duong V. D., Nguyen X. H., Phan N. S., Cao D. V., *"Results of operation and utilization of the Dalat nuclear research reactor"*, Nuclear Science and Technology 4 (2014) 1–9.

[64] Nguyen N., *"Safety Analysis Report for the Dalat Nuclear Research Reactor"*, Tech. rep., Nuclear Research Institute, Vietnam Atomic Energy Commission (2003).

[65] Dau D. T., Nguyen M. T., Le V. V., Huynh T. N., Nguyen K. C., Tran Q. D., Bui P. N., *"Reactivity induced transient analysis when the occurrence of leakage in the dry irradiation channels of the Dalat Nuclear Research Reactor"*, Nuclear Science and Technology 8 (2018) 01–09.

[66] Mohammad M., Seock K. I., *"WIMS-ANL User Manual"*, Argonne National Laboratory (2004) 1739–1812.

[67] Kulesza J. A., Adams T. R., Armstrong J. C., Bolding S. R., *"MCNP Code Theory and User Manual"*, Tech. rep., Los Alamos National Laboratory (2022).

[68] Tikhonchev M. Y., Shimansky G., Lebedeva E., Lichadeev V., Ryazanov D., Tellin A., *"The role of computer simulation in nuclear technologies development"*, in: Conference: IYNC 2000: International Youth Nuclear Congress 2000, Bratislava (Slovakia), 9-14 Apr (2001).

[69] Wieselquist W. A., Lefebvre R. A., *"SCALE 6.3.1 User Manual"*, Tech. rep., US Department of energy (2023).

[70] Halsall M., Tauman C., *"WIMS-D: a neutronics code for standard lattice physics analysis"*, Distributed by the NEA Databank, NEA (1507) 02 (1997).

[71] Fowler T., Vondy D. R., Cunningham G., *"Nuclear reactor core analysis code: CITATION."*, Tech. rep., Oak Ridge National Laboratory, Tenn. (1971).

[72] Okumura K., Kugo T., Kaneko K., Tsuchihashi K., *"SRAC2006: a comprehensive neutronics calculation code system"*, Tech. rep., Japan Atomic Energy Agency (2007).

[73] Zain J. A., Hajjaji O. E., Bardouni T. E., Boukhal H., *"Deterministic evaluation of safety parameters and neutron flux spectra in the MNSR research reactor using Dragon-4 code"*, Journal of Radiation Research and Applied Sciences (11)3, (2018) 255 - 261.

[74] Demaziere C., *"Modelling of Nuclear Reactor Multi-physics: From Local Balance Equations to Macroscopic Models in Neutronics and Thermal Hydraulics"*, Tech. rep., Academic Press Elsevier Inc (2019).

[75] Fleming M., Chadwick M., Brown D., Capote R., Ge Z., Herman M., Ignatyuk A., Ivanova T., Iwamoto O., Koning A., Plompen A., Trkov

A., *"Results of the Collaborative International Evaluated Library Organisation(CIELO) Project"*, Tech. rep., EPJ Web of Conferences 239 (2020).

[76] MacFarlane R. E., Muir D. W., Boicourt R. M., Kahler A. C., Conlin J. L., Haeck W., *"The NJOY Nuclear Data Processing System"*, Tech. rep., Los Alamos National Laboratory (2019).

[77] Koning A. J., Rochman D., *"Modern Nuclear Data Evaluation with the TALYS Code System"*, Nuclear Data Sheets 113 (12) (2012) 2841–2934.

[78] Zuhair , Luthfi W., Dwijayanto R. A. P., Rohanda A., Suwoto , *"Study on kinetic parameters of pebble bed reactor with TRISO duplex fuel"*, Nuclear Technology & Radiation Protection 38 (1) (2023) 1–9.

[79] Zuhair , Luthfi W., Sriyono , Suwoto , Setiadipura T., *"Study on kinetic parameters characteristics of pebble bed reactor using HTR-proteus facility"*, Nuclear Technology & Radiation Protection 37 (2) (2022) 119–127.

[80] Muhammad A., Iqbal M., Mahmoo T., *"Kinetic parameters study based on burn-up for improving the performance of research reactor equilibrium core"*, Nuclear Technology & Radiation Protection 29 (4) (2014) 253–258.

[81] Akyurek T., Shoaib S., Usman S., *"Delayed fast neutron as an indicator of burn-up for nuclear fuel elements"*, Nuclear Engineering and Technology 53 (10) (2021) 3127–3132.

[82] Arkani M., Hassanzadeh M., Khakshournia S., *"Calculation of six-group importance weighted delayed neutron fractions and prompt neutron lifetime of MTR research reactors based on Monte Carlo method"*, Progress in Nuclear Energy 88 (2016) 352–363.

[83] Nagaya Y., *"Calculation of reactor kinetics parameters with Monte Carlo differential operator sampling"*, Annals of Nuclear Energy 82 (2015) 226–229.

[84] Khan M., Sarker M., Islam S., *"Analysis of kinetic parameters of 3MW TRIGA Mark-II research reactor using the SRAC2006 code system"*, Annals of Nuclear Energy 60 (2013) 181–186.

[85] Lamarsh J. R., *"Introduction to nuclear engineering"*, Addison-Wesley Publishing Co.,Reading, MA, (1975).

[86] Do Q. B., Tran H. N., Ngo Q. H., Phan T. T. G., *"Determination of fuel burnup distribution of a research reactor based on measurements at subcritical conditions"*, Nuclear Science and Techniques 29 (12) (2018) 174.

[87] Conlin J. L., Haeck W., Neudecker D., Parsons D. K., White M. C., *"Release of ENDF/B-VIII.0-Based ACE"*, Tech. rep., Los Alamos National Laboratory (2018).

[88] Brown D. A., *"ENDF-6 formats manual-data formats and procedures for the evaluated nuclear data files ENDF/B-VI, ENDF/B-VII and ENDF/B-VIII"*, Tech. rep., Brookhaven National Laboratory (BNL), Upton, NY (United States) (2023).

[89] Trkov A., Brown D. A., *"ENDF-6 formats manual: data formats and procedures for the evaluated nuclear data files"*, Tech. rep., Brookhaven National Laboratory (BNL), Upton, NY (United States) (2018).

[90] Honeck H., *"ENDF/B: Specifications for an evaluated nuclear data file for reactor applications"*, Tech. rep., Brookhaven National Laboratory (BNL), Upton, NY (United States) (1967).

[91] Drake M., *"Data Formats and Procedures for the ENDF Neutron Cross Section Library"*, Tech. rep., Brookhaven National Laboratory (BNL), Upton, NY (United States) (1970).

[92] Dudziak D., *"ENDF Formats and Procedures for Photon Production and Interaction Data"*, Tech. rep., LA-4549, ENDF-102, Rev., Vol. II, Los Alamos Scientific Laboratory (1971).

[93] Garber D., Dunford C., Pearlstein S., *"ENDF-102, Data Formats and Procedures for the Evaluated Nuclear Data File, ENDF"*, Tech. rep., Brookhaven National Laboratory (BNL), Upton, NY (United States) (1975).

[94] Kinsey R., *"ENDF-102, Data Formats and Procedures for the Evaluated Nuclear Data File, ENDF"*, Tech. rep., Brookhaven National Laboratory (BNL), Upton, NY (United States) (1983).

[95] Rose P., Dunford C., McLane V., *"ENDF-102, Data Formats and Procedures for the Evaluated Nuclear Data File, ENDF-6"*, Tech. rep., Brookhaven National Laboratory (BNL), Upton, NY (United States) (2001).

[96] Herman M., Trkov A., Herman M., Trkov A., Brown D., *"ENDF-6, Formats Manual, Data Formats and Procedures for the Evaluated Nuclear Data File ENDF/B-VI and ENDF/B-VII"*, Tech. rep., Brookhaven National Laboratory (BNL), Upton, NY (United States) (2011).

[97] Igarashi S., Nakagawa T., Kikuchi Y., *"Japanese evaluated nuclear data library, version-1 JENDL-1"*, Tech. rep., Japan Atomic Energy Research Institute (1979).

[98] Shibata K., *"JENDL: Nuclear databases for science and technology"*, Journal of Nuclear Science and Technology 50 (5) (2013) 449–469.

[99] Igarasi S. I., *"Japanese Evaluated Nuclear Data Library (JENDL)"*, Journal of Nuclear Science and Technology 26 (1) (1989) 5–10.

[100] Keiichi S., Osamu I., Tsuneo N., Nobuyuki I., Akira I., Satoshi K., Satoshi C., Kazuyoshi F., Naohiko O., Takaaki O., Toru M., Hiroyuki M., Atsushi Z., So K., Jun-ichi K., *"JENDL-4.0: A New Library for Nuclear Science and Engineering"*, Journal of Nuclear Science and Technology 48 (1) (2011) 1–30.

[101] Dunjiu C., Qichang L., Tingjin L., *"Chinese evaluated nuclear data library, version 2"*, Tech. rep., Chinese Nuclear Data Center (1997).

[102] Tingjin L., Qichang L., Zongdi S., *"CENDL-2, Chinese Evaluated Nuclear Data Library, Version-2"*, Springer, (1992) 804–810.

[103] Youxiang Z., Tingjin L., Jingshang Z., Ping L., *"CENDL-3–Chinese Evaluated Nuclear Data Library, version 3"*, Journal of Nuclear Science and Technology 39 (sup2) (2002) 37–39.

[104] Ge Z., Zhao Z., Xia H., Zhuang Y., Liu T., Zhang J., Wu H., *"The updated version of Chinese evaluated nuclear data library (CENDL-3.1)"*, J. Korean Phys. Soc 59 (2) (2011) 1052–1056.

[105] Kodeli I., *"Multidimensional deterministic nuclear data sensitivity and uncertainty code system: method and application"*, Nuclear Science and Engineering 138 (1) (2001) 45–66.

[106] Sellaoui N., Zidi T., Belgaid M., *"Nuclear data uncertainty propagation to the main physical parameters of NUR research reactor"*, Progress in Nuclear Energy 130 (2020) 103557.

[107] Kiedrowski B., *"Methodology for Sensitivity and Uncertainty-Based Criticality Safety Validation"*, Tech. rep., Los Alamos National Laboratory (LANL), Los Alamos, NM (United States) (2014).

[108] Vu T. M., Kitada T., *"Impact of Thorium Capture Cross Section Uncertainty on the Thorium Utilized ADS Reactivity Calculation"*, Science and Technology of Nuclear Installations 2014 (2014) 1–4.

[109] Michálek S., Števo S., Farkas G., Haščík J., Slugeň V., Rataj J., Kolros A., *"Determination of the effective delayed neutron fraction for training reactor VR-1"*, Progress in Nuclear Energy 52 (8) (2010) 735–742.

[110] Hanson A., Diamond D., *"Calculation of Kinetics Parameters for the NBSR"*, Tech. rep., Brookhaven National Laboratory: Upton, NY, USA (2012).

[111] Keepin G., *"Physics of Nuclear Kinetics"*, Addison-Wesley, (1965).

[112] Kiedrowski B., Brown F., Wilson P., *"Calculating kinetics parameters and reactivity changes with continuous-energy Monte Carlo"*, Tech.

rep., Los Alamos National Laboratory (LANL), Los Alamos, NM (United States) (2009).

[113] Romero B. J., Damian J. I. M., Molina F., Zambra M., Aguilera P., Lopez U. F., Parra B., *"Calculation of kinetic parameters β_{eff} and Λ with modified open source Monte Carlo code OpenMC(TD)"*, arXiv preprint arXiv:2107.11197 (2021).

[114] Spriggs G. D., Busch R. D., Campbell J. M., *"Calculation of the delayed neutron effectiveness factor using ratios of k-eigenvalues"*, Annals of Nuclear Energy 28 (5) (2001) 477–487.

[115] Chiba G., *"Calculation of Effective Delayed Neutron Fraction Using a Modified k-Ratio Method"*, Journal of Nuclear Science and Technology 46 (5) (2009) 399–402.

[116] Michalek S., Hascik J., Farkas G., *"MCNP5 delayed neutron fraction (β_{eff}) calculation in training reactor VR-1"*, Journal of Electrical Engineering 59 (2008).

[117] Goorley T., James M., Booth T., Brown F., Bull J., Cox L., Durkee J., Elson J., Fensin M., Forster R., *"Initial MCNP6 release overview"*, Nuclear technology 180 (3) (2012) 298–315.

[118] Louis H. K., *"Evaluation of effective prompt neutron lifetime for pressurized water reactors"*, Nuclear Technology 188 (1) (2014) 1–7.

[119] Liem P. H., Surbakti T., Hartanto D., *"Kinetics parameters evaluation on the first core of the RSG GAS (MPR-30) using continuous energy Monte Carlo method"*, Progress in Nuclear Energy 109 (2018) 196–203.

[120] Snoj L., Kavčič A., Žerovnik G., Ravnik M., *"Monte Carlo calculation of kinetic parameters for the TRIGA Mark II research reactor"*, Nuclear Energy for New Europe (2008).

Appendix A Evaluation of kinetic parameters of the DNRR using Serpent 2 code

A.1 Methodology

A.1.1 Meulekamp-Spriggs method

The effective delayed neutron fraction, β_{eff}, represents the ratio of delayed neutrons to the total neutron yield per fission event. The Meulekamp estimates β_{eff} using the ratio of fission events induced by delayed neutrons to the total number of fissions caused by both prompt and delayed neutrons. The expression for β_{eff} is formulated in terms of the adjoint weighted neutron flux as follows:

$$\beta_{\text{eff}} = \frac{\int \phi^{+}(\vec{r},\Omega',E') \int \chi_d(E')\,\nu_d(E')\,\Sigma_f(\vec{r},E')\,\phi(\vec{r},\Omega,E)\,dE\,d\Omega\,d\vec{r}\,d\Omega'\,dE'}{\int \phi^{+}(\vec{r},\Omega',E') \int \chi(E')\,\nu(E')\,\Sigma_f(\vec{r},E')\,\phi(\vec{r},\Omega,E)\,dE\,d\Omega\,d\vec{r}\,d\Omega'\,dE'}. \tag{A.1}$$

where, $\phi(\vec{r},\Omega,E)$ is neutron flux; $\phi^{+}(\vec{r},\Omega',E')$ is adjoint neutron flux; $\Sigma_f(\vec{r},E')$ is macroscopic fission cross section; $\chi(E')$ is fission neutron energy spectrum; $\nu(E')$ is total number of neutrons emitted per fission; $\chi_d(E')$ is delayed neutron energy spectrum; $\nu_d(E')$ is number of delayed neutrons emitted per fission. This expression can be reformulated using the inner product notation $\langle f,g\rangle$, which represents integration over all spatial coordinates, energy, and angular directions. With appropriate simplifications, the full integral form of the equation can be expressed in a more compact and generalized representation as:

$$\beta_{\text{eff}} = \frac{\langle \phi^{+}, \chi_d\nu_d\Sigma_f\phi\rangle}{\langle \phi^{+}, \chi\nu\Sigma_f\phi\rangle} \approx \frac{\langle \chi_d\nu_d\rangle}{\langle \chi\nu\rangle}. \tag{A.2}$$

Spriggs reformulated the expression for β_{eff} to emphasize the contribution of delayed neutrons. As a result, the so called *k ratio* approach was introduced to estimate the effective delayed neutron fraction based solely on the delayed neutron yield:

$$\beta_{\text{eff}} \approx \frac{\langle \chi_d\nu\rangle}{\langle \chi\nu\rangle} \cdot \frac{\langle \chi_d\nu_d\rangle}{\langle \chi\nu\rangle} \approx \frac{\langle \chi_d\nu_d\rangle}{\langle \chi\nu\rangle} \cdot \frac{\langle \chi_d\nu\rangle}{\langle \chi\nu\rangle} \approx \beta_0 \cdot \frac{\langle \chi_d\nu\rangle}{\langle \chi\nu\rangle} \approx \beta_0 \cdot \frac{k_d}{k}. \tag{A.3}$$

In which β_0 represents the delayed neutron fraction derived from nuclear data based on neutrons emitted by precursor decay. The factor k_d accounts for the energy dependent contribution of delayed neutrons to fission.

A.1.2 Chiba method

Chiba proposed a refinement to the k ratio formulation. By introducing the prompt neutron yield $\nu_p(E_0) = \nu - \nu_d$ and recognizing that the delayed neutron fraction is typically small, the total neutron production term $\chi\nu$ can be approximated by $\chi_p\nu_p$, given the close similarity between prompt and total spectra. Continuous further simplified the delayed neutron contribution by replacing $\chi_d\nu_d$ with $\chi\nu - \chi_p\nu_p$, resulting in an alternative expression for β_{eff}:

$$\beta_{\text{eff}} \approx \frac{\langle \chi_d \nu_d \rangle}{\langle \chi\nu \rangle} \approx \frac{\langle \chi\nu - \chi_p\nu_p \rangle}{\langle \chi\nu \rangle} \approx 1 - \frac{\langle \chi_p\nu_p \rangle}{\langle \chi\nu \rangle} \approx 1 - \frac{k_p}{k}. \tag{A.4}$$

The ratio $\langle \chi_p\nu_p \rangle / \langle \chi\nu \rangle$ defines the prompt neutron k ratio. Since prompt neutrons constitute approximately 99% of the total, the values of k_p and k are nearly equal. However, this formulation enhances the resolution of small differences between k and k_p, which can significantly impact the quantification of uncertainty in neutron transport calculations:

$$L\phi = \frac{1}{k} F\phi, \tag{A.5}$$

where, L denotes the neutron loss operator in the transport equation, encompassing both absorption processes and leakage effects:

$$L = \Omega \cdot \nabla + \Sigma_t - \iint \Sigma_s(E', \vec{\Omega}')\, dE\, d\vec{\Omega}', \tag{A.6}$$

where, F represents the neutron production operator, which accounts for the generated neutrons:

$$F = \frac{1}{4\pi} \iint \chi(E')\, \nu(E')\, \Sigma_f(E')\, dE'\, d\vec{\Omega}', \tag{A.7}$$

which applies to the adjoint neutron flux under a hypothetical condition in which delayed neutrons are excluded from the reactor:

$$L^+\phi^+ = \frac{1}{k} F^+\phi^+ \quad \text{and} \quad L\phi_p = \frac{1}{k_p} F_p\phi_p. \tag{A.8}$$

In which,

$$F_p = \frac{1}{4\pi} \iint \chi_p(E')\, \nu_p(E')\, \Sigma_f(E')\, dE'\, d\vec{\Omega}'. \tag{A.9}$$

Therefore, the ratio $\frac{k_p}{k}$ can be approximated under the assumption that $\phi_p \approx \phi$, which simplifies the calculation but may introduce a degree of approximation related error.

$$\frac{k_p}{k} = \frac{\langle \phi^+, F_p\phi_p \rangle}{\langle \phi^+, F\phi_p \rangle} \approx \frac{\langle \phi^+, F_p\phi \rangle}{\langle \phi^+, F\phi \rangle}, \tag{A.10}$$

Chiba introduced further refinements to the k ratio formulation by incorporating an additional hypothetical state, where a scaling parameter a is used to quantify deviations or perturbations relative to the reference condition.

$$L\,\overline{\phi} = \frac{1}{k}\,\overline{F}\,\overline{\phi}, \tag{A.11}$$

where, the $\overline{F}$ includes contributions from both prompt and delayed neutrons, and is defined as:

$$\overline{F} = \frac{1}{4\pi}\iint (\chi\nu + a\chi_d\nu_d)\,\Sigma_f\,dE'\,d\vec{\Omega}', \tag{A.12}$$

The β_{eff} can be approximated by the following expression:

$$\beta_{\text{eff}} \approx \frac{1}{a}\left(\frac{\overline{k}}{k} - 1\right). \tag{A.13}$$

A.1.3 Nauchi and Kameyama method

An alternative approximation for β_{eff} involves using the adjoint neutron flux ϕ^+ as a weighting function for delayed neutron contributions. Nauchi and Kameyama proposed a method that estimates β_{eff} based on the number of fission neutrons produced in the subsequent generation, rather than the number of fissions they induce. This approach replaces the conventional adjoint flux $\phi^+(\vec{r}, \Omega', E')$ with a modified function $M(\vec{r}, \Omega', E')$, which represents the probability of neutron production from fission. Equation (A.2) can thus be reformulated accordingly,

$$\beta_{\text{eff}} = \frac{\langle \phi^+, \chi_d\nu_d\Sigma_f\phi\rangle}{\langle \phi^+, \chi\nu\Sigma_f\phi\rangle} \approx \frac{\langle M, \chi_d\nu_d\Sigma_f\phi\rangle}{\langle M, \chi\nu\Sigma_f\phi\rangle}. \tag{A.14}$$

Nauchi further proposed a technique for evaluating the neutron generation time, Λ, by deriving it from a generalized and modified form of the fundamental equation used to define this parameter as:

$$\Lambda = \frac{\int \phi^+(\vec{r}, \Omega', E')\,\frac{1}{v}\phi(\vec{r}, \Omega, E)\,d\vec{r}\,d\Omega'\,dE'}{\int \phi^+(\vec{r}, \Omega', E')\,\frac{1}{4\pi}\int \chi(E')\nu(E')\Sigma_f(E')\,\phi(\vec{r}, \Omega, E)\,dE'\,d\vec{r}\,d\Omega'\,dE'}. \tag{A.15}$$

In Monte Carlo simulations, the neutron velocity v, which depends on energy, direction, and position governs the flight time along its stochastic path through reactor materials. This velocity, combined with track length, is evaluated at each collision or absorption event. In Nauchi's method, the adjoint weighting function ϕ^+ is replaced by M, which represents the expected

number of fission neutrons contributing to the subsequent generation:

$$\Lambda = \frac{\left\langle \phi^+, \frac{1}{v}\phi \right\rangle}{\langle \phi^+, F\phi \rangle} \approx \frac{\left\langle M, \frac{1}{v}\phi \right\rangle}{\langle M, F\phi \rangle}. \tag{A.16}$$

A.1.4 Iterated Fission Probability (IFP) method

Nauchi and Kameyama proposed a new weighting function for calculating the Iterated Fission Probability (IFP), which forms the basis of their method. The IFP function shares a physical interpretation with the adjoint neutron flux, as the spatial and energy distribution of fission neutrons is proportional to the adjoint flux. This enables the estimation of the probability that a neutron induces fission in the next generation under critical conditions. The IFP is evaluated as the number of fission events induced by neutrons, derived from the power distribution and flux using continuous energy or multigroup cross sections. Using the IFP function $I_{FP}(\vec{r}, \Omega', E')$, both β_{eff} and Λ can be calculated with expressions analogous to those in adjoint weighted methods, with a modified weighting scheme:

$$\beta_{\text{eff}} = \frac{\langle \phi^+, \chi_d \nu_d \Sigma_f \phi \rangle}{\langle \phi^+, \chi \nu \Sigma_f \phi \rangle} \approx \frac{\langle I_{FP}, \chi_d \nu_d \Sigma_f \phi \rangle}{\langle I_{FP}, \chi \nu \Sigma_f \phi \rangle}. \tag{A.17}$$

$$\Lambda = \frac{\left\langle \phi^+, \frac{1}{v}\phi \right\rangle}{\langle \phi^+, F\phi \rangle} \approx \frac{\left\langle I_{FP}, \frac{1}{v}\phi \right\rangle}{\langle I_{FP}, F\phi \rangle}. \tag{A.18}$$

A.1.5 Perturbation method

Verboomen et al. developed a perturbation based method for estimating neutron generation time in both thermal and fast reactors. This approach introduces localized perturbations in the macroscopic absorption cross section, allowing reactivity changes to be quantified and mathematically described using formulations such as:

$$L_p \phi_p = \frac{1}{k_p} F_p \phi_p, \tag{A.19}$$

and adjoint equation

$$L^+ \phi^+ = \frac{1}{k^+} F^+ \phi^+, \tag{A.20}$$

which can be expressed using precise perturbation formulation to evaluate changes in reactivity:

$$\Delta\rho = \frac{\left\langle \phi^+, \left(\frac{1}{k^+}\Delta F - \Delta L\right) \phi_p \right\rangle}{\langle \phi^+, F_p \phi_p \rangle}, \tag{A.21}$$

In this formulation, the perturbation operators are defined as: $\Delta F = F_p - F^+$ and $\Delta L = L_p - L^+$. Here, the term $\frac{c}{v}$ represents a uniform neutron absorber introduced as a perturbation, with c being a scaling constant for homogeneous poison $\frac{1}{v}$ and v denoting neutron speed. Based on this representation, the resulting change in reactivity due to the perturbation can be expressed as follows:

$$\Delta\rho = \rho_p - \rho^+ = \frac{\left\langle \phi^+, \frac{c}{v}\,\phi_p \right\rangle}{\langle \phi^+, F^+\phi_p \rangle}. \tag{A.22}$$

Taking the derivative of this expression with respect to c as $c \to 0$ yields the negative of the adjoint neutron generation time. More generally, the neutron generation time can be interpreted as the negative slope of the reactivity curve with respect to the perturbation amplitude:

$$\Lambda = -\frac{\Delta\rho}{c} = -\lim_{c\to 0}\frac{1}{c}\cdot\frac{\left\langle \phi^+, \frac{c}{v}\phi_p \right\rangle}{\langle \phi^+, F^+\phi_p \rangle} = \frac{\left\langle \phi^+, \frac{1}{v}\phi^+ \right\rangle}{\langle \phi^+, F^+\phi^+ \rangle}. \tag{A.23}$$

A.2 Results and discussion

Table A.1 presents the group wise delayed neutron parameters, specifically the delayed neutron fractions (β_i) and decay constants (λ_i), obtained using three different computational methods: Meulekamp, Nauchi, and IFP methods. The values of λ_i increase monotonically from Group 1 to Group 6, ranging from approximately 0.013 s^{-1} to 2.857 s^{-1} across all methods. The β_i exhibits good agreement among the methods. Group 4 contributes the most to the total delayed neutron fraction, accounting for over 280 pcm across all methods. Group 2 and Group 3 also make significant contributions, each around 130 pcm, while Groups 1 and 6 contribute the least. Table A.2 provides a comparative summary of the kinetic parameters, including the β_{eff}, Λ, and l_p, evaluated using various computational methods: Meulekamp, Chiba, Nauchi, IFP, and Perturbation, along with a comparison of these methods to MCNP6.

Table A.1: Delayed neutron parameters group using Meulekamp, Nauchi, and IFP methods.

Group i	Meulekamp Method		Nauchi Method		IFP Method	
	β_i (pcm)	λ_i (s^{-1})	β_i (pcm)	λ_i (s^{-1})	β_i (pcm)	λ_i (s^{-1})
1	25.76 ± 0.10	0.013	25.61 ± 0.11	0.013	25.50 ± 0.39	0.013
2	131.98 ± 0.26	0.033	132.01 ± 0.26	0.033	132.20 ± 0.86	0.033
3	127.47 ± 0.24	0.121	127.37 ± 0.26	0.121	126.94 ± 0.87	0.121
4	282.45 ± 0.35	0.303	281.80 ± 0.37	0.303	282.70 ± 1.20	0.303
5	117.12 ± 0.22	0.851	117.09 ± 0.24	0.851	118.14 ± 0.79	0.851
6	49.05 ± 0.14	2.857	48.99 ± 0.15	2.857	50.67 ± 0.52	2.857

Table A.2: Comparison of kinetic parameters obtained through different methods.

Parameters	Meulekamp	Chiba	Nauchi	IFP	Perturbation	MCNP6
β_{eff} (pcm)	733.83 ± 0.57	734.07 ± 0.82	732.87 ± 0.61	736.13 ± 2.02	735.36 ± 0.40	735 ± 5
Λ (μs)	-	-	81.92 ± 0.02	81.08 ± 0.05	81.62 ± 0.01	80.96 ± 0.10
l_p (μs)	-	-	81.96 ± 0.02	81.12 ± 0.05	81.66 ± 0.01	80.98 ± 0.10

The β_{eff} obtained by all methods ranges from approximately 732.87 to 736.13 pcm. The average value of the methods is 734.85 pcm. The IFP method yields the highest β_{eff} value (736.13 ± 2.02 pcm). The perturbation technique provides a close estimate (735.36 ± 0.40 pcm), while the Meulekamp, Chiba, and Nauchi methods show a deviation range of less than 1%. The Λ data is only available from the Nauchi, IFP, and Perturbation methods. The results range from 81.08 ± 0.05 μs (IFP) to 81.92 ± 0.02 μs (Nauchi), indicating good agreement. The l_p was determined using three different approaches: Nauchi, IFP, and Perturbation. The corresponding values obtained are 81.96 μs, 81.12 μs, and 81.66 μs, respectively. The average value across these methods is 81.58 μs. The results from all three methods are in agreement, with relative deviations from the mean value being within 0.6%.

The kinetic parameters obtained with the methods are compared to those obtained using MCNP6 as shown in Table A.2, where β_{eff} is 735 pcm. Compared to this value, the Meulekamp, Chiba, and Nauchi methods produce slightly lower results, with deviations of –0.16%, –0.13%, and –0.29%, respectively. In contrast, the IFP and perturbation methods show higher results, with deviations of +0.15% and +0.05%, respectively. For the Λ,

MCNP6 yields a value of 80.96 μs. In comparison, the Nauchi method produces 81.92 μs, which is a relative difference of +1.19%. The perturbation method gives 81.62 μs (+0.81%), while the IFP method reports 81.08 μs, with the smallest deviation of +0.15%. For the l_p, the MCNP6 result is 80.98 μs. Compared to this, the Nauchi, IFP, and perturbation methods yield values of 81.96 μs, 81.12 μs, and 81.66 μs, corresponding to relative deviations of +1.21%, +0.17%, and +0.84%, respectively. Overall, the IFP method aligns most closely with MCNP6 results across all kinetic parameters.

Kinetic parameters of the DNRR with LEU fuel, including the β_{eff}, the Λ, and the l_p, were determined using the various built in methods of the Serpent 2 code and the ENDF/B-VIII.0 library. The values of β_{eff} obtained with the methods are within the range of 732.87–736.13 pcm, respectively. The values of Λ ranges from 81.08 μs (IFP) to 81.92 μs (Nauchi), while the values of l_p varies from 81.12 μs (IFP) to 81.96 μs (Nauchi). The differences between the methods are less than 1.07%. Comparing with those obtained with MCNP6 calculations, the kinetic parameters calculated by Serpent 2 show good agreement with the MCNP6 reference values, demonstrating the consistency and reliability of the two codes for the DNRR analysis.

Appendix B Covariance data

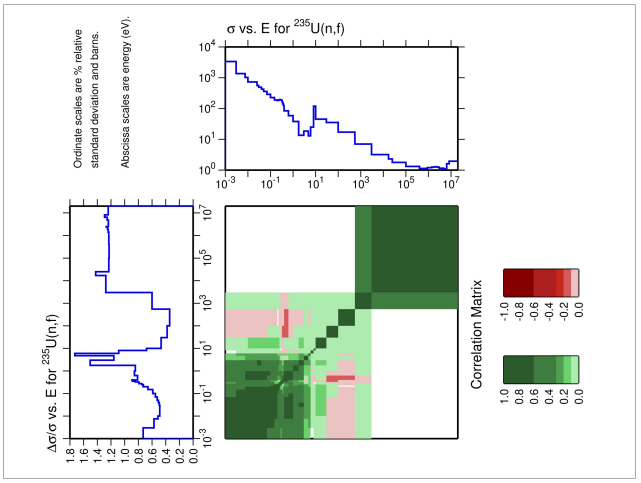

(a) ENDF/B-VIII.0

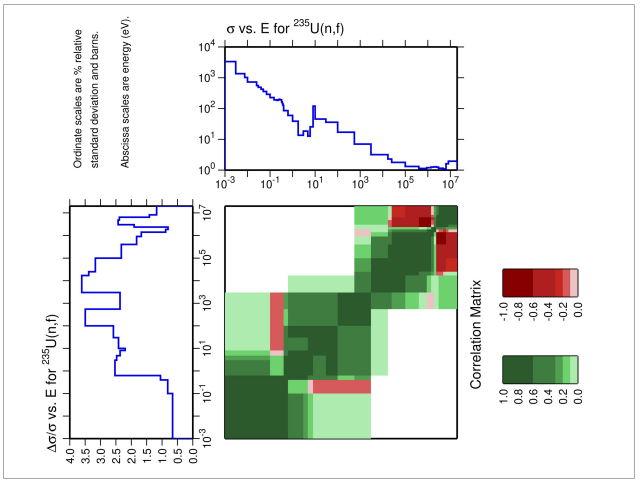

(b) JEFF-3.3

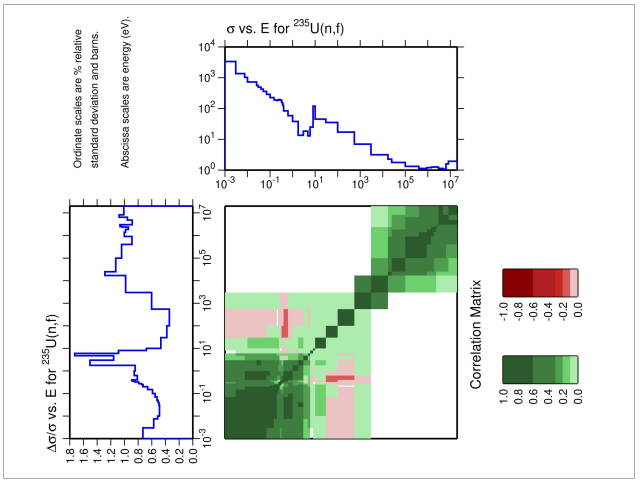

(c) JENDL-5

Figure B.1: Covariance data of U-235 (n,fission) taken from the ENDF/B-VIII.0, JEFF-3.3 and JENDL-5 libraries.

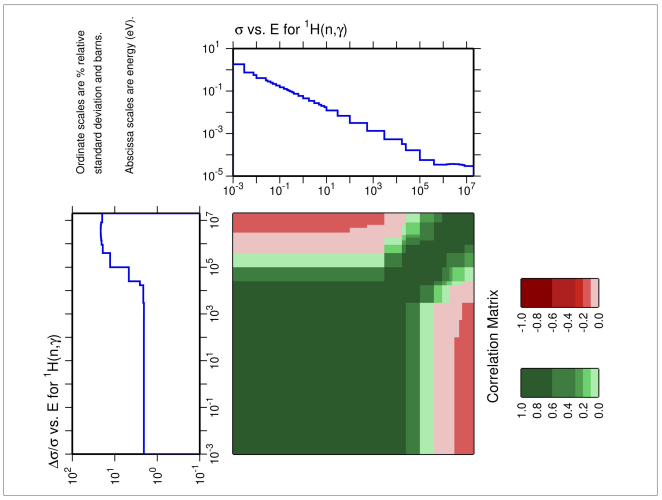

(a) ENDF/B-VIII.0

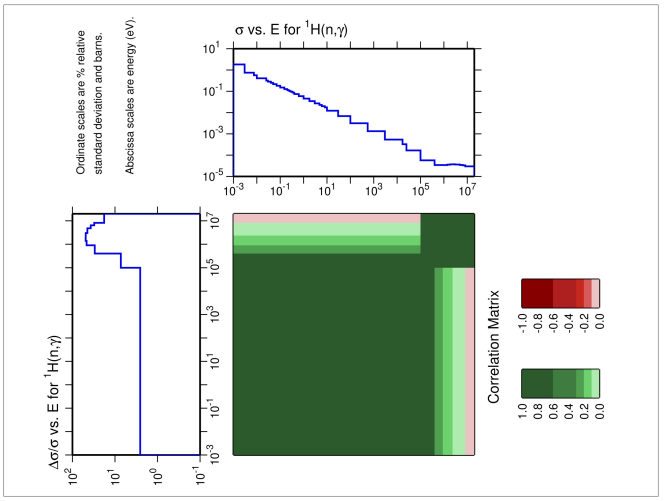

(b) JEFF-3.3

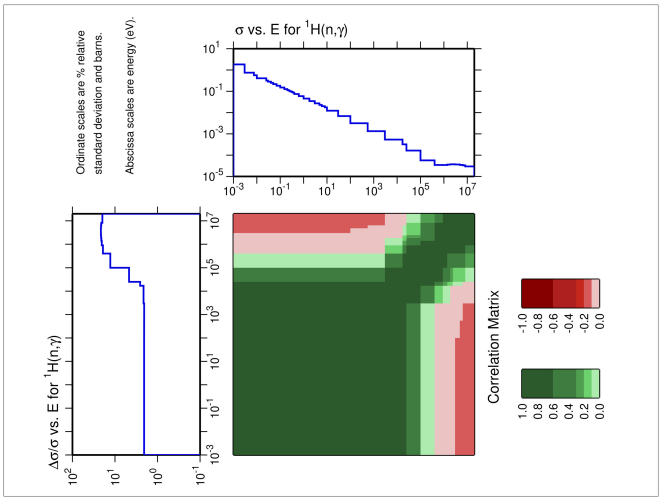

(c) JENDL-5

Figure B.2: Covariance data of H-1 (n,γ) taken from the ENDF/B-VIII.0, JEFF-3.3 and JENDL-5 libraries.

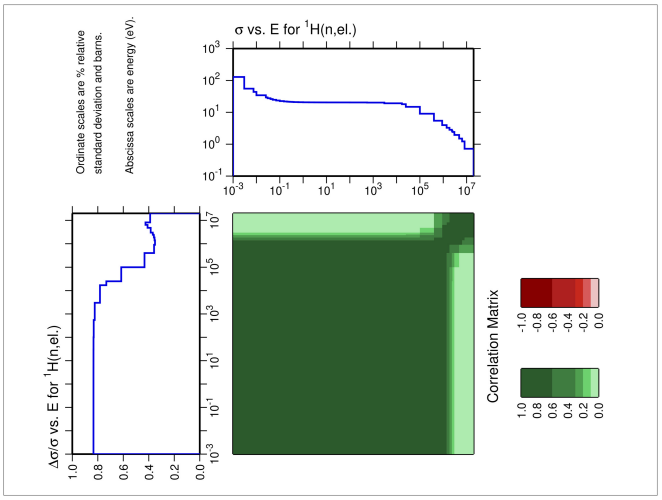

(a) ENDF/B-VIII.0

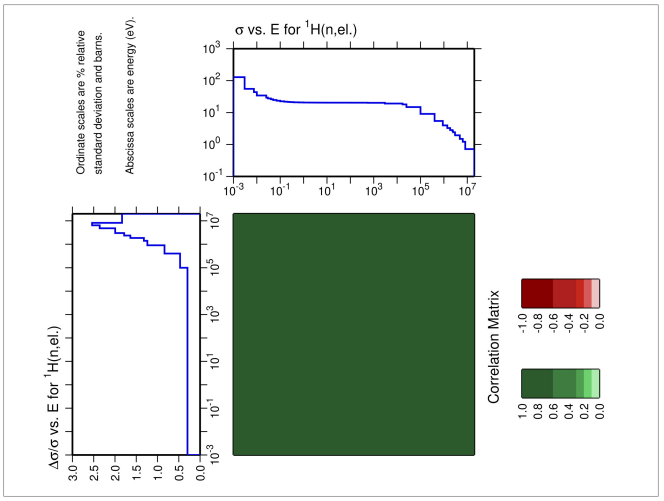

(b) JEFF-3.3

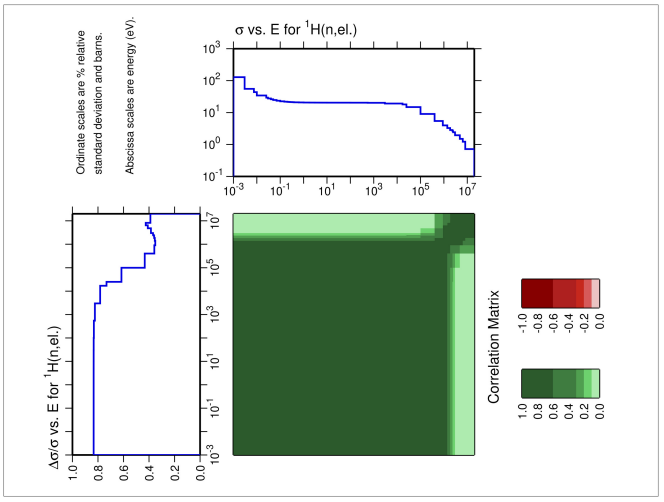

(c) JENDL-5

Figure B.3: Covariance data of H-1 (n,elastic) taken from the ENDF/B-VIII.0, JEFF-3.3 and JENDL-5 libraries.

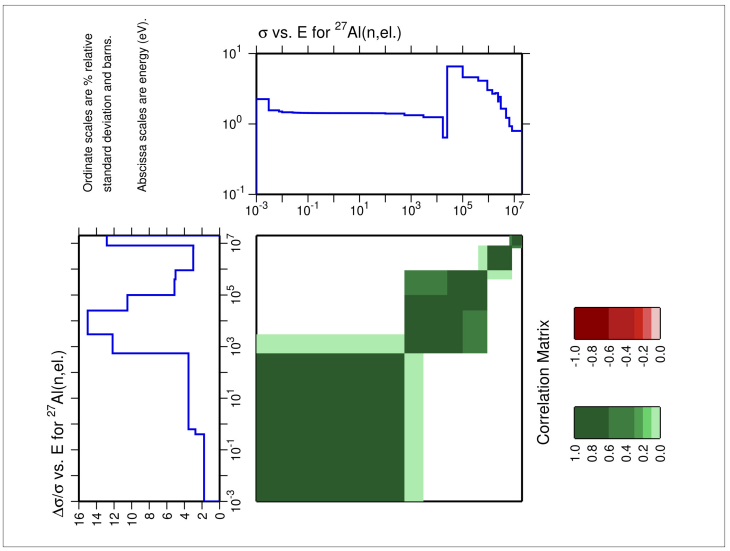

(a) ENDF/B-VIII.0

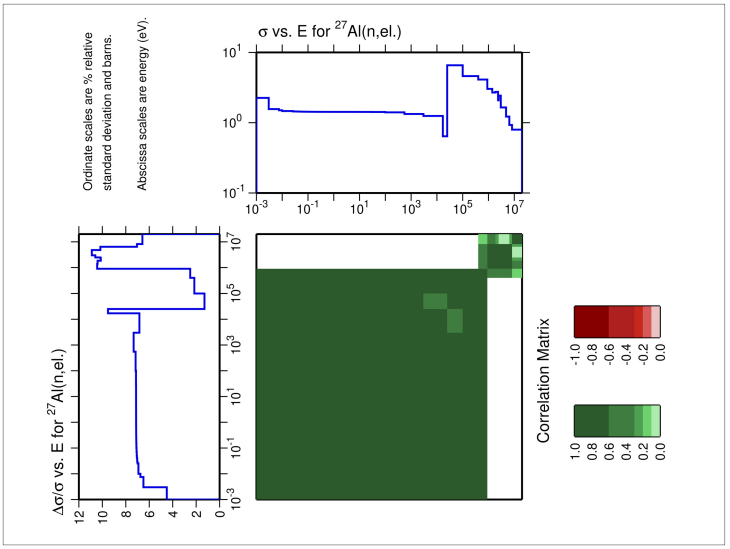

(b) JEFF-3.3

Figure B.4: Covariance data plot for Al-27 (n,elastic).

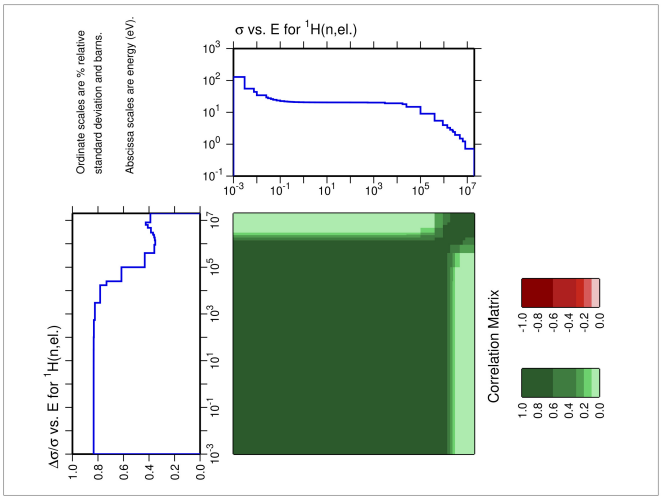

(a) ENDF/B-VIII.0

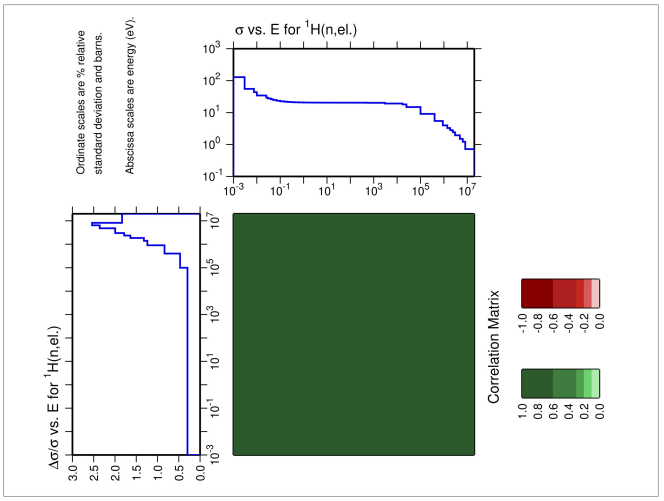

(b) JEFF-3.3

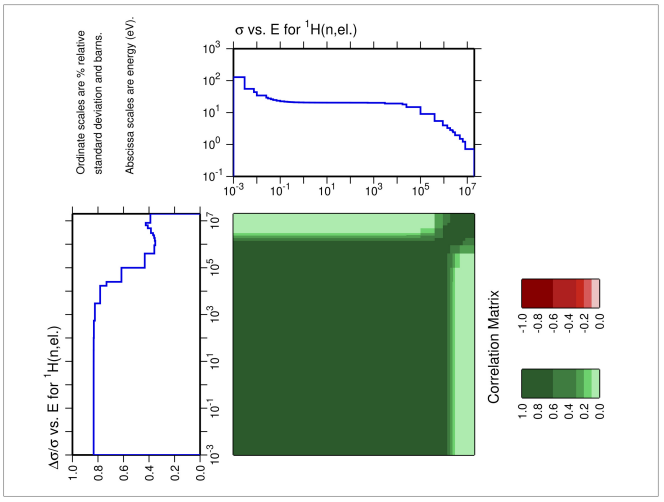

(c) JENDL-5.0

Figure B.5: Covariance data plot for H-1 (n,elastic).

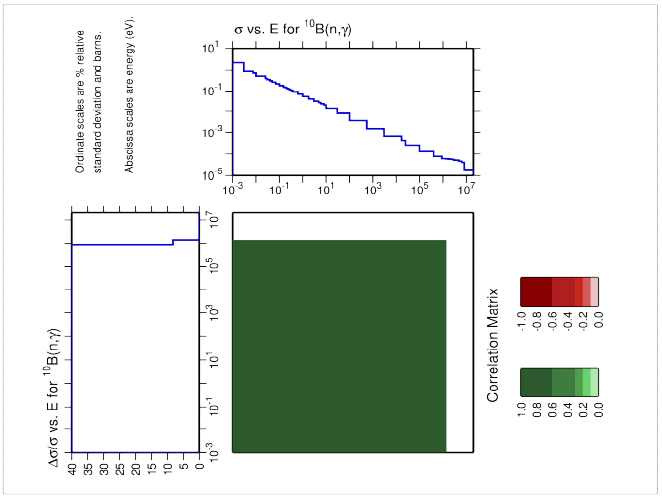

(a) ENDF/B-VIII.0

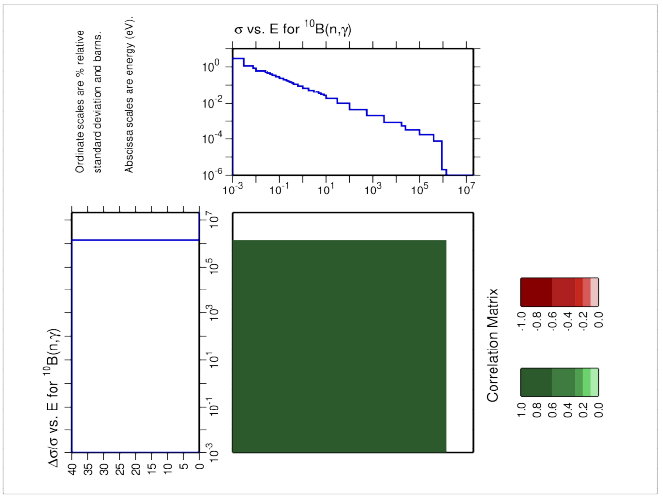

(b) JEFF-3.3

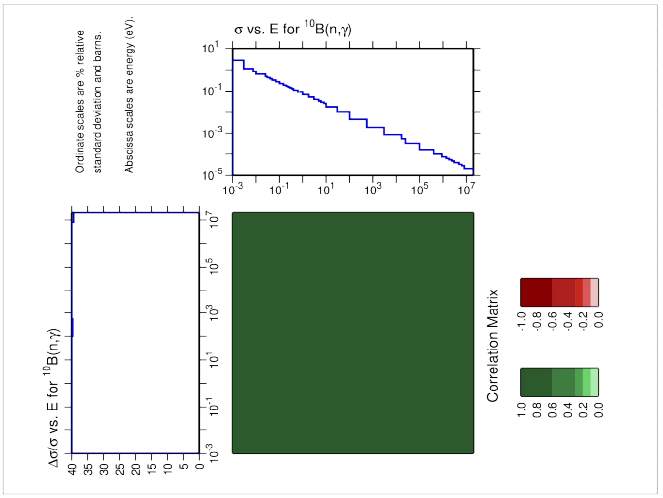

(c) JENDL-5.0

Figure B.6: Covariance data plot for Bo-10 (n,γ).

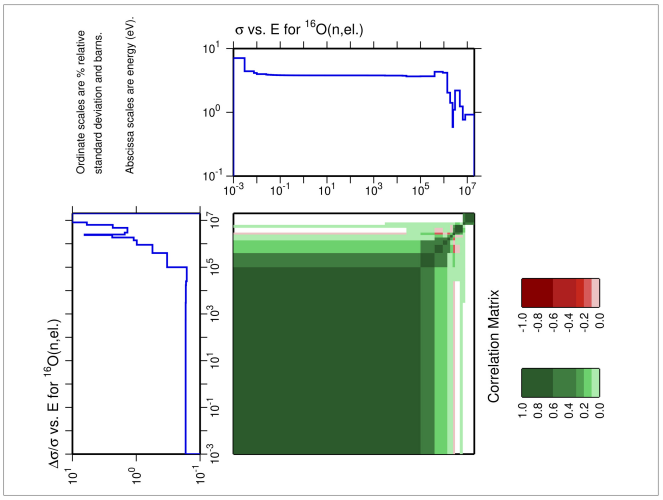

(a) ENDF/B-VIII.0

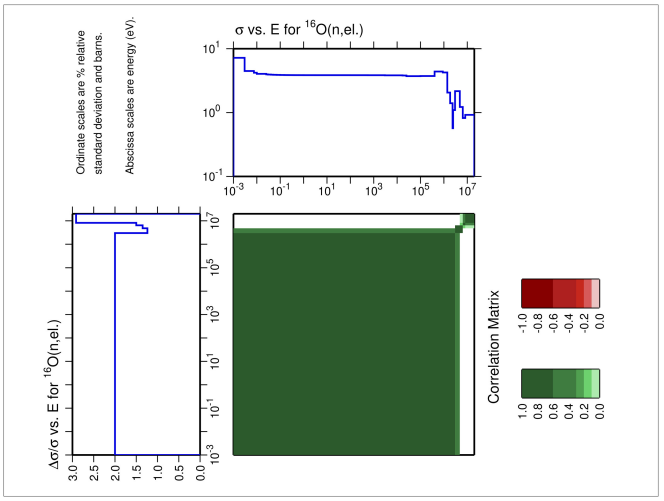

(b) JEFF-3.3

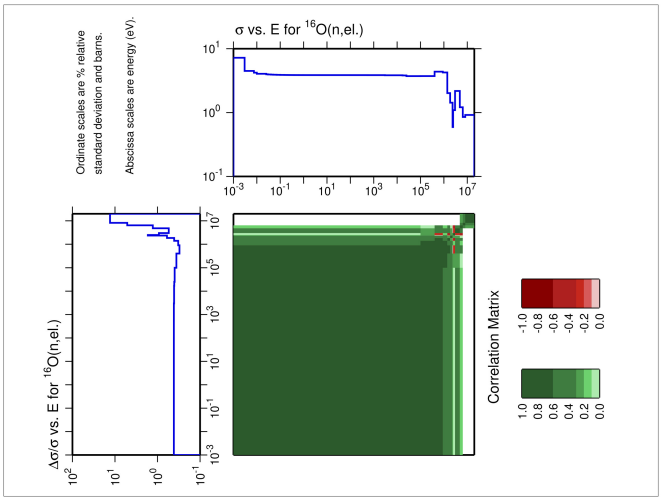

(c) JENDL-5.0

Figure B.7: Covariance data plot for O-16 (n,elastic).

Appendix C Neutron spectrum

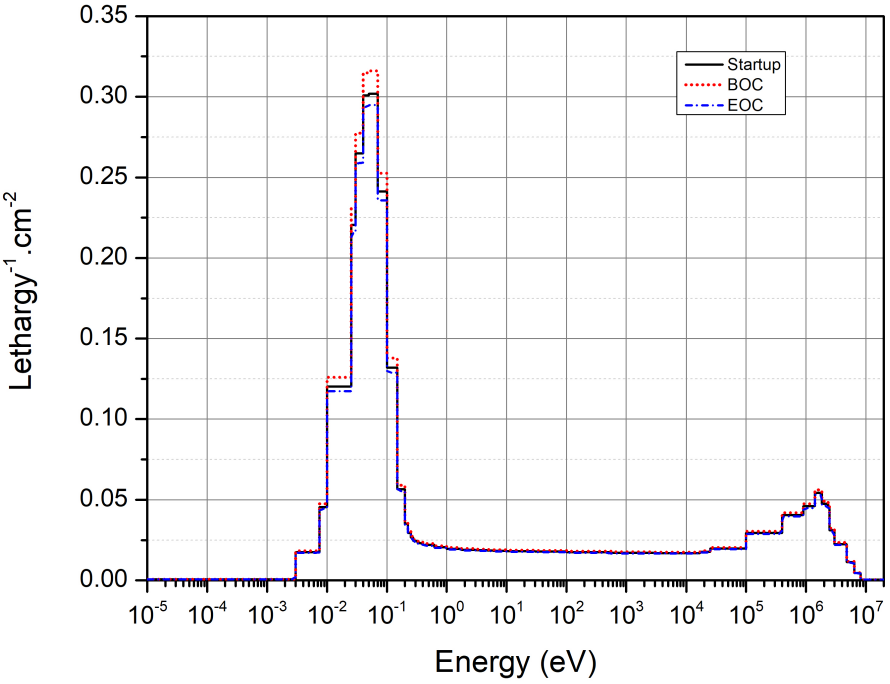

Figure C.1: The neutron spectrum was calculated at the neutron trap using 44 energy groups and the ENDF/B-VIII.0.

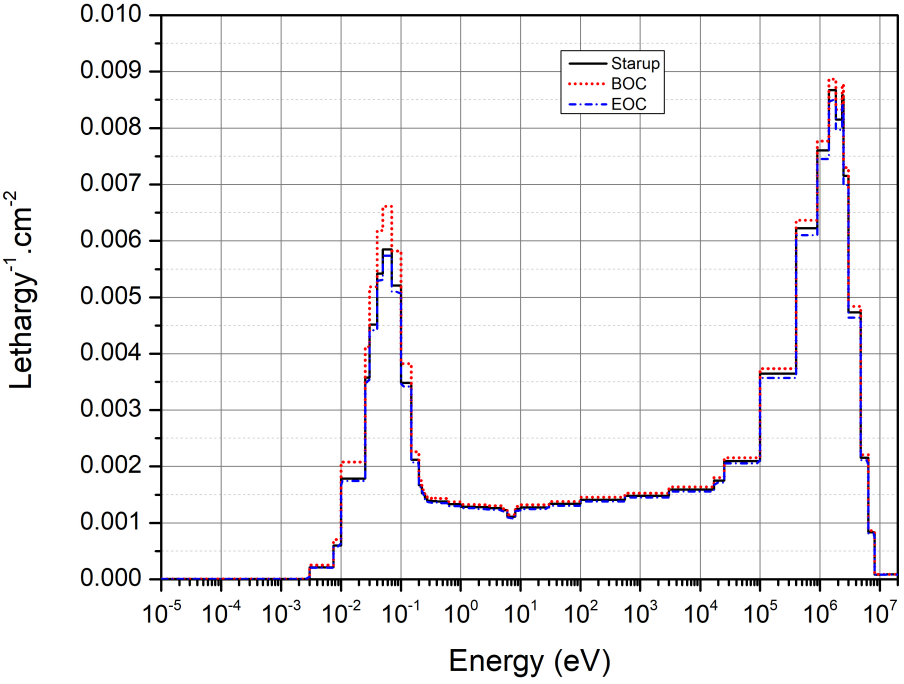

Figure C.2: The neutron spectrum was calculated at the fuel rod using 44 energy groups and the ENDF/B-VIII.0 library.